

## CONTENTS

**Biochemistry**

- V. D. Dragičević, S. Sredojević, M. B. Spasić and M. M. Vrvic*: Ageing-induced changes of reduced and oxidized glutathione in fragments of maize seedlings ..... 911

**Inorganic Chemistry**

- V. M. Leovac, Lj. S. Vojinović, K. Mészáros Szécsényi and V. I. Češljević*: Transition metal complexes with thiosemicarbazide-based ligands. Part 46. Synthesis and physico-chemical characterization of mixed ligand cobalt(III)-complexes with salicylaldehyde semi-, thiosemi- and isothiosemicarbazone and pyridine..... 919

- V. S. Jevtović, Lj. S. Jovanović, V. M. Leovac and L. J. Bjelica*: Transition metal complexes with thiosemicarbazide-based ligands. Part 47. Synthesis, physicochemical and voltammetric characterization of iron(III) complexes with pyridoxal semi-, thiosemi- and *S*-methylisothiosemicarbazones..... 929

**Physical Chemistry**

- I. Gutman, B. Furtula and J. Belić*: Note of the Hyper-Wiener index (Note) ..... 943
- I. Gutman*: Hyper-Wiener index and Laplacian spectrum..... 949
- I. Hinić, G. Stanišić and Z. Popović*: Influence of the synthesis conditions on the photoluminescence of silica gels..... 953
- B. F. Abramović, V. B. Anderluh, A. S. Topalov and F. F. Gaál*: Direct photolysis and photocatalytic degradation of 2-amino-5-chloropyridine ..... 961
- M. M. Ačanski*: Normal-phase high performance liquid chromatography of estradiol derivatives on amino- and diol-columns..... 971

**Electrochemistry**

- V. V. Panić, A. B. Dekanski, V. B. Mišković-Stanković, S. K. Milonjić and B. Ž. Nikolić*: The role of the concentration profile of titanium oxide on the electrochemical behavior of RuO<sub>2</sub>-TiO<sub>2</sub> coatings obtained by the sol-gel procedure ..... 979
- K. Babić-Samarđžija, S. P. Sovilj and V. M. Jovanović*: Comparative electrochemical study of some cobalt(III) and cobalt(II) complexes with azamacrocycles and β-diketonato ligands . 989

**Materials**

- A. Golubović, S. Nikolić, R. Gajić, S. Djurić and A. Valčić*: The growth of Nd:CaWO<sub>4</sub> single crystals . 1001

**Book Review**

- M. M. Vrvic*: Comprehensive enzyme kinetics by V. Leskovac..... 1011
- Contents of Volume 68 ..... 1013
- Subject index..... 1021
- Author index..... 1025

## Ageing-induced changes of reduced and oxidised glutathione in fragments of maize seedlings

VESNA D. DRAGIČEVIĆ<sup>\*1</sup>, SLOBODANKA SREDOJEVIĆ<sup>1#</sup>, MIHAJLO B. SPASIĆ<sup>2#</sup> and  
MIROSLAV M. VRVIĆ<sup>3#</sup>

<sup>1</sup>Maize Research Institute “Zemun Polje”, 11185 Belgrade-Zemun, Slobodana Bajića 1, <sup>2</sup>Institute for Biological Research “Siniša Stanković”, 11000 Belgrade, 29. Novembra 142 and <sup>3</sup>Faculty of Chemistry, University of Belgrade, 11001 Belgrade, Studentski trg 16, P. O. Box 158, Serbia and Montenegro

(Received 15 April 2003)

**Abstract:** A trial with four maize inbred lines with the ability to have different durations of seed germination in the course of the accelerated ageing (AA) treatment was set up. Changes of the content of total, reduced and oxidized glutathione (expressed as monomers) were observed in the seeds and seedlings before and after the treatment. For the first time, changes of glutathione in whole seedlings, as well as in the rest of the seed, were analysed. It was noticed that maize inbreds with a smaller decrease of the total glutathione but with an increase of the oxidized form had the ability of prolonged germination. In the control seedlings, the amount of total glutathione was lower than in the treated ones. Maize seeds which lost germination faster had greater losses of total glutathione with an increased content of the oxidized form in seedlings. The ability of prolonged germination together with the possibility of glutathione synthesis in seedlings are genotypic traits.

**Keywords:** ageing, maize seedling, reduced and oxidised glutathione.

### INTRODUCTION

The processes of ageing have primarily been investigated in anthropo-animal organisms, as they were initially observed in them. The development of new trends in agriculture required ageing processes in plant organisms to be investigated, firstly in seed material for biological (germplasm conservation) and economic reasons (production of commercial seeds). The reason for this phenomenon lies in complex biochemical changes of the reserve substances of seeds, the production of toxic reactants and inhibitory substances (free radicals, methyl jasmonates, *etc.*).<sup>1,2</sup> Glutathione is synthesized in living systems as a highly important antioxidant for the maintenance of equilibrium.

The role of glutathione has been much more investigated within anthropo-animal systems,<sup>3,4</sup> but in recent times the increase in the knowledge of its functions in plants has be-

<sup>\*</sup> Corresponding author. Phone: +381-11-3756-704. Fax: +381-11-3756-707.

E-mail: mmvchem@drenik.net.

<sup>#</sup> Serbian Chemical Society active member.

come more essential. The glutathione system is one of the most important non-enzymic protective factors.<sup>4</sup> From a biochemical point of view, it is a small, mobile molecule consisting of three amino acids: glutamine, cysteine and glycine, and it is important in oxidation-reduction reactions in tissues. In physiologically active tissues, reduced glutathione (GSH) presents a reducing substrate, whereby oxidized glutathione (GSSG) is generated. Then glutathione reductase catalyses the NADPH-dependent reduction of GSSG to glutathione GSH by a reversible reaction. Water elimination out from a system over a series of reactions is known as the ascorbate-glutathione cycle.<sup>4</sup> Since there is no free ascorbate in seeds, GSH directly participates in the oxidation, by the proposed mechanism of substitution:<sup>5,6</sup>



The GS• radical is relatively stable, while the formed GSSG is non-toxic to living systems.

Pastori and Trippi<sup>7</sup> and Kocsy *et al.*<sup>8</sup> indicated in their studies that plants with a higher resistance to stress factors are characterized by an increased level of glutathione. Furthermore, changes in the content of the total, as well as the reduced and oxidized glutathione were observed in aged seed.<sup>9–11</sup> Therefore, it is important to determine the influence of seed ageing on changes of the content of total, as well as of reduced and oxidised glutathione in maize genotypes of different germination ability. Additionally, changes of the glutathione levels in seedlings retarded in growth, originating from aged seeds, should be determined and, therefore, these are also the objectives of this investigation.

#### EXPERIMENTAL

The following four maize inbreds were used in the experiment: two dent inbreds (ZP PL 175-L<sub>1</sub> and ZP PL 188-L<sub>2</sub>) and two sweet maize inbreds (ZP PL 51-L<sub>3</sub> and ZP PL 67-L<sub>4</sub>). Maize seeds were subjected to the AA treatment<sup>12</sup> at a temperature of 42 °C and a relative air humidity of 100 %, for a duration of three, six or nine days up to the moment when the slope of the germination curve becomes steep and the seedlings are significantly retarded in growth. This occurred with L<sub>1</sub> and L<sub>2</sub> after 9 and 6 days (germination decreased from the initial 91.5 to 46 %, *i.e.*, 89 to 15.2 % respectively), while with the inbreds L<sub>3</sub> and L<sub>4</sub> it was registered after 3 days (germination decreased from the initial 28.7 to 13.7 %, *i.e.*, 88.5 to 77 %, respectively). Further exposure of the seeds to the treatment led to germination hold-up.

A further step was to determine the germination capacity according to the ISTA Rules<sup>13</sup> in four replicates of 100 uniform seeds. The germination capacity was evaluated seven days later. All seedlings were grouped into four replicates of 25 plants, and then the radicle, shoots and the rest of seed were fractioned. Also, four replicates of 25 uniform seeds were formed of the treated and untreated seeds, and average weight of a seed was determined.

The plant material was dried in a ventilation drier at 60 °C to constant weight from which the average weight of each fraction individually was determined and expressed per unit, *i.e.*, seedling. Then, the plant material was pulverised (pulveriser Fritsch IZP-119-UP11).

The content of reduced (GHS) and oxidized glutathione (GSSG) was determined according to the method of Kok *et al.*<sup>14</sup> After shaking 1 g of sample with 10 mL 0.15 % Na ascorbate solution in a shaker, the sample was centrifuged at 20,000 g for 20 minutes, and then the supernatant was deproteinised in a water bath

at 95 °C for 3 min. After repeated centrifugation at 15,000 g for 15 min, the content of total glutathione in the supernatant was analysed in the following manner: 1.5 mL 0.2 M potassium phosphate buffer (pH 8.0) and 0.2 mL 10 mM DTNB [5,5'-dithiobis(2-nitrobenzoic acid)] were added to 1.5 mL of the extract, as well as to 1.5 mL 0.02 M potassium phosphate buffer (pH 7.0). The absorbance was read at 415 nm. In the other 1.5 mL of supernatant, 0.5 mL 0.25 M potassium phosphate buffer (pH 6.8), 0.3 mL albumin, 0.02 mL glyoxalase I (Sigma grade IV) and 0.08 mL 0.1 M methylglyoxal are added. After incubation at 30 °C for 15 min, the content of reduced glutathione (GSH) was determined in the above described manner. GSH (Sigma Ultra 98–100 %) in the concentration range 0–0.1  $\mu\text{mol GSH mL}^{-1}$  was used as the standard. The content of oxidized glutathione (GSSG), calculated as the difference between the total and the reduced glutathione, was expressed as monomer.

Statistical evaluation was performed using the Student's *t*-test. The control without AA treatment was used as the reference. The minimum level of statistical significance accepted was  $p < 0.05$ .

## RESULTS

Changes of the GSH and GSSG contents were observed in seeds, as well as in parts of the seedlings originating from the seeds, before and after AA treatment.

The AA treatment lowered the level of total glutathione in the seeds (Table I). Thus, the total glutathione in  $L_1$ ,  $L_2$ ,  $L_3$  and  $L_4$  decreased by 12 %, 20 %, 30 % and even 55 %, compared to the control. Furthermore, the treatment resulted in an increase of the GSSG content in seeds of  $L_1$  and  $L_2$  from 90 to 395 and from 716 to 726  $\text{nmol g}^{-1}$ . In contrast, the levels of GSH and GSSG decreased significantly from 814 to 619 and from 161 to 62  $\text{nmol g}^{-1}$ , respectively, in  $L_3$ , and from 894 to 548 and from 822 to 222  $\text{nmol g}^{-1}$ , respectively, in  $L_4$ .

TABLE I. The impact of accelerated ageing on the distribution of GSH and GSSG among seedling parts, [ $\text{nmol g}^{-1}$ ].

Genotype	Ageing treatment	Seed			Radicle			Shoot			Rest of seed		
		GSH	GSSG	$\Sigma$	GSH	GSSG	$\Sigma$	GSH	GSSG	$\Sigma$	GSH	GSSG	$\Sigma$
$L_1$	control	963	90	1053	1090	672	1762	435	1453	1888	624	401	1025
	treatment	528	395	923	1312	1132	2444	664	993	1657	913	536	1449
$L_2$	control	793	716	1509	553	2407	2960	404	1949	2353	689	191	880
	treatment	474	726	1200	1196	2067	3263	378	1688	2066	805	394	1262
$L_3$	control	814	161	975	5778	4312	10090	3384	1613	4997	2241	2994	5235
	treatment	619	62	681	5019	2126	7145	3709	2273	5982	2173	3866	6039
$L_4$	control	894	822	1716	4900	2245	7145	356	1837	2193	1589	3328	4917
	treatment	548	222	770	4509	1032	5541	141	2400	2541	1730	3910	5640
$p < 0.05^*$		18	21	37	44	86	130	43	66	108	28	72	101

\*Significant differences from controls (*t*-tests)

It is interesting that the employed treatment provided a classification of the seedlings into two groups. Namely, the content of total glutathione increased from 4,675 to 5,550  $\text{nmol g}^{-1}$  and from 6,193 to 6,528  $\text{nmol g}^{-1}$  in the whole seedlings of  $L_1$  and  $L_2$  respectively (Table I). On the other hand, this content decreased in  $L_3$  and  $L_4$  from 20,322 to 19,166  $\text{nmol g}^{-1}$  and from 14,255 to 13,722  $\text{nmol g}^{-1}$  in the whole seedlings of  $L_3$  and  $L_4$ ,

respectively. The increase in the level of total glutathione in  $L_1$  and  $L_2$  was pronounced in the radicle (39 and 10 %) and the rest of the seed (41 and 43 %), while in  $L_3$  and  $L_4$  it was in the shoots (20 and 16 %) and the rest of the seed (15 %).

In order to express the changes in the glutathione levels in maize seeds and seedlings after AA treatment more clearly, the GSH:GSSG ratio was calculated (Fig. 1).

The GSH:GSSG ratio in the seeds of  $L_1$  (the genotype most resistant to the treatment in whose seeds the ability to germinate is preserved for up to 9 days) decreased from 10.7:1 to 1.3:1 (Fig. 1). There were no significant changes of this ratio in seeds of  $L_2$  (the ability to germinate is preserved for up to 6 days in the course of accelerated ageing), *i.e.* the share of GSH in relation to GSSG decreases only from 1.1:1 to 0.7:1. However, this ratio increases in  $L_3$  and  $L_4$  (inbreds with the shortest ability to germinate, up to 3 days) from 5.1:1 to 10.3:1, and from 1.1:1 to 2.4:1, respectively.

The GSH:GSSG ratio distinguishes seedlings of  $L_1$  from seedlings of the other inbreds (Fig. 1) - the GSH share in relation to GSSG decreases in the radicle from 1.6:1 to 1.2:1, while it increases in the shoots from 0.3:1 to 0.7:1, and shows no changes in the rest of the seed. Significantly higher variations of this ratio were recorded for all other inbreds. Thus, the treatment increased the GSH level in the radicle by 94 % on average, and increased the GSSG level in the shoots and the rest of the seed on average by 32 and 72 %, respectively.

#### DISCUSSION

The inbreds investigated under the effects of AA treatment were classified into the following groups: more sensitive ( $L_3$  and  $L_4$ ), in whose seeds the level of total glutathione decreased (Table I), in accordance with the results observed in tomatoes<sup>10</sup> and less sensitive ( $L_1$  and  $L_2$ ), in which the decrease of the level of total glutathione in the seeds was not significant, but with increased share of GSSG, similar to sunflower seeds.<sup>11</sup> The increase in the content of GSSG dimers in the seeds of the maize inbreds more resistant to the treatment can indicate an interruption of further propagation of radicals by the mechanism of substitution.<sup>5,6</sup> The antioxidative capacity of glutathione should be based on this mechanism.<sup>4,7,8</sup>

Considering numerous studies of other authors, such as Narayan *et al.*<sup>1</sup>, McDonald,<sup>5</sup> Torres *et al.*,<sup>11</sup> Walters,<sup>15</sup> seed ageing is foremost oxidative stress that leads to a decline of germination and to the loss of viability. In contrast to seeds, where metabolic processes are mild and slow, seedlings are an active metabolic system in which catabolic and anabolic processes are simultaneously present. Therefore, changes of the glutathione content in seedlings are more complex. Oxidation of the greatest part of the GSH into GSSG in the fractions of seedlings originating from treated  $L_1$  seeds (Fig. 1) did not affect changes of the GSH:GSSG ratio. It can be assumed that a lower content of total glutathione (Table I) and a smaller range of the GSH:GSSG ratio in seeds (Fig. 1) of other genotypes result in a lowering of the total glutathione content in the whole seedlings, with an increased accumulation of GSSG in the radicle and its decrease in the

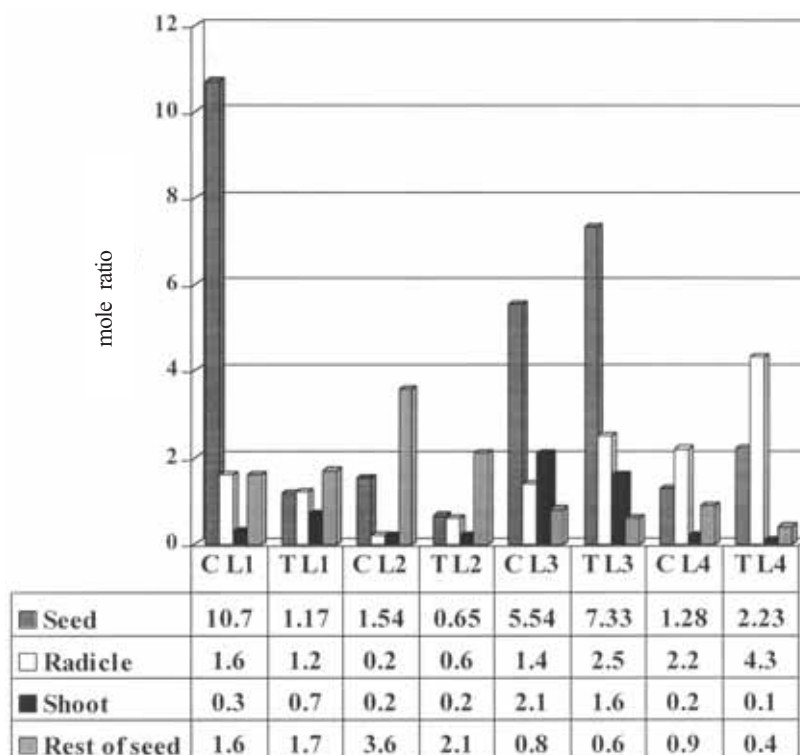


Fig. 1. The GSH:GSSG mole ratio before and after accelerated ageing of seeds and seedling parts. C- control. T- treatment.

shoots and the rest of the seed in comparison with control seedlings, which is in accordance with the results of De Vos *et al.*,<sup>9</sup> De Paula *et al.*,<sup>10</sup> and Torres *et al.*,<sup>11</sup> obtained with sunflowers and tomatoes. These results were also confirmed by investigations of Pastori and Trippi<sup>7</sup> and Kocsy *et al.*,<sup>8</sup> according to which the accumulation of total glutathione in the radicle and shoots of maize seedlings increased after they had been subjected to a stress factor. In the presented studies, changes of glutathione in the rest of the seed were analysed for the first time. Based on the significant share of glutathione in this part of seedlings, especially in inbreds more sensitive to the treatment, it seems that the seed rest plays a significant role in the synthesis and distribution of glutathione in 7-day old maize seedlings. This was confirmed by studies of Rueggsegger and Brunold<sup>16</sup> who determined that synthesis of GSH *de novo* in the 7-day period is mainly done in the scutellum (as a maize seed fraction).

According to our results, maize inbreds with a prolonged ability to germinate (9 and 6 days of treatment of L<sub>1</sub> and L<sub>2</sub>) are characterized by a slower decrease of the total glutathione with an increased GSSG share, in contrast to seeds of L<sub>3</sub> and L<sub>4</sub>, which lose their ability to germinate after a 3-day treatment, with the greatest decrease of the total glutathione. On the other hand, seedlings originating from treated seeds have a higher or a

lower content of total glutathione depending on their sensitivity to the treatment. The total glutathione in seedlings of L<sub>3</sub> and L<sub>4</sub>, as sensitive inbreds, was lower, while the equilibrium was shifted towards GSSG accumulation, in contrast to seedlings of L<sub>1</sub> and L<sub>2</sub> where total glutathione was higher, with the equilibrium shifted towards GSH accumulation. Therefore, the obtained results indicate that seeds of dent maize inbreds (L<sub>1</sub> and L<sub>2</sub>) can preserve their ability to germinate for a longer period of time due to both the smaller loss of total glutathione and a greater GSH synthesis *de novo* and/or GSSG reduction during germination and emergence, which could be bined to the rest of the seed. Seeds of sweet maize inbreds (L<sub>3</sub> and L<sub>4</sub>) are less capable of preserving germination, which is probably a result of the greater loss of total glutathione during the ageing treatment. The significantly higher share of GSSG in these seedlings indirectly indicates oxidative stress which makes germination more difficult.

#### CONCLUSION

From the obtained results, it could be assumed that changes in content and form of the glutathione redox system have a significant influence on the retention of germination ability of seeds. Firstly, the degree of sensitivity of an individual genotype (maize inbreds) to the treatment can be caused by the decrease of total glutathione in the seeds, and, on the other hand, by its uneven distribution and *de novo* synthesis in certain parts of formed seedlings (greater glutathione content in the rest of the seed), as well as by the increased share of GSSG within the total glutathione. These processes result in the classification of maize genotypes into more sensitive, such as sweet maize (L<sub>3</sub> and L<sub>4</sub>) and less sensitive, such as dent maize (L<sub>1</sub> and L<sub>2</sub>); furthermore, within each group, more sensitive (L<sub>2</sub> and L<sub>4</sub>) and less sensitive genotypes (L<sub>1</sub> and L<sub>3</sub>) are observed. Based on the presented results, it could be purported that the retention of germination ability, as well as the potential of GSH synthesis *de novo* are genotypic traits, and as such, could be used in practice, *i.e.*, in selection of less sensitive genotypes, as carriers of these traits.

#### ИЗВОД

##### УТИЦАЈ УБРЗАНОГ СТАРЕЊА НА ПРОМЕНЕ РЕДУКОВАНОГ И ОКСИДОВАНОГ ГЛУТАТИОНА У КЛИЈАНЦИМА КУКУРУЗА

ВЕСНА Д. ДРАГИЧЕВИЋ<sup>1</sup>, СЛОБОДАНКА СРЕДОЛЕВИЋ<sup>1</sup>, МИХАЈЛО Б. СПАСИЋ<sup>2</sup> И МИРОСЛАВ М.  
ВРВИЋ<sup>3</sup>

<sup>1</sup>Институт за кукуруз "Земун Поље", 11185 Београд-Земун, Слободана Бајића 1, <sup>2</sup>Институт за биолошка  
истраживања "Синиша Стојанковић", 11000 Београд, 29. новембра 142 и <sup>3</sup>Хемијски факултет, Универзитет у  
Београду, Студентски йрз 16, й. йр. 158, Београд

Постављен је оглед са четири линије кукуруза различите дужине очувања клијавости семена током третмана убрзног старења. Испитиване су промене укупног, као и редукованог и оксидованог глутатиона (изражени као мономери) у семену и клијанцима пре и након убрзаног старења. У истраживањима су први пут анализиране промене глутатиона у целим клијанцима, као и остатку семена. У семену линија кукуруза које имају способност дужег очувања клијавости био је мањи губитак укупног глутатиона, уз повећање удела оксидованог



облика. Код њихових клијанаца дошло је до повећања садржаја укупног глутатиона у односу на контролне клијанце. Семе кукуруза које брже губи клијавост имало је веће губитке укупног глутатиона, уз већи садржај оксидованог облика код формираних клијанаца. Дужина очувања клијавости, као и синтеза глутатиона код клијанаца је генотипска особина.

(Примљено 15. априла 2003)

#### REFERENCES

1. R. Narayan, G. S. Chauhan, N. S. Verma, *Food Chem.* **27** (1988) 13
2. W. Q. Sun, A. C. Leopold, *Physiol. Plant.* **94** (1995) 94
3. J. B. Schulz, J. Lindenau, J. Dichyons, *Eur. J. Biochem.* **267** (2000) 4904
4. G. Noctor, L. Gomez, H. Vanacker, C. H. Foyer, *J. Exp. Bot.* **53** (2002) 1283
5. M. B. Mc Donald, *Seed Sci. Technol.* **27** (1999) 177
6. Ž. Čeković, *XL Meeting of Serbian Chemical Society, Book of Abstracts*, Serbian Chemical Society, Belgrade, 2001, p. 3 (in Serbian)
7. G. M. Pastori, V. S. Trippi, *Physiol. Plant.* **87** (1993) 227
8. G. Kocsy, M. Brunner, A. Rueggsegger, P. Stamp, C. Brunold, *Planta* **198** (1996) 365
9. C. H. R. De Vos, H. L. Kraak, R. J. Bino, *Physiol. Plant.* **92** (1994) 131
10. M. De Paula, M. Pérez-Otaola, M. Darder, M. Torres, G. Frutos, C. J. Martínez-Honduvilla, *Physiol. Plant.* **96** (1996) 543
11. M. Torres, M. De Paula, M. Perez-Otaola, M. Darder, G. Frutos, C. J. Martínez-Honduvilla, *Physiol. Plant.* **101** (1997) 807
12. J. M. Waltz, D. M. Tekrony, *Seed Sci. Technol.* **23** (2001) 21
13. ISTA Rules, *Seed Sci. Technol.* **21**, Supplement V-21 (1993) 141
14. L. J. de Kok, P. J. L. de Kan, O. G. Tánczos, P. J. C. Kupier, *Physiol. Plant.* **53** (1981) 435
15. C. Walters, *Seed Sci. Res.* **8** (1998) 223
16. D. M. Hodges, C. J. Andrews, D. A. Johnson, R. I. Hamilton, *Physiol. Plant.* **98** (1996) 685
17. A. Rueggsegger, C. Brunold, *Plant Physiol.* **101** (1993) 561.



## Transition metal complexes with thiosemicarbazide-based ligands. Part 46. Synthesis and physico-chemical characterization of mixed ligand cobalt(III)-complexes with salicylaldehyde semi-, thiosemi- and isothiosemicarbazone and pyridine

VUKADIN M. LEOVAC\*<sup>#</sup>, LJILJANA S. VOJINOVIĆ, KATALIN MÉSZÁROS SZÉCSÉNYI and VALERIJA I. ČEŠLJEVIĆ<sup>#</sup>

Department of Chemistry, Faculty of Science, University of Novi Sad, Trg Dositeja Obradovića 3, 21000 Novi Sad, Serbia and Montenegro

(Received 25 June, revised 12 September 2003)

**Abstract:** Mixed ligand octahedral cobalt(III) complexes with the tridentate salicylaldehyde semi-, thiosemi- and isothiosemicarbazone and pyridine of general formula  $[\text{Co}^{\text{III}}(\text{L}^{1-3})(\text{py})_3]\text{X}$  ( $\text{H}_2\text{L}^1$  = salicylaldehyde semicarbazone,  $\text{X} = [\text{Co}^{\text{II}}\text{Cl}_3(\text{py})]^-$ ,  $\text{ClO}_4^- \cdot \text{H}_2\text{O}$ ,  $\text{I}^- \cdot 0.5 \text{I}_2$ ;  $\text{H}_2\text{L}^2$  = salicylaldehyde thiosemicarbazone,  $\text{X} = [\text{Co}^{\text{II}}\text{Cl}_3(\text{py})]^-$ ,  $[\text{Co}^{\text{II}}\text{Br}_3(\text{py})]^-$ ,  $\text{ClO}_4^- \cdot \text{H}_2\text{O}$ ,  $\text{I}_3^-$ ;  $\text{H}_2\text{L}^3$  = salicylaldehyde *S*-methylisothiosemicarbazone,  $\text{X} = [\text{Co}^{\text{II}}\text{Br}_3(\text{py})]^-$ ,  $\text{ClO}_4^- \cdot \text{H}_2\text{O}$ ,  $\text{BF}_4^-$ ) were synthesized. The tridentate coordination of all the three dianionic forms of the ligands involves the phenol oxygen, hydrazine nitrogen and the chalcogen (O or S) in case of salicylaldehyde semi-, thiosemicarbazone and the terminal nitrogen atom in the case of isothiosemicarbazone. For all the complexes, a meridial octahedral arrangement is proposed, which is a consequence of the planarity of the chelate ligand. The compounds were characterized by elemental analysis, molar conductivity, magnetic susceptibility, IR and electronic absorption spectra. The thermal decomposition of the complexes was investigated by thermogravimetry, coupled TG-MS measurements and DSC.

**Keywords:** mixed Co(III) complexes, salicylaldehyde semi-, thiosemi-, isothiosemicarbazone, pyridine.

### INTRODUCTION

Due to their good complexing properties,<sup>1–4</sup> biological activity<sup>5,6</sup> and analytical application,<sup>7,8</sup> semi-/thiosemi-/isothiosemicarbazides and their Schiff bases of different denticity, as well as their metal complexes, have been subject of many studies. Apparently, the most numerous among them are the complexes with tridentate salicylaldehyde semi-/thiosemi-/isothiosemicarbazones. In contrast to salicylaldehyde semi-/thiosemicarbazones, whose donor atoms are O, N, X ( $\text{X}=\text{O}$

\* Corresponding author.

<sup>#</sup> Serbian Chemical Society active member

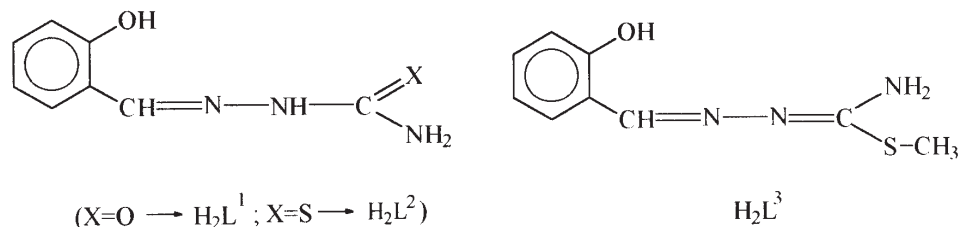


Fig. 1. Structural formulas of salicylaldehyde semi- ( $H_2L^1$ ), thiosemi- ( $H_2L^2$ ) and *S*-methylisothiosemicarbazone ( $H_2L^3$ ).

or S),<sup>1-3</sup> the third donor atom with isothiosemicarbazone derivatives is the nitrogen of the isothioamide group.<sup>4,9</sup>

Cobalt(III) and various tridentate ligands form mainly mixed bis(ligand) complexes, whereas mixed complexes such as  $[Co(L)A_3]^0$ ,  $[Co(L)A_2B]^+$ ,  $[Co(L)B_3]^{3+}$  ( $L$ =diethylenetriamine, cyclohexanitroamine, bis(2-aminoethyl)-sulphide, *N*-(3-aminopropyl)-1,3-propanetriamine;  $A=NO_2$ ,  $N_3$ ,  $CN$ ,  $Cl$ ;  $B=NH_3$ ), are much rarer.<sup>10</sup> In our previous work,<sup>11</sup> the crystal structure of mixed Co(III) complexes of the formula  $[Co^{III}(L^3)(py)_3]X$  ( $X=[Co^{II}Cl_3(py)]^- \cdot EtOH$ ,  $I_3^-$ ), in which three pyridine molecules are in the meridial position, was described. As a continuation of these studies, the syntheses and some physico-chemical characteristics of some new, also mixed, Co(III) complexes with salicylaldehyde semi- ( $H_2L^1$ ), thiosemi- ( $H_2L^2$ ) and *S*-methylisothiosemicarbazone ( $H_2L^3$ ) (Fig. 1), are presented in this work.

## EXPERIMENTAL

### Reagents

All chemicals used were commercially available products of analytical reagent grade, except for the ligands salicylaldehyde semicarbazone ( $H_2L^1$ ), thiosemicarbazone ( $H_2L^2$ ) and *S*-methylisothiosemicarbazone ( $H_2L^3$ ), the preparation of which has been described earlier.<sup>12,13</sup>

### Synthesis of the complexes

$[Co(L^1)(py)_3][CoCl_3(py)]$ . EtOH (5.0 cm<sup>3</sup>) and pyridine ( $\approx 5$  mmol) were added to a mixture of  $CoCl_2 \cdot 6H_2O$  (1.2 mmol) and salicylaldehyde semicarbazone, ( $H_2L^1$ ) (0.6 mmol) in the presence of LiOAc (4 mmol). The reactants were dissolved by stirring and mild heating. After 4 days at room temperature, the green crystals were separated by filtration and washed with EtOH and Et<sub>2</sub>O. The yield was 0.27 g (61 %).

$[Co(L^2)(py)_3][CoCl_3(py)]$  and  $[Co(L^{2,3})(py)_3][CoBr_3(py)]$ . EtOH (5.0 cm<sup>3</sup>) and pyridine ( $\approx 5$  mmol) were added to a mixture of  $CoX_2 \cdot 6H_2O$  ( $X = Cl, Br$ ) (2.5 mmol) and salicylaldehyde thiosemi- ( $H_2L^2$ )/*S*-methylisothiosemicarbazone ( $H_2L^3$ ) (1.25 mmol). After 24 h, the green crystals were separated by filtration and washed with EtOH and Et<sub>2</sub>O. The yield was 0.10 g (11 %), 0.29 g (27 %), 0.48 g (52 %) respectively.

$[Co(L^{1-3})(py)_3]ClO_4 \cdot H_2O$ . To a mixture of the ligands ( $H_2L^{1-3}$ ) (0.5 mmol) and  $Co(ClO_4)_2$  (1 mmol), EtOH (5.0 cm<sup>3</sup>) and pyridine ( $\approx 5$  mmol) were added, and the mixture was heated for a few minutes. After 24 h, the brown crystals were separated by filtration and washed with EtOH and Et<sub>2</sub>O. The yield was 0.27 g (63 %), 0.20 g (64 %), 0.19 g (65 %), respectively.

$[Co(L^1)(py)_3]I_3$  and  $[Co(L^2)(py)_3]I_3$ . To a warm solution of NaI (5 mmol) in EtOH (5.0 cm<sup>3</sup>), 2.5 mmol  $CoCl_2 \cdot 6H_2O$  were added and the resulting solution was heated for a few minutes. After 15 min the precipitated NaCl was separated by filtration. To the  $CoI_2$  solution was then added  $H_2L^1/H_2L^2$  (1.25 mmol) and pyridine ( $\approx 5$  mmol), and the mixture was dissolved by heating. After 24 h, the obtained brown crystals were separated by filtration and washed with EtOH and Et<sub>2</sub>O. The yield was 0.30 g (34 %), 0.30 g (28 %), respectively.

$[\text{Co}(\text{L}^3)(\text{py})_3]\text{BF}_4$ . A mixture of  $\text{CoCl}_2 \cdot 6\text{H}_2\text{O}$  (2 mmol) and  $\text{NaBF}_4$  (4 mmol) in EtOH (6.0 cm<sup>3</sup>) was heated for a few minutes. After 15 minutes, the precipitated NaCl was separated by filtration. To the  $\text{Co}(\text{BF}_4)_2$  solution were then added  $\text{H}_2\text{L}^3$  (2 mmol) and pyridine ( $\approx 5$  mmol), and the mixture was dissolved by heating. After 2 days, the obtained green monocrystals of composition  $[\text{Co}(\text{L}^3)(\text{py})_3][\text{CoCl}_3(\text{py})] \cdot \text{EtOH}^{11}$  were separated by filtration. After 24 h (r. t.), the brown crystals which formed in the filtrate were separated by filtration and washed with EtOH and Et<sub>2</sub>O. The yield was: 0.33 g (28 %).

#### Analytical methods

*Elemental analysis* (C, H, N) was carried out by standard micromethods.

*The content of the metal* in the complexes was determined after previous sample decomposition by heating in a Kjeldahl flask in conc.  $\text{H}_2\text{SO}_4$  and conc.  $\text{HNO}_3$ , followed by evaporation to dryness. The dry residue was dissolved in water and the metal content determined by complexometric titration (EDTA).

*Magnetic susceptibility* measurements were performed at room temperature using an MSB-MKI magnetic susceptibility balance (Sherwood Scientific Ltd., Cambridge, England). The data were corrected for diamagnetic susceptibilities.

*Molar conductivities* of freshly prepared  $1 \times 10^{-3}$  mol/dm<sup>3</sup> DMF solutions were measured using a Janway 4010 conductivity meter.

*IR spectra* (KBr disc) were recorded using a Perkin-Elmer 457 Infracord spectrophotometer.

*Electronic absorption spectra* were recorded using a Carl Zeiss spectrophotometer.

*Thermal measurements* were carried out in dynamic air and argon atmospheres at a heating rate of 10 K min<sup>-1</sup>. The thermogravimetric curves were registered up to 1000 K by means of a DuPont 2000 TA system with a thermobalance DuPont 951 TGA using sample masses of about 5 mg in a platinum crucible. The DSC curves were recorded up to 600 K in an open aluminium pan as the sample holder with an empty aluminium pan as the reference. TG-MS measurements were performed on a TA Instruments SDT 2960 coupled with Balzers Thermstar GSD 300 T capillary MS in dynamic helium and air atmospheres.

## RESULTS AND DISCUSSION

Mixed-ligand octahedral complex of cobalt(III) with salicylaldehyde semi- ( $\text{H}_2\text{L}^1$ ), thiosemi- ( $\text{H}_2\text{L}^2$ ) and *S*-methylisothiosemicarbazone ( $\text{H}_2\text{L}^3$ ), of the type  $[\text{Co}^{\text{III}}(\text{L})(\text{py})_3]\text{X}$  ( $\text{L} = \text{L}^1$ ,  $\text{X} = [\text{Co}^{\text{II}}\text{Cl}_3(\text{py})]^-$ ,  $\text{ClO}_4^- \cdot \text{H}_2\text{O}$ ,  $\text{I}^- \cdot 0.5\text{I}_2$ ;  $\text{L} = \text{L}^2$ ,  $\text{X} = [\text{Co}^{\text{II}}\text{Cl}_3(\text{py})]^-$ ,  $[\text{Co}^{\text{II}}\text{Br}_3(\text{py})]^-$ ,  $\text{ClO}_4^- \cdot \text{H}_2\text{O}$ ,  $\text{I}_3^-$ ;  $\text{L} = \text{L}^3$ ,  $\text{X} = [\text{Co}^{\text{II}}\text{Br}_3(\text{py})]^-$ ,  $\text{ClO}_4^- \cdot \text{H}_2\text{O}$ ,  $\text{BF}_4^-$ ) were obtained by reacting warm ethanolic solutions of cobalt(II) salts and the mentioned ligands and pyridine in the ratio 2:1:5 (Table I). In the first stage of the preparation of the complex with  $\text{BF}_4^-$ , the complex  $[\text{Co}(\text{L}^3)(\text{py})_3][\text{CoCl}_3(\text{py})] \cdot \text{EtOH}^{11}$  was formed, which means that the metathetical reaction between  $\text{CoCl}_2$  and  $\text{NaBF}_4$  yielded no complete precipitation of the chloride (NaCl). It should be mentioned that attempts to isolate complexes with the mixed anion  $[\text{Co}^{\text{II}}\text{I}_3(\text{py})]^-$  were unsuccessful.

All the complexes are well soluble in DMF, less in MeOH, EtOH and  $\text{Me}_2\text{CO}$ , and insoluble in  $\text{H}_2\text{O}$  and  $\text{Et}_2\text{O}$ .

On the basis of the obtained results it can be concluded that the complexes  $[\text{Co}^{\text{III}}(\text{L}^{1-3})(\text{py})_3]^+$  are formed only in combination with large counterions, such as  $[\text{Co}^{\text{II}}\text{X}_3(\text{py})]^-$  ( $\text{X} = \text{Cl}, \text{Br}$ ) or  $\text{ClO}_4^-$ . The formation of complexes with the smaller  $\text{BF}_4^-$  ion is hindered, which was observed in the synthesis of  $[\text{Co}(\text{L}^3)(\text{py})_3]\text{BF}_4$ , as this complex could be obtained only after separation of the primarily formed  $[\text{Co}^{\text{III}}(\text{L}^3)(\text{py})_3][\text{Co}^{\text{II}}\text{Cl}_3(\text{py})]$ .

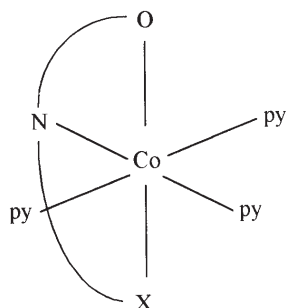
The necessity of the presence of a relatively large anion in combination with the large  $[\text{Co}^{\text{III}}(\text{L}^{1-3})(\text{py})_3]^+$  cation has also been confirmed on the examples of the  $[\text{Co}^{\text{III}}(\text{L}^2)(\text{py})_3]\text{I}_3$  complex, similar to the previously synthesized isothiosemicarbazone complexes,<sup>11</sup> such as  $[\text{Co}^{\text{III}}(\text{L}^1)(\text{py})_3]\text{I}\cdot 0.5\text{I}_2$ , in which a significant interaction exists between  $\text{I}_2$  and two  $\text{I}^-$  anions from the neighbouring molecules. A similar situation was also found in the crystal structure of the  $[\text{Co}^{\text{III}}(\text{H}_2\text{L})\text{I}_2]\text{I}\cdot 0.5\text{I}_2$  ( $\text{H}_2\text{L}$  = bis(hydrazone 2,6 diacetylpyridine)) complex.<sup>14</sup>

TABLE I. Some physico-chemical characteristics and analytical data of the complexes

Complex	Colour	$\mu_{\text{eff}}/\mu_{\text{B}}$	$\lambda_{\text{M}}$ $\text{Scm}^2/\text{mol}$	Found (Caled.) / %			
				C	H	N	Co
$[\text{Co}(\text{L}^1)(\text{py})_3][\text{CoCl}_3(\text{py})]$	green	4.39	43.6	47.34 (46.85)	4.07 (3.79)	13.95 (13.66)	15.94 (16.42)
$[\text{Co}(\text{L}^2)(\text{py})_3][\text{CoCl}_3(\text{py})]$	green	4.45	44.7	46.14 (45.83)	4.03 (3.71)	13.10 (13.66)	16.27 (16.06)
$[\text{Co}(\text{L}^2)(\text{py})_3][\text{CoBr}_3(\text{py})]$	green	4.25	101.7	38.08 (38.77)	3.61 (3.14)	11.14 (11.30)	13.27 (13.59)
$[\text{Co}(\text{L}^3)(\text{py})_3][\text{CoBr}_3(\text{py})]$	green	4.98	158.0	38.89 (39.52)	3.66 (3.32)	11.04 (11.12)	13.03 (13.37)
$[\text{Co}(\text{L}^1)(\text{py})_3]\text{ClO}_4\cdot\text{H}_2\text{O}$	brown	diam	61.0	47.22 (46.75)	4.25 (4.10)	14.05 (14.22)	9.42 (9.97)
$[\text{Co}(\text{L}^2)(\text{py})_3]\text{ClO}_4\cdot\text{H}_2\text{O}$	brown	diam	67.8	46.06 (45.51)	4.10 (3.99)	13.35 (13.58)	9.41 (9.69)
$[\text{Co}(\text{L}^3)(\text{py})_3]\text{ClO}_4\cdot\text{H}_2\text{O}$	brown	diam	83.0	44.50 (46.42)	3.35 (4.22)	13.54 (13.53)	9.15 (9.49)
$[\text{Co}(\text{L}^1)(\text{py})_3]\text{I}\cdot 0.5\text{I}_2$	brown	diam	69.6	41.94 (37.99)	3.78 (3.05)	12.33 (11.55)	8.00 (8.10)
$[\text{Co}(\text{L}^2)(\text{py})_3]\text{I}_3$	brown	diam	23.6	33.45 (31.75)	2.79 (2.55)	11.08 (9.66)	6.46 (6.67)
$[\text{Co}(\text{L}^3)(\text{py})_3]\text{BF}_4$	brown	diam	54.3	49.07 (48.83)	4.57 (4.10)	13.20 (14.24)	10.21 (9.98)

Finally, the obtained results indicate the differences in the possibility of the formation of tri-halogenopyridinecobaltate(II) ions which, to our knowledge,<sup>10</sup> have only been found in combination with the complex cation  $[\text{Co}^{\text{III}}(\text{L}^{1-3})(\text{py})_3]^+$ .<sup>15</sup> Namely, under identical experimental conditions, the  $[\text{CoCl}_3(\text{py})]^-$  anion is very easily formed,  $[\text{CoBr}_3(\text{py})]^-$  is much more difficult to prepare, whereas the analogous iodo-complex is not formed at all.

As can be seen from their coordination formulas (Table I), all the complexes contain the same complex cation  $[\text{Co}^{\text{III}}(\text{L}^{1-3})(\text{py})_3]^+$  with dianionic form of the Schiff bases formed by deprotonation of the most acidic phenolic OH group and deprotonated enolised keto/thioketo group in the case of  $\text{H}_2\text{L}^{1,2}$ , and the isothioamide group in the case of

Scheme 1. Structure of  $[\text{Co}(\text{L})(\text{py})_3]^+$ .

$\text{H}_2\text{L}^3$ . The formation of double-deprotonated form of these ligands is undoubtedly facilitated by the presence of excess pyridine. At the same time, the deprotonation of these groups is chemical proof of the participation of their donor atoms in their coordination. There is no doubt that in addition to the mentioned atoms, another participant in the coordination is the azomethine nitrogen. Thus, one six-membered (salicylidene) and one five-membered (semi-/thiosemi-/isothiosemicarbazide) metalocycles are formed, which has been confirmed by X-ray analysis of  $[\text{Co}(\text{L}^3)(\text{py})_3]\text{X}$  ( $\text{X}=[\text{CoCl}_3(\text{py})]^- \cdot \text{EtOH}$ ,  $\text{I}_3^-$ ).<sup>11</sup> Therefore, in these complexes too, the mentioned ligands are coordinated in the usual tridentate mode with a meridial arrangement of the O, N, X ( $\text{X} = \text{O}, \text{S}, \text{N}$ ) donor atoms<sup>1-4</sup> (Scheme 1).

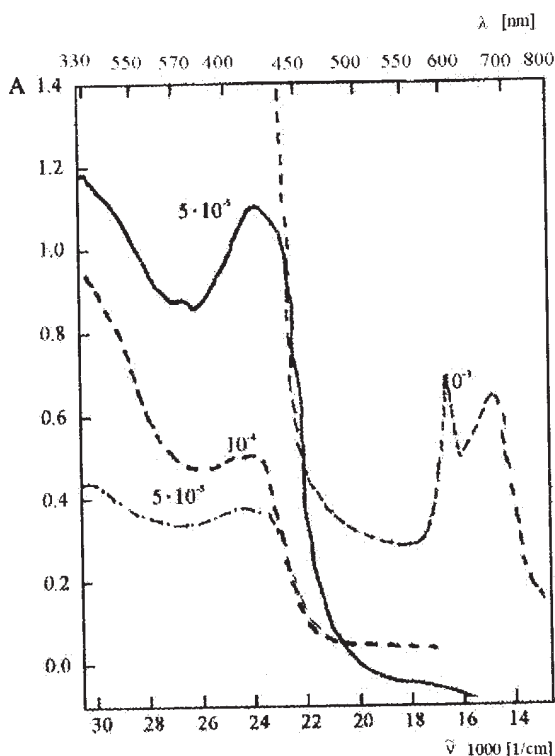


Fig. 2. Electronic spectra of the complexes:  
 (—)  $[\text{Co}^{\text{III}}(\text{L}^2)(\text{py})_3][\text{CoCl}_3(\text{py})]$  in DMF;  
 (---)  $[\text{Co}^{\text{III}}(\text{L}^2)(\text{py})_3][\text{CoCl}_3(\text{py})]$  in  $\text{Me}_2\text{CO}$ ;  
 (.....)  $[\text{Co}^{\text{III}}(\text{L}^2)(\text{py})_3]\text{ClO}_4 \cdot \text{H}_2\text{O}$  in DMF.

In concordance with the mentioned coordination mode is also the absence of the characteristic  $\nu(\text{OH})$  bands in the IR spectra of the complexes, which in the ligand spectra appear at  $\approx 3470\text{ cm}^{-1}$ , as well as the shift to lower energies (*ca.*  $60\text{ cm}^{-1}$ ) of the bands  $\nu(\text{C}=\text{O})$  and  $\nu(\text{C}=\text{S})$ , which in the spectra of  $\text{H}_2\text{L}^1$  and  $\text{H}_2\text{L}^2$  appear at  $1690$  and  $1275\text{ cm}^{-1}$ ,<sup>16</sup> respectively. In the spectra of complexes with  $\text{H}_2\text{L}^3$ , the bands  $\nu(\text{NH})$  and  $\delta(\text{NH}_2)$ , observed in the ligand spectrum at  $3330$  and  $1640\text{ cm}^{-1}$ , are also shifted to lower energies:  $3200$ ,  $1605\text{ cm}^{-1}$ , respectively. In the spectra of the complexes containing  $\text{ClO}_4$  and  $\text{BF}_4$  there are characteristic very strong single bands at  $\approx 1100\text{ cm}^{-1}$ , indicating the ionic character of the acid residues.<sup>16</sup>

With the exception of the complexes that contain tetrahedral anions  $[\text{Co}^{\text{II}}\text{X}_3(\text{py})]^-$  ( $\text{X} = \text{Cl}, \text{Br}$ ), all the others are diamagnetic. Magnetic moments of the paramagnetic complexes correspond to the usual values observed for tetrahedral  $\text{Co}(\text{II})$  complexes<sup>17</sup> (Table I).

The electronic spectra of the brown DMF and  $\text{Me}_2\text{CO}$  solutions of complexes are similar to each other and exhibit an absorption maximum at  $\approx 400\text{ nm}$  corresponding to d-d transitions of  $\text{Co}(\text{III})$ .<sup>18</sup> The green solutions of the complexes con-

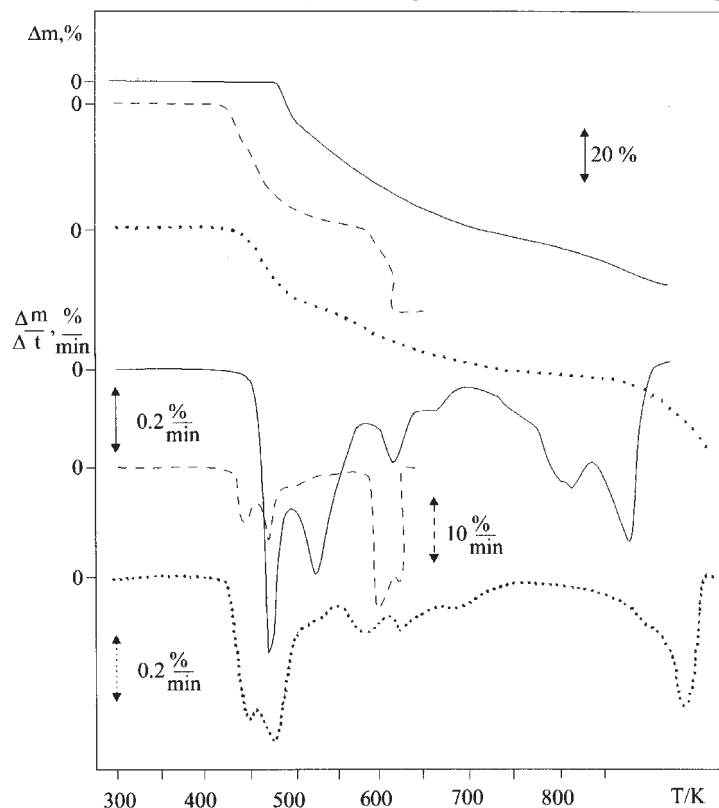


Fig. 3. Thermal curves of: (—)  $[\text{Co}^{\text{III}}(\text{L}^1)(\text{py})_3][\text{CoCl}_3(\text{py})_3]$ ; (---)  $[\text{Co}^{\text{III}}(\text{L}^1)(\text{py})_3]\text{I} \cdot 0.5\text{I}_2$ ; (····)  $[\text{Co}^{\text{III}}(\text{L}^2)(\text{py})_3][\text{CoCl}_3(\text{py})_3]$ .

taining the tetrahedral  $[\text{CoX}_3(\text{py})]^-$  ( $\text{X} = \text{Cl}, \text{Br}$ ) anion also exhibit a weak absorption in the range of 600–700 nm, belonging to d-d transitions of Co(II).

It should be mentioned that the DMF solutions of the complexes with a tetrahedral Co(II)-anion are evidently less stable than the  $\text{Me}_2\text{CO}$  solutions of the same compounds. Namely, in DMF solutions of these complexes, known complexes of a nonelectrolyte type  $[\text{Co}^{\text{III}}(\text{HL})(\text{L})]^{19-21}$  are formed in the course of time, which is accompanied by a change in the colour of the solution from green to brown and by the disappearance of the absorption in the range of 600–700 nm (Fig. 2). Such instability is most pronounced with the  $[\text{Co}^{\text{II}}\text{Br}_3(\text{py})]^-$  ion, which is also evident from its enhanced molar conductivity in comparison with 1:1 type electrolytes (Table I). On the other hand, the molar conductivities of the other complexes are in agreement with their coordination formulas.<sup>22</sup>

The thermal decomposition of all the compounds is continuous. As examples, the TG and DTG curves of selected compounds are presented in Fig. 3. The decomposition pattern does not depend on the gas carrier up to 600 K. In argon, above this temperature the decomposition rate decreases, and the decomposition is not completed up to 1000 K. In air, the decomposition of some compounds is accompanied by burning of the sample. In all cases, the decomposition of the compounds begins with the departure of the pyridine ligand, followed by decomposition of the Schiff base and the end product is cobalt(III) oxide.

The thermal stability of the compounds is about the same and the decomposition begins around 420 K. The highest thermal stability is exhibited by the  $[\text{Co}(\text{L}^1)(\text{py})_3][\text{CoCl}_3(\text{py})]$  complex, which decomposes above 470 K.

In order to propose a decomposition mechanism, the decomposition of  $[\text{Co}(\text{L})(\text{py})_3]\text{I} \cdot 0.5\text{I}_2$  was followed by coupled mass spectrometry up to 600 K. As the first departing group, pyridine and its decomposition products were identified. The decrease in mass supports this proposition not only in the case of the investigated compound but in the cases of other complexes too.

The DSC curves in an inert atmosphere (argon) refer to endothermic decomposition processes.

*Acknowledgement:* This work was supported by the Ministry of Science, Technology and Development of the Republic of Serbia (Grant N° 1318).



## ИЗВОД

КОМПЛЕКСИ ПРЕЛАЗНИХ МЕТАЛА СА ЛИГАНДИМА НА БАЗИ  
 ТИОСЕМИКАРБАЗИДА. ДЕО 46. СИНТЕЗЕ И ФИЗИЧКО-ХЕМИЈСКА  
 КАРАКТЕРИЗАЦИЈА КОБАЛТ(III) КОМПЛЕКСА СА МЕШОВИТИМ  
 ЛИГАНДИМА СЕМИ-, ТИОСЕМИ- И ИЗОТИОСЕМИКАРБАЗОНОМ  
 САЛИЦИЛАЛДЕХИДА И ПИРИДИНОМ

ВУКАДИН М. ЛЕОВАЦ, ЉИЉАНА С. ВОЈИНОВИЋ, КАТАЛИН МЕСАРОШ СЕЧЕЊИ И ВАЛЕРИЈА И  
 ЧЕШЉЕВИЋ

*Дейарџман за хемију, Природно-математички факултет, Универзитет у Новом Саду,  
 Трг Доситеја Обрадовића 3, 21000 Нови Сад*

Реакцијом топлих етанолних раствора соли кобалта(II) и пиридина са семи- $(\text{H}_2\text{L}^1)$ , тиосеми- $(\text{H}_2\text{L}^2)$  и *S*-метилизотиосемикарбазоном салицилалдехида  $(\text{H}_2\text{L}^3)$ , у молском односу 2:5:1, респективно, добијени су октаедарски комплекси кобалта(III), са мешовитим лигандима, опште формуле  $[\text{Co}^{\text{III}}(\text{L})(\text{py})_3]\text{X}$  ( $\text{L} = \text{L}^1$ ,  $\text{X} = [\text{Co}^{\text{II}}\text{Cl}_3(\text{py})]^-$ ,  $\text{ClO}_4^- \cdot \text{H}_2\text{O}$ ,  $\Gamma^- \cdot 0.5 \text{I}_2$ ;  $\text{L} = \text{L}^2$ ,  $\text{X} = [\text{Co}^{\text{II}}\text{Cl}_3(\text{py})]^-$ ,  $[\text{Co}^{\text{II}}\text{Br}_3(\text{py})]^-$ ,  $\text{ClO}_4^- \cdot \text{H}_2\text{O}$ ,  $\text{I}_3^-$ ;  $\text{L} = \text{L}^3$ ,  $\text{X} = [\text{Co}^{\text{II}}\text{Br}_3(\text{py})]^-$ ,  $\text{ClO}_4^- \cdot \text{H}_2\text{O}$ ,  $\text{BF}_4^-$ ). Претпостављена је уобичајена тридентатна (O, N, X ( $\text{X} = \text{O}, \text{S}, \text{N}$ )) координација дианјонске форме хелатних лиганата са меридијалним распоредом донорних атома. Комплекси су окарактерисани подацима елементалне анализе, моларне проводљивости, магнетним мерењима, те IR и електронским апсорпционим спектрима. Термичка разградња комплекса је испитана термогравиметријском и DSC методом, а код одабраног комплекса куплованим TG-MS мерењем.

(Примљено 25. јуна, ревидирано 12. септембра 2003)

## REFERENCES

1. M. J. M. Campbell, *Coord. Chem. Rev.* **15** (1975) 279
2. S. Padhye, G. B. Kauffman, *Coord. Chem. Rev.* **63** (1985) 127
3. J. S. Casas, M. S. Garsia-Tasende, J. Sordo, *Coord. Chem. Rev.* **209** (2000) 197
4. V. M. Leovac, V. I. Češljević, *Coordination Chemistry of Isothiosemicarbazides and their Derivates*, University of Novi Sad, Faculty of Sciences, Novi Sad, 2002
5. D. X. West, S. B. Padhye, P. B. Sonawane, *Struct. Bond.* **76** (1991) 1
6. D. X. West, A. E. Liberta, S. B. Padhye, R. C. Chikate, P. B. Sonawane, A. S. Kumbhar, R. G. Yeranade, *Coord. Chem. Rev.* **123** (1993) 49
7. R. B. Singh, B. S. Garg, R. P. Singh, *Talanta* **25** (1978) 619
8. R. B. Singh, H. Ishii, *Cryst. Rev. Anal. Chem.* **22** (1991) 381
9. T. I. Malinovskii, Yu. A. Simonov, N. V. Gerbeleu, M. A. Yampolskaya, M. D. Revenko, S. G. Shova, *Problemi kristalloghimii*, Nauka, Moskva, 1985, p. 39
10. R. Grobelny, M. Melnik, J. Mrozinski, *Cobalt Coordination Compounds: Classification and Analysis of Crystallographic and Structure Data*, Wroclaw, 1997
11. G. A. Bogdanović, V. B. Medaković, Lj. S. Vojinović, V. I. Češljević, V. M. Leovac, A. Spasojević-de Biré, S. D. Zarić, *Polyhedron* **20** (2001) 2231
12. A. I. Vogel, *A Text-book of Practical Organic Chemistry*, Longman, London 1972, p. 344
13. Gy. Argay, A. Kálmán, B. Ribár, V. M. Leovac, A. F. Petrović, *Monatsch. Chem.* **114** (1983) 1205
14. M. Ferrari Belicchi, G. Gasparri Fava, C. Pelizzi, *Acta Cryst.* **B37** (1981) 924
15. V. Divjaković, V. M. Leovac, B. Ribár, *Acta Cryst.* **B37** (1982) 1738
16. K. Nakamoto, *Infrared and Raman Spectra of Inorganic and Coordination Compounds*, Wiley-Interscience, New York, 1997
17. F. A. Cotton, G. Wilkinson, *Advanced Inorganic Chemistry*, Wiley-Interscience, New York, 1998

18. A. B. Lever, *Inorganic Electronic Spectroscopy*, Elsevier, Amsterdam, 1984
19. N. M. Samus, V. G. Chebanu, *Zh. Neorg. Khim.* **15** (1970) 2182
20. A. V. Ablov, N. V. Gerbeleu, *Zh. Neorg. Khim.* **9** (1964) 2325
21. V. M. Leovac, N. V. Gerbeleu, V. D. Canić, *Zh. Neorg. Khim.* **27** (1982) 918
22. W. J. Geary, *Coord. Chem. Rev.* **7** (1971) 81.

**Transition metal complexes with thiosemicarbazide-based ligands. Part 47. Synthesis, physicochemical and voltammetric characterization of iron(III) complexes with pyridoxal semi-, thiosemi- and *S*-methylisothiosemicarbazones**

VIOLETA S. JEVTIČIĆ, LJILJANA S. JOVANOVIĆ<sup>#</sup>, VUKADIN M. LEOVAC<sup>\*#</sup> and LUKA J. BJELICA<sup>#</sup>

*Faculty of Science, University of Novi Sad, Trg D. Obradovića 3, 21000 Novi Sad, Serbia and Montenegro*

(Received 14 July 2003)

**Abstract:** The reaction of warm EtOH solutions of  $\text{FeX}_3 \cdot n\text{H}_2\text{O}$  ( $\text{X} = \text{Cl}, \text{NO}_3$ ) with tridentate ONX ( $\text{X} = \text{O}, \text{S}, \text{N}$ ) pyridoxal semi-, thiosemi- and *S*-methylisothiosemicarbazones ( $\text{H}_2\text{L}^1$ ,  $\text{H}_2\text{L}^2$ ,  $\text{H}_2\text{L}^3$ , respectively) yielded high-spin octahedral mono- and bis(ligand) complexes of the formula  $[\text{Fe}(\text{H}_2\text{L}^{1-3})\text{Cl}_2(\text{H}_2\text{O})]\text{Cl}$ ,  $[\text{Fe}(\text{HL}^{1,2})_2]\text{Cl} \cdot n\text{H}_2\text{O}$  and  $[\text{Fe}(\text{H}_2\text{L}^3)(\text{HL}^3)](\text{NO}_3)_2 \cdot \text{H}_2\text{O}$ . The compounds were characterized by elemental analysis, conductometric and magnetochemical measurements, IR and UV-Vis spectra. Besides, a detailed voltammetric study of the complexes was carried out in DMF solution in the presence of several supporting electrolytes, to characterize the nature of the electrode processes and solution equilibria.

**Keywords:** iron(III) complexes, pyridoxal semi-, thiosemi- and isothiosemicarbazones, physicochemical and voltammetric studies.

INTRODUCTION

Transition metal complexes with Schiff bases derivatives of pyridoxal, *e.g.* 3-hydroxymethyl-2-methylpyridine-4-carboxaldehyde (one of the forms of vitamin B<sub>6</sub>), amines and amino acids, are the subject of strong interest for many researchers.<sup>1–5</sup> The reason for this lies in the fact that these compounds can serve as models for studying a wide range of biological reactions catalyzed by enzymes in which pyridoxal phosphate appears as an essential component.<sup>1–3</sup> It has been shown that, in the presence of metal ions, free pyridoxal can catalyze most of the known enzymatic reactions in which pyridoxal phosphate acts as a co-enzyme.<sup>1,6</sup>

A special group of Schiff bases pyridoxal derivatives as ligands are the tridentate semi-, thiosemi- and isothiosemicarbazones ( $\text{H}_2\text{L}^1$ ,  $\text{H}_2\text{L}^2$  and  $\text{H}_2\text{L}^3$ , respec-

<sup>#</sup> Serbian Chemical Society active member.

<sup>\*</sup> Corresponding author.

tively) (Fig. 1). In contrast to the metal complexes with pyridoxal thiosemicarbazones, the study of which began in 1986, so that a substantial number of complexes not only with transition but also with non-transition metals have been synthesized,<sup>7–9</sup> complexes with pyridoxal semi- and isothiosemicarbazones appeared much later. Namely, in our previous works,<sup>10–12</sup> the syntheses and some physicochemical and structural characteristics of the complexes of Cu(II) and Pt(IV) with  $H_2L^1$ , and Cu(II) complexes with  $H_2L^3$  were described.

In continuation of our studies on the complexing properties of these ligands, the syntheses and some physicochemical and voltammetric characteristics of their iron(III) complexes are described in this paper.

## EXPERIMENTAL

### *Chemicals and methods*

All chemicals used were commercially available products of analytical reagent grade. The exceptions were the ligands  $H_2L^1 \cdot 2H_2O$ ,  $H_2L^2 \cdot 3H_2O$ ,  $H_2L^3 \cdot H_2O$  and complex  $[Fe(HL^2)_2]Cl$ , which were synthesized following previously described procedures.<sup>7,10–13</sup>

*Elemental (C, H, N) analysis* of air-dried samples was carried out by standard micromethods in the Centre for Instrumental Analysis, Faculty of Chemistry, Belgrade.

*Magnetic susceptibility* measurements were made at room temperature using a magnetic susceptibility balance MSB-MKL (Sherwood Scientific Ltd., Cambridge, England). The data were corrected for diamagnetic susceptibilities.

*Molar conductivities* of freshly-prepared  $1 \times 10^{-3}$  M solution were measured on a Jenway 4010 conductivity meter.

*IR-spectra* (KBr disc) were recorded using a Perkin-Elmer FTIR 31725X.

*Electronic spectra* were recorded in DMF solutions (Merck, spectroscopic grade) on the Secomam instrument (Anthelie 2, advanced).

*Voltammetric experiments* were performed in freshly distilled DMF solutions. The salts serving as supporting electrolytes (tetrabutylammonium perchlorate, TBAP, and lithium perchlorate and chloride) were used after recrystallization, usually at a concentration of 0.1 M. The ligands and complexes were dried at 120–140 °C and 1 mM solutions were thoroughly purged with nitrogen. An AMEL three-electrode voltammetric set-up was used together with a Hewlett Packard X-Y recorder and a storage oscilloscope for recording the voltammograms. A glassy carbon (3 mm diameter) disc (the working electrode) was coupled to a Pt wire (counter electrode) and an aqueous calomel electrode (SCE, reference electrode) connected to the working solution *via* a salt bridge. The potentials, referred to SCE, were frequently checked with ferrocene as an internal standard.

Since most of the complexes and ligands, and especially the products of electrochemical reactions exhibited strong adsorption, the GC electrode surface had to be frequently polished with a fine alumina suspension, in some cases before each scan. The experiments were performed in the range of scan rates from 10 mV s<sup>-1</sup> to 10 V s<sup>-1</sup>.

### *Preparation of the protonated forms of the ligands and complexes*

$H_2L^{1,2} \cdot HCl \cdot H_2O$ . To a mixture of pyridoxal hydrochloride (10 mmol, Aldrich) and semicarbazide hydrochloride (10 mmol, Aldrich), *i.e.*, thiosemicarbazide hydrochloride (10 mmol, Merck), water (10 cm<sup>3</sup>) was added and the mixture heated to complete dissolution of the reactants. After 10 h, the precipitated yellowish needle-like crystals were separated by filtration and washed with EtOH. Yield: 86 and 68 %, respectively.

$[Fe(H_2L^{1-3})Cl_2(H_2O)]Cl$ . To a warm suspension of the neutral forms of the ligands (1 mmol) in EtOH (10 cm<sup>3</sup>),  $FeCl_3 \cdot 6H_2O$  (1 mmol) was added and the mixture heated to complete dissolution of the ligand. The brown solution was left for 20 h at room temperature. The brown crystals which formed were filtered and washed with EtOH. Yield: 62, 87 and 69 %, respectively.

$[Fe(HL^1)_2]Cl \cdot 4H_2O$ . To 0.26 g (1 mmol) of  $H_2L^1 \cdot 2H_2O$  in EtOH (10 cm<sup>3</sup>) was added 0.14 g (0.5 mmol) of  $FeCl_3 \cdot 6H_2O$  and the mixture heated to complete dissolution of the ligand. Then, 0.06 g (1 mmol) of LiOAc was added to the brown solution and dissolved by heating. The brown-black glittering crystals which formed in the course of 50 h were filtered and washed with EtOH. Yield: 0.14 g (46 %).

$[Fe(HL^2)_2]Cl$ . The complex was synthesized according to the previously described procedure.<sup>13</sup>

$[Fe(H_2L^3)(HL^3)](NO_3)_2 \cdot H_2O$ . A mixture of 0.20 g (0.5 mmol) of  $Fe(NO_3)_3 \cdot 9H_2O$ , 0.14 g (0.5 mmol) of  $H_2L^3 \cdot H_2O$  and 0.05 g of LiOAc was dissolved with heating in EtOH (10 cm<sup>3</sup>). The warm brown solution was filtered and left at room temperature for 50 h. The black crystals were filtered and washed with EtOH. Yield: 0.14 g (79 %).

## RESULTS AND DISCUSSION

### *Synthesis, general physicochemical characteristics and geometrical configuration of the complexes*

Until now, the only known complexes of iron with the mentioned ligands were the complexes  $[Fe(HL^2)_2]Cl \cdot nH_2O$  ( $n = 0, 2$ )<sup>13</sup> and  $[Fe(HL^2)Cl_2]$ .<sup>14</sup> The data of elemental analysis and some physico-chemical characteristics of the newly-synthesized iron complexes with  $H_2L^1$  and  $H_2L^3$  in general, as well as of the novel mono(ligand) complex with  $H_2L^2$  are given in Table I. Taking into account these results and those of the previously known complex  $[Fe(HL^2)_2]Cl$ , it can be concluded that all the three ligands form both mono- and bis(ligand) complexes with Fe(III). The mono(ligand) complexes considered in this work, whose composition can be described by the general formula  $Fe(H_2L)Cl_3 \cdot H_2O$ , were obtained in a good yield by the reaction of warm EtOH solutions of  $FeCl_3 \cdot 6H_2O$  and the ligands in a mole ratio of 1:1. It should be pointed out that complexes of analogous composition were obtained with  $H_2L^1$  and  $H_2L^2$ , *i.e.*, with the neutral forms of the ligands, and in the case of the reaction of  $FeCl_3 \cdot 6H_2O$  with their protonated forms  $H_3L^+$ . Also, it is important to emphasize that the previously known  $[Fe(HL^2)Cl_2]$  complex,<sup>14</sup> involving the once-deprotonated form of the ligand, was synthesized starting from  $FeCl_2$ , and that, despite performing the reaction in a nitrogen atmosphere, the result was an iron(III) complex.

Bis(ligand) monocationic  $[Fe(HL^1)_2]Cl \cdot 4H_2O$  and dicationic  $[Fe(H_2L^3)(HL^3)](NO_3)_2 \cdot H_2O$  complexes, were also obtained in the reaction of EtOH solutions of the ligands with the corresponding iron(III) salt in the respective mole ratios 2:1 and 1:1 after partial neutralization (LiOAc) of the reaction solution. To our knowledge, the obtained cationic complex with  $H_2L^3$ , containing both the neutral and once-deprotonated forms of the ligand, represents the first Fe(III) complex with this charge with a diprotic tridentate Schiff base. The previously known  $[Fe(HL^2)_2]Cl$ ,<sup>13</sup> whose voltammetric behaviour is also included here, was obtained by the reaction of anhydrous  $FeCl_3$  and  $H_2L^2$  in absolute EtOH.

On the basis of the conditions of synthesis of all three bis(ligand) complexes, it can be concluded that the deprotonation of  $H_2L^2$  is the easiest and that of  $H_2L^3$  the hardest. From the structures of these ligands (Fig. 1) it is evident that the phenolic

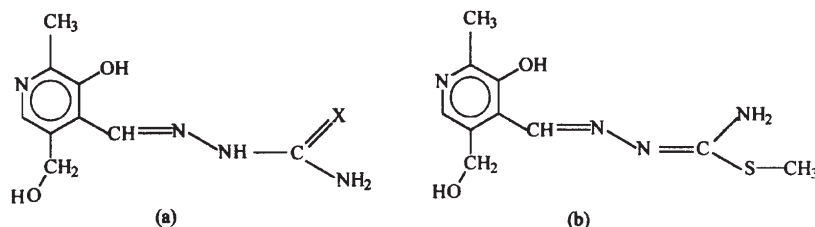


Fig. 1. Structural formulas of pyridoxal semi/thiosemicarbazones ( $X = O \rightarrow H_2L^1$ ,  $X = S \rightarrow H_2L^2$ ) (a) and *S*-methylisothiosemicarbazone ( $H_2L^3$ ) (b).

hydroxyl and enol/thiol form of  $H_2L^1/H_2L^2$ , *i.e.*, isothioamide group of  $H_2L^3$ , can be deprotonated.

The results of X-ray structural analysis<sup>14,15</sup> of the complex with the once-deprotonated form of  $H_2L^2$  show that this form of the ligand results from deprotonation of the thiol form of the thiosemicarbazide moiety, whereby the pyridoxal fragment is in the form of a zwitter ion, *i.e.*, the pyridine nitrogen is protonated on account of the deprotonation of the phenolic hydroxyl. Further deprotonation (the pyridine nitrogen) yields the dianionic form of the ligand.<sup>16</sup> There is no doubt that an analogous deprotonation sequence also holds for the other two ligands. Such a deprotonation sequence is the consequence of the strong basicity of the pyridine nitrogen, which explains the zwitter-ionic nature of not only the coordinated but also the uncoordinated  $H_2L^2$  ligand.<sup>7</sup>

The occurrence of one or more bands of different intensity at *ca.* 2800  $\text{cm}^{-1}$ , belonging to the  $\nu(\text{NH}^+)$  vibrations of the protonated pyridine nitrogen,<sup>7</sup> in the IR spectra of both the coordinated and uncoordinated ligand in the complexes is proof of the zwitter-ionic form of both.

X-Ray structural analyses of a number of complexes of various metals with the  $H_2L^2$  ligand,<sup>14–17</sup> as well as of Cu(II) complexes with the other two ligands,<sup>10,11</sup> showed that all three ligands are coordinated as a tridentate entity. Thus, two donor atoms are the same – the phenolic oxygen and the hydrazinic nitrogen N(1). The third donor atom in the case of  $H_2L^1$  and  $H_2L^2$  is the oxygen or sulphur of the amide or thioamide group,  $-\text{C}(-\text{NH}_2) = \text{X}$  ( $X = \text{O}, \text{S}$ ), respectively, whereas the third donor atom in the case of  $H_2L^3$  is the nitrogen of the isothioamide group,  $=\text{C}(-\text{NH}_2)-\text{SCH}_3$ . In all cases, one six-membered (pyridoxal) and one five-membered (semi/thiosemi/isothiosemicarbazide) metallocycles are formed. Most probably, such a mode of coordination of these ligands is also realized in all the obtained complexes with iron(III), which has been confirmed by X-ray structural analysis<sup>18</sup> in the case of the complexes with  $H_2L^1$  and  $H_2L^2$ .

Simultaneously, these analyses showed that the mentioned two complexes have, apart from one molecule of the tridentate ONX ( $X = \text{O}, \text{S}$ ) ligand, also an octahedral configuration formed by coordination of two chloride ions and one molecule of water. Probably, the  $\text{Fe}(\text{H}_2\text{L}^3)\text{Cl}_3 \cdot \text{H}_2\text{O}$  complex also has such a structure, *i.e.*, in addition to the organic ONN ligand there are two chloro- and one aqua-ligand. That one water

molecule is coordinated is also indicated by its relatively high temperature of evolution ( $\approx 150^\circ\text{C}$ ), at which temperature the other two complexes are also dehydrated. It should be noticed that the previously synthesized  $[\text{Fe}(\text{HL}^2)\text{Cl}_2]$  has a square-pyramidal structure.<sup>14</sup>

All three mono(ligand) complexes are well soluble in  $\text{H}_2\text{O}$  and DMF and somewhat less soluble in MeOH and EtOH. Their stability in  $\text{H}_2\text{O}$  and MeOH solutions are markedly different, which is also evident from the values of their molar conductivities  $\lambda_{\text{M}}$  (Table I). Namely, the  $\lambda_{\text{M}}$  values of their MeOH solutions are in the range of  $124\text{--}150\text{ S cm}^2\text{ mol}^{-1}$ , *i.e.*, between the  $\lambda_{\text{M}}$  values for 1:1 and 1:2 types of electrolytes,<sup>19</sup> whereas the  $\lambda_{\text{M}}$  values of the aqueous solutions correspond to those of a 1:3 type of electrolytes (for the  $\text{H}_2\text{L}^1$  and  $\text{H}_2\text{L}^3$  complexes) or to a 1:5 type of electrolyte ( $\text{H}_2\text{L}^2$  complex).<sup>20</sup> This means that in methanolic solution, partial replacement of the coordinated chloride ions by solvent molecules occurs, the replacement in aqueous solution being complete. The extremely high value of  $\lambda_{\text{M}}$  of aqueous solutions of the  $\text{H}_2\text{L}^2$  complex could also be explained by the formation of the very mobile  $\text{H}_3\text{O}^+$  ion as a consequence of the deprotonation of the thiosemicarbazide fragment. In view of the fact that the  $\lambda_{\text{M}}$  value of the aqueous solutions of the other two complexes is at the upper limit of the  $\lambda_{\text{M}}$  range of values for a 1:3 type of electrolyte, it is possible that the same phenomenon is also involved, but at a lower concentration of  $\text{H}_3\text{O}^+$  ion. All these observations are in agreement with the previous supposition that deprotonation of  $\text{H}_2\text{L}^2$  is the easiest and that of  $\text{H}_2\text{L}^3$  the hardest, which corresponds to the trend of decreasing  $\lambda_{\text{M}}$  values of the corresponding complexes.

TABLE I. Some physical characteristics and analytical data of the newly synthesized compounds

Ligands/Complex	Found (Calcd)/%			$\mu_{\text{eff}}^*/\mu_{\text{B}}$	$\lambda_{\text{M}}^{**}/\text{S cm}^2\text{ mol}^{-1}$ (solvent)
	C	H	N		
$\text{H}_2\text{L}^1\cdot\text{HCl}\cdot\text{H}_2\text{O}$	39.80 (39.48)	5.80 (5.43)	19.86 (20.11)	—	126 ( $\text{H}_2\text{O}$ )
$\text{H}_2\text{L}^2\cdot\text{HCl}\cdot\text{H}_2\text{O}$	37.28 (36.67)	5.27 (5.13)	19.19 (19.01)	—	162 ( $\text{H}_2\text{O}$ )
$[\text{Fe}(\text{H}_2\text{L}^1)\text{Cl}_2(\text{H}_2\text{O})]\text{Cl}$	26.66 (26.73)	3.59 (3.49)	13.76 (13.86)	5.44	467 ( $\text{H}_2\text{O}$ ) 124 (MeOH)
$[\text{Fe}(\text{H}_2\text{L}^2)\text{Cl}_2(\text{H}_2\text{O})]\text{Cl}$	25.32 (25.70)	3.41 (3.36)	13.52 (13.33)	5.34	580 ( $\text{H}_2\text{O}$ ) 150 (MeOH)
$[\text{Fe}(\text{H}_2\text{L}^3)\text{Cl}_2(\text{H}_2\text{O})]\text{Cl}$	27.74 (27.64)	3.81 (3.71)	12.62 (12.90)	6.01	420 ( $\text{H}_2\text{O}$ ) 136 (MeOH)
$[\text{Fe}(\text{HL}^1)_2]\text{Cl}\cdot 4\text{H}_2\text{O}$	35.46 (35.45)	4.81 (4.16)	18.25 (18.38)	5.29	78 (MeOH)
$[\text{Fe}(\text{H}_2\text{L}^3)(\text{HL}^3)](\text{NO}_3)_2\cdot\text{H}_2\text{O}$	34.42 (34.64)	4.42 (4.15)	19.82 (19.86)	4.43	143 (MeOH)

\* At  $23^\circ\text{C}$ ; \*\*  $c = 1\text{ mM}$



As far as the bis(ligand) complexes are concerned, there is no doubt that they have an octahedral configuration in which, because of its planarity, the ligands assume *mer*- positions. As with mono(ligand) complexes, they are also well soluble in H<sub>2</sub>O and DMF (with exception of the H<sub>2</sub>L<sup>2</sup> complex) and less soluble in MeOH and EtOH. The molar conductivities of their MeOH solutions are in full agreement with the proposed coordination formulas.

With the exception of [Fe(H<sub>2</sub>L<sup>3</sup>)Cl<sub>2</sub>(H<sub>2</sub>O)]Cl (Table I) and [Fe(HL<sup>2</sup>)<sub>2</sub>]Cl,<sup>13</sup> which have  $\mu_{\text{eff}}$  values characteristic of pure high-spin Fe(III) complexes, the other complexes have somewhat lower  $\mu_{\text{eff}}$  values, which could be explained in terms of the “admixture” of low-spin complexes. In relation to this, it is important to mention that there are literature data<sup>21</sup> about Fe(III) complexes, mainly with the tridentate thiosemicarbazones, the spin state of which depends even on the outer-sphere ion, as well as on the number of molecules of crystalline water. An example of this is just the [Fe(HL<sup>2</sup>)<sub>2</sub>]Cl complex, which at room temperature is high-spin ( $\mu_{\text{eff}}$  = 5.75  $\mu_{\text{B}}$ ), while its dihydrate is low-spin ( $\mu_{\text{eff}}$  = 2.05  $\mu_{\text{B}}$ ).<sup>13</sup>

#### Electronic spectra

The spectra of the neutral and protonated forms of the ligands were recorded over the available region in DMF, from 270 to 800 nm, as well in the presence of LiCl (serving as supporting electrolyte in the voltammetric measurements). The spectra of the complexes were also recorded under similar conditions, and the characteristic parameters are given in Table II.

TABLE II. Electronic spectral data for the ligands and complexes in DMF

Compound	$\lambda_{\text{max}}^{\text{a}}$ ( $\epsilon^{\text{b}}$ )
H <sub>2</sub> L <sup>1</sup> ·2H <sub>2</sub> O	290(1.79); 329(0.77 <i>sh</i> <sup>c</sup> )
H <sub>2</sub> L <sup>1</sup> ·HCl·H <sub>2</sub> O	306(1.40 <i>sh</i> ); 321(1.47); 339(1.45)
H <sub>2</sub> L <sup>2</sup> ·3H <sub>2</sub> O	284(1.04); 333(2.10)
H <sub>2</sub> L <sup>2</sup> ·HCl·H <sub>2</sub> O	321(1.38); 349(1.43); 361(1.39 <i>sh</i> )
H <sub>2</sub> L <sup>3</sup> ·H <sub>2</sub> O	325(2.81 <i>bp</i> <sup>d</sup> ); 352(2.69); 365 (2.39 <i>sh</i> )
[Fe(H <sub>2</sub> L <sup>1</sup> )Cl <sub>2</sub> (H <sub>2</sub> O)]Cl	291(1.92); 355(1.20)
[Fe(H <sub>2</sub> L <sup>2</sup> )Cl <sub>2</sub> (H <sub>2</sub> O)]Cl	320(1.82); 356(1.97); 442(0.48 <i>sh</i> )
[Fe(H <sub>2</sub> L <sup>3</sup> )Cl <sub>2</sub> (H <sub>2</sub> O)]Cl	323(1.72); 353(1.72); 367(1.73); 404(1.17 <i>sh</i> )
[Fe(HL <sup>1</sup> ) <sub>2</sub> ]Cl·4H <sub>2</sub> O	282(2.71); 348(1.40)
[Fe(HL <sup>2</sup> ) <sub>2</sub> ]Cl	326(3.53); 351(3.66); 438(0.73 <i>sh</i> )
[Fe(H <sub>2</sub> L <sup>3</sup> )(HL <sup>3</sup> )](NO <sub>3</sub> ) <sub>2</sub> ·H <sub>2</sub> O	316(1.65 <i>sh</i> ); 327(1.72); 351(1.72); 367(1.73)

<sup>a</sup>In nm. <sup>b</sup>In M<sup>-1</sup> cm<sup>-1</sup> × 10<sup>-4</sup>. <sup>c</sup>Shoulder. <sup>d</sup>Broad peak.

The spectra of all three ligands are characterized by 2–3 bands in the range of 270–450 nm. The difference in the spectral patterns is due to the structural differ-

ences of the compounds. As could be expected, the addition of LiCl to the ligand solutions caused no significant changes in their spectra. Ligand protonation, however, resulted in a decrease of the absorption at  $\lambda < 360$  nm, with the simultaneous appearance of new bands characteristic of the absorption of  $\text{H}_3\text{L}^+$  and  $\text{H}_4\text{L}^{2+}$  species in the range of 315–400 nm.

The spectra of all the ligands of the type  $\text{H}_2\text{L}$  and  $\text{H}_2\text{L}\cdot\text{HCl}$  protonated to the same extent by adding  $\text{HClO}_4$  ( $> 2\text{H}^+/\text{ligand}$ ) have similar characteristics. The protonated  $\text{H}_2\text{L}^2$  and  $\text{H}_2\text{L}^3$  exhibit similar absorption, while the spectrum of the semicarbazone derivative is different, suggesting a different nature of the chromophore.

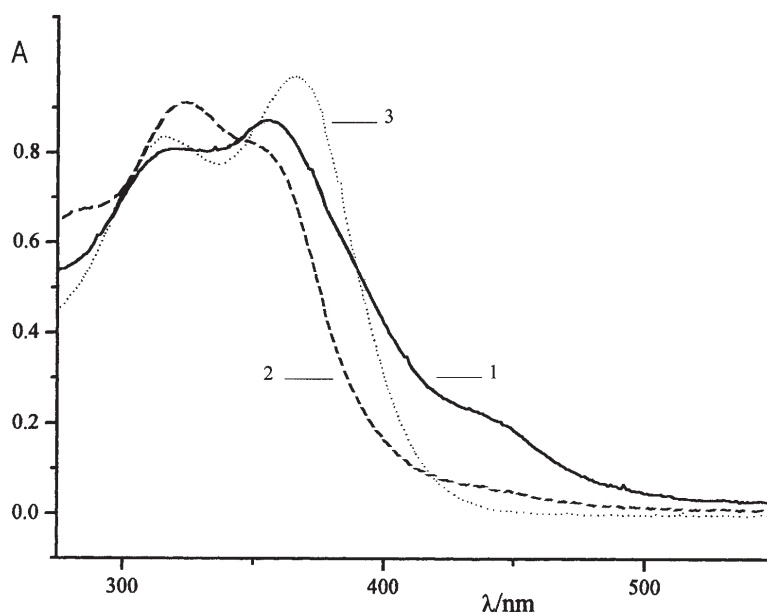


Fig. 2. Electronic spectra of  $[\text{Fe}(\text{H}_2\text{L}^2)\text{Cl}_2(\text{H}_2\text{O})]\text{Cl}$  in DMF: pure solvent (1) and after the addition of 0.1 M LiCl (2) and  $\text{HClO}_4$  to the mole ratio  $2 \text{H}^+/\text{Fe}$  (3).

The complexes absorb in the range of 270–600 nm, the appearance of a particular spectrum depending mainly on the coordinated ligand. A common characteristic of all these spectra is the absence of bands that could be ascribed to  $d-d$  transitions (Fig. 2). The band at  $\lambda < 400$  nm corresponds to the absorption of the ligand part of the molecule ( $\pi \rightarrow \pi^*$ ), which is evident from the absorption of the ligand itself, especially with the  $\text{H}_2\text{L}^1$  complexes. This means that the bonds in the Fe(III) complex with this ligand are weakest, which was also confirmed by voltammetric experiments.

The addition of LiCl to a solution of a complex changes the appearance of the absorption curve, which becomes more similar to the spectrum of the ligand itself, suggesting a partial dissociation of the molecule (Fig. 2, curve 2). This was also confirmed by the disappearance of the charge-transfer bands ( $\lambda > 400$  nm) in the spectra of all the complexes. On addition of  $\text{HClO}_4$  to a mole ratio of (2–3)  $\text{H}^+/\text{Fe}$ ,

the resulting spectra have two characteristic bands at somewhat different wavelengths (in the region of 305–332 and 340–390 nm), depending on the nature of the complex. Moreover, the bands correspond to those obtained under the same conditions for a solution of the corresponding protonated ligand. Hence, the protonation product could be represented as  $H_4L^{2+}$ , whereby the protonation sites may be the phenolic oxygen and one of the nitrogen atoms of the hydrazine moiety.

#### *Voltammetric studies*

In view of the experience gained in studying Fe(III) complexes with similar ligands – salicylaldehyde semi-, thiosemi and *S*-methylisothiosemicarbazone in DMF,<sup>22–24</sup> it was interesting to study the behaviour of the new complexes under the same conditions.

A marked characteristic of the newly synthesized mono(ligand) and bis(ligand) complexes of the cationic type is their pronounced dissociation in DMF, especially in the presence of chloride. In contrast to this, the previous series of complexes, being stable enough, was characterized by well-defined cyclic voltammograms. The reaction of the new complexes taking place in the presence of LiCl is accompanied by a visual change in their colour from brown to ruby-red and a spectrum characterizing the absorption of the displaced ligand.

For the sake of legibility the results will be presented according to the complex type with reference to specific features of a particular coordinated ligand.

#### *Mono(ligand) complexes*

The previously studied complexes of this type with salicylaldehyde derivatives as ligands behaved as coordination dimers  $[Fe(HL)_2][FeCl_4]$ , dissociating in DMF into equimolar amounts of  $[Fe(HL)]^{2+}$ ,  $[FeCl_4]^-$  and  $(HL^-)$ .<sup>22</sup> In contrast to them, the new ligands, coordinated as neutral molecules, give unstable  $[Fe(H_2L)]^{3+}$  complexes, dissociating almost completely to Fe(III) and  $H_2L$ .

The appearance of the cyclic voltammogram for  $[Fe(H_2L^3)Cl_2(H_2O)]Cl$  recorded in TBAP, as the least “aggressive” medium, is presented in Fig. 3. The reduction peaks, observed at three potential amplitudes (to  $-1.0$  V), belong to one-electron processes, the first for  $FeCl_4^-$ , then that for  $Fe(HL^3)^{2+}$  with perchlorate/chloride in the coordination sphere. The two most negative peaks represent the reduction of  $H_2L^3$ , occurring on the pyridoxal and hydrazine fragment, respectively. The reduced complexes also exhibit instability:  $[FeCl_4]^{2-}$  dissociates rapidly to  $FeCl_2$  and  $Fe(ClO_4)_2$ , which are oxidized in two close peaks at about  $0.0$  V.<sup>22</sup>

Oxidation of the complexes (in the amplitude range from  $+0.6$  to  $+1.6$  V) is represented by 2–3 multi-electron peaks involving processes on the ligand part, followed by decomposition of the molecule. The detailed electrochemistry of the ligand will be described in a subsequent paper.<sup>25</sup>

*LiClO<sub>4</sub>.* The addition of  $LiClO_4$  to the solution of these complexes results in changes of the voltammogram in the part corresponding to ligand reduction, the

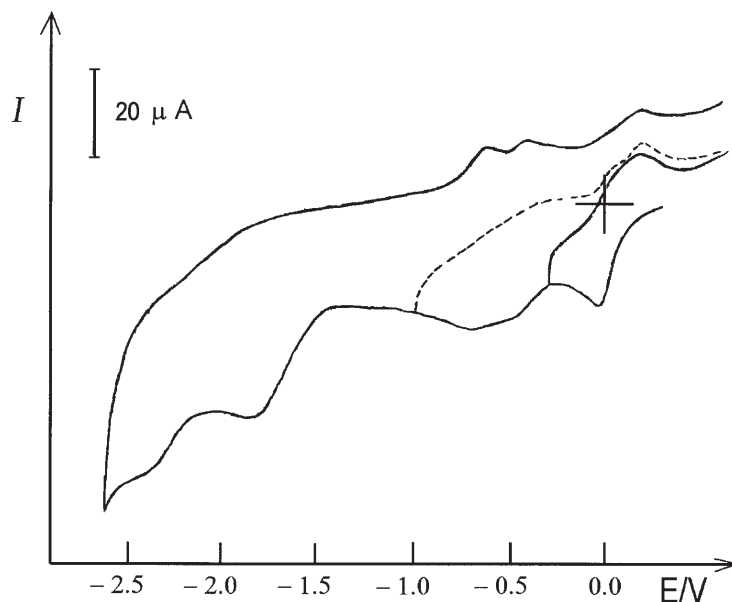


Fig. 3. Cyclic voltammograms for  $[\text{Fe}(\text{H}_2\text{L}^3)\text{Cl}_2(\text{H}_2\text{O})]\text{Cl}$  in 0.1 M TBAP;  $0.20 \text{ V s}^{-1}$ .

cathodic peaks being shifted to more positive potentials, overlapping thus with the first peak. This effect is probably a consequence of ion-pairing of  $\text{Li}^+$  and the product of the multielectron reduction of the ligand.<sup>22</sup>

*LiCl*. The voltammogram of the mono(ligand) complex (Fig. 4) shows that excess of  $\text{Cl}^-$  stabilizes the reaction of  $\text{FeCl}_4^-$ , yielding a pair of quasi-reversible peaks

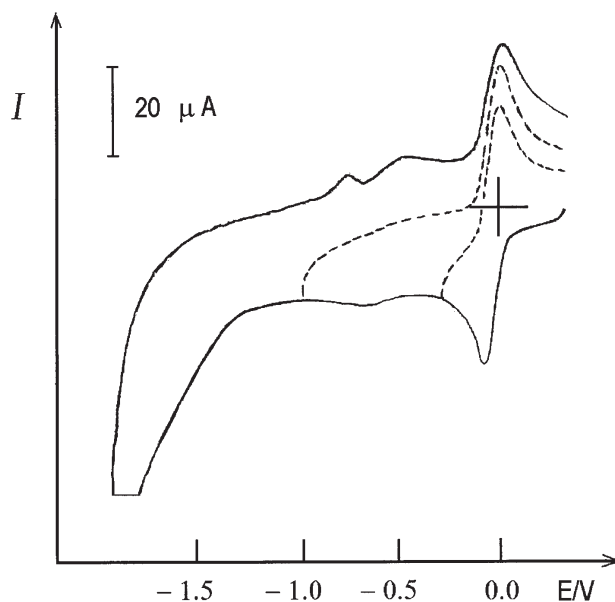


Fig. 4. Cyclic voltammograms for  $[\text{Fe}(\text{H}_2\text{L}^3)\text{Cl}_2(\text{H}_2\text{O})]\text{Cl}$  in 0.1 M LiCl;  $0.20 \text{ V s}^{-1}$ .

at  $E_p^c = -0.08$  V. The current corresponding to this peak is approximately equivalent to the total Fe(III) content, which is also evident from the voltammogram, in which the peak current for  $\text{Fe}(\text{HL}^3)^{2+}$  ( $E_p^c = -0.68$  V) does not exceed 10–20 %. At potentials more negative than  $-1.5$  V, partial overlap of several reduction processes at the ligand is observed. The electron transfer processes are followed by irreversible chemical reactions whereby the complex decomposes into several species with marked tendency of adsorption (*e.g.*, the oxidative peak at  $-0.8$  V).

#### *Bis(ligand) complexes*

**Monocationic complexes.** Complexes of this type, represented in the crystalline state by the formulas  $[\text{Fe}(\text{HL}^1)_2]\text{Cl}$  and  $[\text{Fe}(\text{HL}^2)_2]\text{Cl}$ , dissociate in DMF solution into several complex species. Another problem is the very poor solubility of the  $\text{H}_2\text{L}^2$  complex – complete dissolution at a level of 1 mM required 3 h.

**TBAP and  $\text{LiClO}_4$ .** Both the investigated complexes in these two electrolytes (Fig. 5, curve 1) behave in basically the same way to a potential of  $-1.60$  V: 2–3 reduction peaks with  $E_p^c > -0.7$  V are characteristic of the different Fe(III)-containing species. The dominant peak at  $-0.05$  V belongs to  $\text{FeCl}_4^-$  and contains about 30 % of the total iron(III) in the case of the  $\text{H}_2\text{L}^1$  and about 50 % in the case of the  $\text{H}_2\text{L}^2$  complexes (determined after protonation, *vide infra*). In the potential region more negative than  $-1.4$  V, the free ligand is reduced in an irreversible one-electron process. However, the peak is actually composed of two peaks of similar potentials ( $\Delta E_p^c < 150$  mV), the more positive of which is supposed to belong to the residual

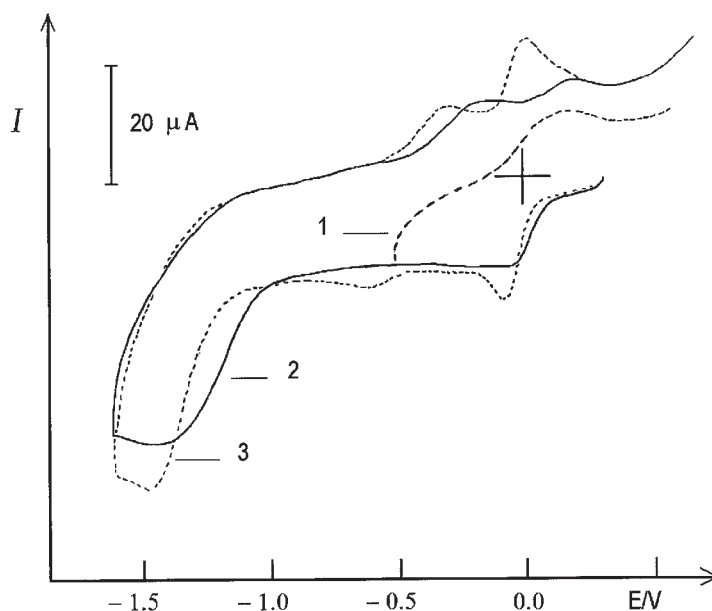


Fig. 5. Cyclic voltammograms for  $[\text{Fe}(\text{HL}^2)_2]\text{Cl}$  in 0.1 M  $\text{LiClO}_4$  – narrow (1) and broad (2) amplitude and after the addition of 0.1 M  $\text{LiCl}$  (3);  $0.20 \text{ V s}^{-1}$ .

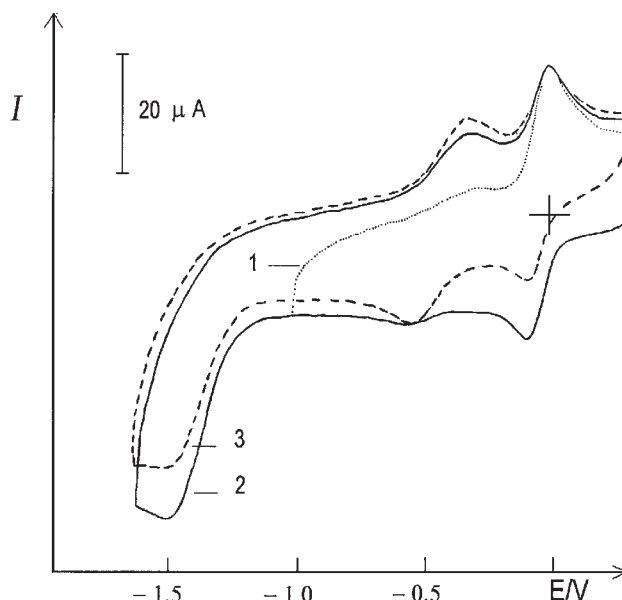


Fig. 6. Cyclic voltammograms for  $[\text{Fe}(\text{HL}^2)_2]\text{Cl}$  in 0.1 M LiCl: 1st sweep, narrow (1) and broad (2) amplitude; 2nd sweep (3) at  $0.20 \text{ V s}^{-1}$ .

undissociated bis(ligand) complex and the more negative one represents the irreversible one-electron reduction of the free ligand.

In TBAP, a further ligand reduction is represented by two peaks at  $-1.9$  and  $-2.2 \text{ V}$ , corresponding to a process on the thiosemicarbazide moiety.<sup>26</sup> However, the two processes merge in  $\text{LiClO}_4$ , as described for the mono(ligand) complexes. Ligand oxidation, up to  $+1.5 \text{ V}$ , proceeds in three partially overlapped peaks, after which the complex decomposes into  $\text{Fe(III)}$  and the products of chemical reactions on the free ligand.

*LiCl.* The voltammetric behaviour of the complexes in this electrolyte is better defined (Fig. 5, curve 3). In addition to the dominant reduction peak of  $\text{FeCl}_4^-$ , containing about 70 % of the total iron(III), there is a peak with  $E_p^c = -0.56 \text{ V}$ , corresponding to the reduction of  $[\text{Fe}(\text{HL}^2)]^{2+}$ . The irreversible one-electron peak at  $-1.47 \text{ V}$  represents the reduction of free ligand. Further reduction in this electrolyte occurs in one multielectron peak formed by the overlapping of the two previous peaks, the processes taking place on the thiosemicarbazide fragment. Besides, in the same potential range ( $< -2.0 \text{ V}$ ),  $\text{Fe(II)}$  is reduced to  $\text{Fe(0)}$ .<sup>26</sup>

A certain insight into the fine equilibria between the  $(\text{HL}^2)^-$  and  $\text{Cl}^-$  complexes of  $\text{Fe(III)}$  and  $\text{Fe(II)}$  can be gained by considering the voltammograms obtained after repetitive cycling in the working potential amplitude (Fig. 6). It is evident that a potential excursion to include the reduction of the ligand results in an increase of the oxidation peak for  $\text{Fe}(\text{HL}^2)^+$  ( $E_p^a \approx -0.30 \text{ V}$ ) on account of a decrease of the peak for  $\text{FeCl}_2$  ( $E_p^a = +0.02 \text{ V}$ ). This ratio of concentrations of the complex

species, altered in comparison with the initial one, is evident from the second sweep (curve 3), amounting almost to 1:1 for the chloride and  $(\text{HL}^2)^-$  complexes. Such behaviour provokes the conclusion that in contrast to Fe(III), which exhibits high affinity toward  $\text{Cl}^-$ , Fe(II) shows a greater stability in the  $\text{Fe}(\text{HL}^2)^+$  complex.

*Dicationic complex.* The complex  $[\text{Fe}(\text{H}_2\text{L}^3)(\text{HL}^3)](\text{NO}_3) \cdot \text{H}_2\text{O}$ , like the analogous semicarbazone compound, already dissociates to a large extent in the presence of an inert electrolyte, the dissociation into  $\text{FeCl}_4^-$  and  $\text{H}_2\text{L}^3$  being practically complete in the presence of excess  $\text{Cl}^-$ . The poorly defined peaks at potentials more negative than  $-1.35$  V do not allow the establishment whether, in addition to  $\text{H}_2\text{L}^3$ , the  $(\text{HL}^3)^-$  species exists also. It can be supposed that the ligand can be protonated to  $\text{H}_2\text{L}^3$  by a proton from the traces of water or acidic impurities, which is confirmed by the electronic spectrum which in the presence of LiCl looks more like that of the ligand itself.

#### *Complexes in the presence of $\text{H}^+$*

The addition of  $\text{H}^+$  (aqueous solution of  $\text{HClO}_4$ ) served both to assess the stability of the complexes in acidic media and check the composition of particular species.<sup>27</sup> Protonation was carried out discontinuously and cyclic voltammograms were recorded after each increment of acid addition.

The cyclic voltammograms for  $[\text{Fe}(\text{H}_2\text{L}^1)\text{Cl}_2(\text{H}_2\text{O})]\text{Cl}$  complex recorded before and after the addition of 2  $\text{H}^+$ /complex molecule are shown in Fig. 7. The peak for  $\text{FeCl}_4^-$ , obtained as the final product of protonation of all complex species in

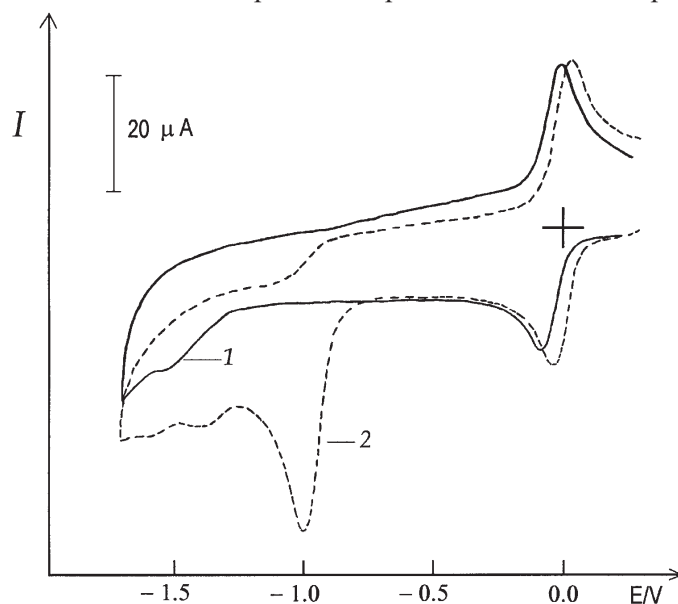


Fig. 7. Cyclic voltammograms for  $[\text{Fe}(\text{H}_2\text{L}^1)\text{Cl}_2(\text{H}_2\text{O})]\text{Cl}$  in 0.1 M LiCl before (1) and after the addition of  $\text{HClO}_4$  to the mole ratio 2  $\text{H}^+/\text{Fe}$  (2);  $0.10 \text{ V s}^{-1}$ .



the presence of LiCl, does not change essentially with respect to the initial peak. A small increase in the peak current after the addition of  $H^+$  is a consequence of the somewhat enhanced reversibility of the process and a shift of the potential to more positive values has been observed in mixed DMF-water solutions.<sup>28</sup>

The fact that there is no increase in the current of the  $FeCl_4^-$  peak which could be ascribed to ligand displacement, suggests that none of the ligand forms are bound into the complex. The height of the new peak, that for all three ligands appears at about  $-0.95$  to  $-1.0$  V, increases two fold for the mono(ligand) and four fold for the bis(ligand) complexes compared to that of  $FeCl_4^-$  and attains its maximum at  $(2-3) H^+/Fe$ . The process has the characteristics of a successive transfer of two electrons, coupled most probably with protonation,<sup>29</sup> which will be dealt with in more detail in another paper.<sup>25</sup>

Of all the investigated iron complexes, protonation of  $HL^-$  to  $H_2L$  was possible only with  $[Fe(HL^1)_2]Cl$  and  $[Fe(HL^2)_2]Cl$ . However, in both cases the  $H^+$  consumption was significantly lower than the theoretical one, which may be a consequence of the partial extraction of protons from the medium itself.

*Acknowledgement.* This work was supported by the Ministry of Science, Technologies and Development of the Republic of Serbia (Grant No. 1318).

#### ИЗВОД

#### КОМПЛЕКСИ ПРЕЛАЗНИХ МЕТАЛА НА БАЗИ ТИОСЕМИКАРБАЗИДА. ДЕО 47. СИНТЕЗА, ФИЗИЧКО-ХЕМИЈСКА И ВОЛТАМЕТРИЈСКА КАРАКТЕРИЗАЦИЈА КОМПЛЕКСА $Fe(III)$ СА СЕМИ-, ТИОСЕМИ- И S-МЕТИЛИЗОТИОСЕМИКАРБАЗОНОМ ПИРИДОКСАЛА

ВИОЛЕТА С. ЛЕВТОВИЋ, ЉИЉАНА С. ЈОВАНОВИЋ, ВУКАДИН М. ЛЕОВАЦ И ЛУКА Ј. БЈЕЛИЦА

*Природно-математички факултет, Универзитет Нови Сад, Трг Д. Обрадовића 3, Нови Сад*

Реакцијом топлих EtOH раствора  $FeX_3 \cdot nH_2O$  ( $X = Cl, NO_3$ ) са тридентатним семи-, тиосеми- и S-метилизотиосемикарбазоном пиридоксала ( $H_2L^1$ ,  $H_2L^2$ , односно  $H_2L^3$ ) добијени су високоспински октаедарски моно- и bis(лиганд) комплекси формула  $[Fe(H_2L^{1-3})Cl_2(H_2O)]Cl$ ,  $[Fe(HL^{1,2})_2]Cl \cdot nH_2O$  и  $[Fe(H_2L^3)(HL^3)](NO_3)_2 \cdot H_2O$ . Једињења су окарактерисана елементалном анализом, кондуктометријским и магнетохемијским мерењима, као и IR и UV-Vis спектрима. Извршено је детаљно волтаметријско испитивање добијених једињења у DMF у неколико помоћних електролита, истражене су природа електрохемијских процеса и равнотеже у раствору.

(Примљено 14. јула 2003)

#### REFERENCES

1. E. H. Abott, A. E. Martell, *J. Am. Chem. Soc.* **92** (1970) 5845
2. S. Capasso, F. Giordano, C. Mattia, L. Mazzarella, A. Ripamanti, *J. Chem. Soc. Dalton Trans* (1974) 2228
3. A. G. Sykes, R. D. Larsen, J. R. Fisher, E. H. Abott, *Inorg. Chem.* **30** (1991) 2911
4. P. Gili, M. G. Martin Reyes, M. G. Martin Zarza, M. F. C. Guedes da Silva, Y.-Y. Tong, A. J. L. Pombeiro, *Inorg. Chim. Acta* **225** (1997) 279

5. W. Henderson, L. L. Koh, J. D. Ranford, W. T. Robinson, J. O. Svensson, J. J. Vittal, Yu M. Wang, Y. Xu, *J. Chem. Soc. Dalton Trans* (1999) 3341
6. E. E. Snell, *Chemical and Biological Aspects of Pyridoxal Catalysis*, Pergamon, Oxford, 1963
7. M. Belicchi Ferrari, G. Gasparri Fava, C. Pelizzi, P. Tarasconi, G. Tosi, *J. Chem. Soc. Dalton Trans* (1986) 2455
8. J. S. Casas, E. E. Castellano, M. C. Rodriguez-Argüelles, A. Sanchez, J. Sordo, J. Zukerman-Schpector, *Inorg. Chim. Acta* **260** (1997) 183 and refs. therein
9. J. S. Casas, M. C. Rodriguez-Argüelles, U. Russo, A. Sanchez, J. Sordo, A. Vazques - Lopez, S. Pinelli, P. Lunghi, A. Bonati, R. Albertini, *J. Inorg. Biochem.* **69** (1998) 283
10. V. M. Leovac, V. S. Jevtović, G. A. Bogdanović, *Acta Cryst.* **C58** (2002) 514
11. D. Poleti, Lj. Karanović, V. M. Leovac, V. S. Jevtović, *Acta Cryst.* **C59** (2003) 73
12. N. Z. Knežević, V. M. Leovac, V. S. Jevtović, S. Grgurić-Šipka, T. J. Sabo, *Inorg. Chem. Commun.* **6** (2003) 561
13. M. Mohan, P. H. Modhuranath, A. Kumar, M. Kumar, N. K. Jha, *Inorg. Chem.* **28** (1989) 96
14. M. Belicchi Ferrari, G. Gasparri Fava, S. Pineli, C. Pelizzi, P. Tarasconi, *6th Yugoslav-Italian Crystallographic conference*, Pula, 1989, Abstracts p. 23
15. M. Belicchi Ferrari, G. Gasparri Fava, C. Pelizzi, P. Tarasconi, G. Tosi, *J. Chem. Soc. Dalton Trans* (1987) 227
16. M. Belicchi Ferrari, G. Gasparri Fava, M. Lanfranchi, C. Pelizzi, P. Tarasconi, *J. Chem. Soc. Dalton Trans* (1991) 1951
17. M. Belicchi Ferrari, G. Gasparri Fava, C. Pelizzi, G. Pelosi, P. Tarasconi, *Inorg. Chim. Acta* **269** (1998) 297
18. V. M. Leovac *et al.*, unpublished results
19. W. J. Geary, *Coord. Chem. Rev.* **7** (1971) 81
20. Yu. N. Kukushkin, *Khimiya koordinatsionnykh soedinenii*, Vysshaya shkola, Moskva, 1985
21. V. A. Kogan, V. V. Zelentsov, G. M. Larin, V. V. Lukov, *Kompleksy perekhodnykh metallov s gidrozonami*, Nauka, Moskva, 1990
22. L. Bjelica, Lj. Jovanović, *J. Electroanal. Chem.* **213** (1986) 85
23. L. J. Bjelica, Lj. S. Jovanović, V. M. Leovac, *Z. Phys. Chemie (Leipzig)* **269** (1988) 768
24. V. M. Leovac, Lj. S. Jovanović, L. J. Bjelica, V. I. Češljević, *Polyhedron* **8** (1989) 135
25. Lj. Jovanović *et al.*, in preparation
26. Lj. S. Jovanović, *Ph. D. Thesis*, Faculty of Science, University of Novi Sad, Novi Sad, 1986
27. Lj. Jovanović, L. Bjelica, F. F. Gaál, *Monatsh. Chem.* **116** (1985) 443
28. J. M. Sevilla, G. Cambron, T. Pineda, M. Blázquez, *J. Electroanal. Chem.* **381** (1995) 179
29. L. J. Bjelica, Lj. S. Jovanović, *Electrochim. Acta* **37** (1992) 371.

NOTE

**Note on the Hyper-Wiener Index**

IVAN GUTMAN, BORIS FURTULA and JASMINA BELIĆ

*Faculty of Science, University of Kragujevac, P. O. Box 60, 34000 Kragujevac, Serbia and Montenegro*

(Received 7 July 2003)

**Abstract:** The hyper-Wiener index  $WW$  of a chemical tree  $T$  is defined as the sum of the products  $n_1n_2$ , over all pairs  $u, v$  of vertices of  $T$ , where  $n_1$  and  $n_2$  are the number of vertices of  $T$ , lying on the two sides of the path which connects  $u$  and  $v$ . We examine a slight modification  $WWW$  of the hyper-Wiener index, defined as the sum of the products  $n_1n_2n_3$ , over all pairs  $u, v$  of vertices of  $T$ , where  $n_3$  is the number of vertices of  $T$ , lying between  $u$  and  $v$ . It is found that  $WWW$  correlates significantly better with various physico-chemical properties of alkanes than  $WW$ . Lower and upper bounds for  $WWW$ , and an approximate relation between  $WWW$  and  $WW$  are obtained.

**Keywords:** hyper-Wiener index, Wiener index, chemical trees, alkanes.

INTRODUCTION

The hyper-Wiener index is one of the recently introduced distance-based molecular structure-descriptors.<sup>1</sup> It was put forward<sup>2</sup> in 1993 and since then it has attracted much attention of theoretical chemists.<sup>3–20</sup> In parallel with the symbol  $W$  for the Wiener index,<sup>21,22</sup> the hyper-Wiener index is traditionally denoted by  $WW$ .

Let  $u$  and  $v$  be two vertices of a (chemical) tree  $T$  and let  $\pi_{uv}$  be the unique path connecting  $u$  and  $v$ . Let  $n_1$  and  $n_2$  be the counts of vertices lying on the two sides of  $\pi_{uv}$ . The vertices  $u$  and  $v$  are included in these counts, and therefore  $n_1$  and  $n_2$  are always greater than or equal to unity.

The hyper-Wiener index of a tree  $T$  is defined as

$$WW = \sum_{u,v} n_1 n_2 \quad (1)$$

with the summation going over all pairs of vertices of  $T$ .

By slightly changing the right-hand side of Eq. (1), one arrives at a modified version of the hyper-Wiener index, which is denoted by  $WWW$ :

$$WWW = \sum_{u,v} n_1 n_2 n_3. \quad (2)$$

Here  $n_3$  is the number of vertices of  $T$ , lying between the endpoints of the path  $\pi_{uv}$ . Note that if the tree  $T$  has  $n$  vertices, then for all pairs of its vertices,  $n_1 + n_2 + n_3 = n$ . Further, if  $u$  and  $v$  are adjacent, then  $n_3 = 0$ . A mathematical reason for defining the hyper-Wiener index via Eq. (2) is outlined elsewhere.<sup>23</sup>

#### COMPARING THE PHYSICO-CHEMICAL APPLICABILITY OF THE OLD AND NEW HYPER-WIENER INDICES

The first question that should be asked when  $WW$  is modified into  $WWW$  is whether the new variant has a better correlating ability, as far as the physico-chemical properties of alkanes are concerned. In order to obtain comparative results on  $WW$  and  $WWW$ , the standard data base of Needham, Wei, and Seybold,<sup>24</sup> in which experimental values for boiling point ( $BP$ ), molar volume ( $MV$ ), molar refraction ( $MR$ ), heat of evaporation ( $HE$ ), critical temperature ( $CT$ ), critical pressure ( $CP$ ), surface tension ( $ST$ ) and melting point ( $MP$ ) of alkanes with up to 10 carbon atoms have been collected, was employed.

For  $MR$  and  $MP$  no correlation between either  $WW$  or  $WWW$  could be established, and therefore these two physico-chemical properties have not been considered any further. The remaining six sets of experimental data were correlated with polynomials of various degrees of either  $WW$  or  $WWW$ . Eventually, the optimal value  $p$  for the degree of these polynomials was established. The correlation coefficients thus obtained are given in Table I.

TABLE I. Correlation coefficients,  $R(WW)$  and  $R(WWW)$ , for the correlation between various physico-chemical properties of alkanes<sup>24</sup> and a  $p$ -th degree polynomial in the parameters  $WW$  and  $WWW$ , respectively. The value of  $p$  was chosen so as to be optimal from the point of view of the  $F$ -test, at 95 % confidence level

Property	$p$	$R(WW)$	$R(WWW)$
$BP$	5	0.9809	0.9816
$MV$	2	0.9687	0.9862
$HE$	3	0.9722	0.9804
$CT$	3	0.9560	0.9444
$CP$	5	0.9657	0.9296
$ST$	2	0.8310	0.8762

As can be seen from Table I, the new hyper-Wiener index  $WWW$  is significantly better correlated with the boiling point, molar volume, heat of evaporation, and surface tension than the older version  $WW$ . The new hyper-Wiener index is found to be (slightly) inferior to  $WW$  only in the case of the critical temperature and critical pressure.

The polynomial approximation for the boiling point could be much improved by means of the expressions:

$$\begin{aligned}\ln BP &\approx A_1 \ln WW + B_1 \\ \ln BP &\approx A_2 \ln WWW + B_2\end{aligned}$$

resulting in  $R = 0.9867$  (for  $WW$ ) and  $R = 0.9911$  (for  $WWW$ ). In these formulas  $BP$  is expressed in Kelvin units; by least squares fitting one obtains  $A_1 = 0.154 \pm 0.004$ ,  $B_1 = 0.52 \pm 0.02$  and  $A_2 = 0.103 \pm 0.002$ ,  $B_1 = 5.41 \pm 0.01$ .

In summary: The new hyper-Wiener index  $WWW$ , Eq. (2), outperforms the previous version  $WW$ , Eq. (1), in correlations with almost all physico-chemical properties of alkanes. Therefore, when applying the hyper-Wiener index in QSPR and QSAR studies,<sup>25</sup> preference should be given to  $WWW$ .

#### ESTIMATING THE NEW HYPER-WIENER INDEX

It is first shown that the new hyper-Wiener index is bounded from both below and above by simple functions of the old hyper-Wiener index and the ordinary Wiener index:

$$WW - W \leq WWW \leq (n-2)(WW - W). \quad (3)$$

The summations in (1) and (2) go over all pairs of vertices. They can be divided into two parts as:

$$\sum_{u,v} = \sum_{adj} + \sum_{n,adj}$$

where  $\sum_{adj}$  and  $\sum_{n,adj}$  indicate summation over adjacent and non-adjacent vertex pairs. As  $n_3 = 0$  whenever the vertices  $u$  and  $v$  are adjacent, formula (2) reduces to

$$WWW = \sum_{n,adj} n_1 n_2 n_3 \quad (4)$$

If  $u$  and  $v$  are not adjacent, then  $n_3$  is at least 1 and at most  $n-2$ . Replacing  $n_3$  in (4) by its minimal possible value, one obtains a lower bound for  $WWW$ :

$$WWW \geq \sum_{n,adj} n_1 n_2 = \sum_{u,v} n_1 n_2 - \sum_{n,adj} n_1 n_2 \quad (5)$$

From Eq. (1), the first summation on the right-hand side of (5) is just  $WW$ . According to a well known result of Wiener,<sup>22,26,27</sup> the second summation on the right-hand side of (5) is equal to the Wiener index  $W$ . Thus one arrives at the lower bound in (3).

Replacing  $n_3$  in (4) by its maximal possible value ( $= n-2$ ), one obtains

$$WWW \leq (n-2) \sum_{n,adj} n_1 n_2$$

which, using the same arguments as above, leads to the upper bound in (3).

By means of an analogous, yet somewhat more complicated, reasoning, one can also deduce the following estimates:

$$v(v-1)/2 + (WW - W) \leq WWW \leq v(v-1)/2 + (n-3)(WW - W)$$

where  $\nu$  is the number of vertices of degree one in the chemical tree  $T$ , *i.e.*, the number of methyl groups in the underlying molecule.

#### APPROXIMATING THE NEW HYPER-WIENER INDEX

In order to deduce an approximate expression for the new hyper-Wiener index  $WWW$ , Eq. (2) is rewritten as:

$$WWW \approx \sum_{u,v} n_1 n_2 \langle n_3 \rangle$$

where  $\langle n_3 \rangle$  is the arithmetic mean of  $n_3$ . Then,

$$WWW \approx \langle n_3 \rangle \sum_{u,v} n_1 n_2 = \langle n_3 \rangle WW. \quad (6)$$

In order to apply (6), the value of  $\langle n_3 \rangle$  must be known (at least approximately). In order to achieve this goal, one starts with:

$$\begin{aligned} \langle n_3 \rangle &= \langle n - n_1 - n_2 \rangle = n - \langle n_1 + n_2 \rangle \\ &= n - 2 \langle (n_1 + n_2)/2 \rangle \approx n - 2 \langle \sqrt{n_1 n_2} \rangle \end{aligned}$$

where the arithmetic mean of  $n_1$  and  $n_2$  has been replaced by their geometric mean. Using another plausible approximation, one obtains:

$$\langle n_3 \rangle \approx n - 2 \sqrt{\langle n_1 n_2 \rangle} \quad (7)$$

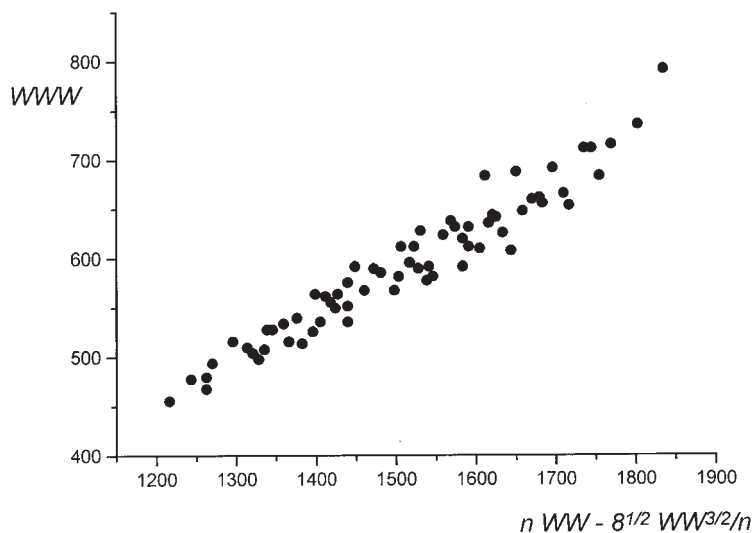


Fig. 1. The new hyper-Wiener index ( $WWW$ , Eq. (2)) vs. the right-hand side of Eq. (9), which is a function of the old hyper-Wiener index ( $WW$ , Eq. (1)). The data points pertain to isomeric decanes,  $C_{10}H_{22}$ , *i.e.*,  $n = 10$ . The correlation coefficient is 0.966.

In view of Eq. (1), the mean value of the product  $n_1 n_2$  is directly related to the hyper-Wiener index  $WW$ :

$$WW = \frac{n(n-1)}{2} \langle n_1 n_2 \rangle \quad (8)$$

where the fact that in an  $n$ -vertex graph there are  $n(n-1)/2$  vertex pairs has been taken into account.

By combining the relations (6)–(8), one finally obtains the expression:

$$WWW \approx n WW - \frac{2\sqrt{2}}{n} WW^{3/2} \quad (9)$$

which relates the old and the new hyper-Wiener index.

The quality of the approximate formula (9) is seen from Fig. 1.

*Acknowledgement:* One author (I.G.) thanks the Alexander von Humboldt Foundation for financial support in 2003.

#### ИЗВОД

#### БЕЛЕШКА О ХИПЕР-ВИНЕРОВОМ ИНДЕКСУ

ИВАН ГУТМАН, БОРИС ФУРТУЛА и ЈАСМИНА БЕЛИЋ

*Природно-математички факултет у Крагујевцу*

Хипер-Винеров индекс  $WW$  хемијског стабла  $T$  дефинисан је као сума производа  $n_1 n_2$ , преко свих парова  $u, v$  чворова стабла  $T$ , где  $n_1$  и  $n_2$  означавају број чворова који леже са две стране пута који повезује  $u$  и  $v$ . У раду испитујемо једну модификацију  $WWW$  хипер-Винеровог индекса, дефинисану као сума производа  $n_1 n_2 n_3$ , преко свих парова  $u, v$  чворова стабла  $T$ , где  $n_3$  означава број чворова који леже између  $u$  и  $v$ . Нађено је да је  $WWW$  значајно боље корелиран са разним физичко-хемијским особинама алкана него  $WW$ . Добивене су доње и горње границе за  $WWW$  као и једна апроксимативна релација између  $WWW$  и  $WW$ .

(Примљено 7. јула 2003)

#### REFERENCES

1. R. Todeschini, V. Consonni, *Handbook of Molecular Descriptors*, Wiley-VCH, Weinheim, 2000
2. M. Randić, *Chem. Phys. Lett.* **211** (1993) 478
3. I. Lukovits, W. Linert, *J. Chem. Inf. Comput. Sci.* **34** (1994) 899
4. I. Lukovits, *J. Chem. Inf. Comput. Sci.* **34** (1994) 1079
5. I. Lukovits, *Comput. Chem.* **19** (1995) 27
6. W. Linert, F. Renz, K. Kleestorfer, I. Lukovits, *Comput. Chem.* **19** (1995) 395
7. W. Linert, K. Kleestorfer, F. Renz, I. Lukovits, *J. Mol. Struct. (Theochem)* **337** (1995) 121
8. D. J. Klein, I. Lukovits, I. Gutman, *J. Chem. Inf. Comput. Sci.* **35** (1995) 50
9. M. V. Diudea, *J. Chem. Inf. Comput. Sci.* **36** (1996) 833
10. W. Linert, I. Lukovits, *MATCH Commun. Math. Comput. Chem.* **35** (1997) 65
11. I. Gutman, W. Linert, I. Lukovits, A. A. Dobrynin, *J. Chem. Inf. Comput. Sci.* **37** (1997) 349
12. I. Gutman, *Indian J. Chem.* **36A** (1997) 128
13. A. A. Dobrynin, I. Gutman, V. N. Pottukh-Peletsii, *J. Struct. Schem.* **40** (1999) 293



14. D. Plavšić, N. Lerš, K. Sertić-Bionda, *J. Chem. Inf. Comput. Sci.* **40** (2000) 516
15. P. Žigert, S. Klavžar, I. Gutman, *ACH Models Chem.* **137** (2000) 83
16. S. Klavžar, P. Žigert, I. Gutman, *Comput. Chem* **24** (2000) 229
17. R. Aringhieri, P. Hansen, F. Malucelli, *J. Chem. Inf. Comput. Sci.* **41** (2001) 958
18. I. Lukovits, in: M. V. Diudea (Ed.), *QSPR/QSAR Studies by Molecular Descriptors*, Nova, Huntington, 2001, pp. 31–38
19. I. Gutman, *Chem. Phys. Lett.* **364** (2002) 352
20. I. Gutman, B. Furtula, *Monatsh. Chem.* **134** (2003) 975
21. I. Gutman, J. H. Potgieter, *J. Serb. Chem. Soc.* **62** (1997) 185
22. A. A. Dobrynin, R. Entringer, I. Gutman, *Acta Appl. Math.* **66** (2001) 211
23. I. Gutman, *J. Serb. Chem. Soc.*, **68** (2003) 947
24. D. E. Needham, I. C. Wei, P. G. Seybold, *J. Am. Chem. Soc.* **110** (1988) 4186
25. J. Devillers, A. T. Balaban (Eds.), *Topological Indices and Related Descriptors in QSAR and QSPR*, Gordon & Breach, Amsterdam, 1999
26. H. Wiener, *J. Am. Chem. Soc.* **69** (1947) 17
27. I. Gutman, B. Arsić, B. Furtula, *J. Serb. Chem. Soc.* **68** (2003) 549.

## Hyper-Wiener index and Laplacian spectrum

IVAN GUTMAN\*

Faculty of Science, University of Kragujevac, P. O. Box 60, 34000 Kragujevac, Serbia and Montenegro

(Received 7 July 2003)

**Abstract:** The hyper-Wiener index  $WWW$  of a chemical tree  $T$  is defined as the sum of the product  $n_1 n_2 n_3$ , over all pairs  $u, v$  of vertices of  $T$ , where  $n_1$  and  $n_2$  are the number of vertices of  $T$ , lying on the two sides of the path which connects  $u$  and  $v$ , and  $n_3$  is the number of vertices lying between  $u$  and  $v$ . An expression enabling the calculation of  $WWW$  from the Laplacian eigenvalues of  $T$  has been deduced.

**Keywords:** hyper-Wiener index, Wiener index, Laplacian spectrum, chemical trees, alkanes.

In the preceding paper<sup>1</sup> a new modification of the hyper-Wiener index, denoted as  $WWW$ , was put forward. It was demonstrated<sup>1</sup> that the  $WWW$  has certain advantages over the original hyper-Wiener index<sup>2</sup>  $WW$ , and relations between  $WWW$  and  $WW$  were established. In this note it will be shown how the  $WWW$  can be computed from the Laplacian eigenvalues of the underlying molecular graph.

The Laplacian graph spectral theory has found recently many chemical applications, see, for instance, the papers<sup>3–11</sup> and the references quoted therein. Details of this theory can be found in several reviews.<sup>12–15</sup>

The Laplacian matrix  $L(G)$  of a graph  $G$  with  $n$  vertices,  $v_1, v_2, \dots, v_n$ , is a square matrix of order  $n$  whose  $(i, j)$ -entry is defined as

$$L(G)_{ij} = \begin{cases} \delta_i & \text{if } i = j \\ -1 & \text{if the vertices } v_i \text{ and } v_j \text{ are adjacent} \\ 0 & \text{otherwise} \end{cases}$$

where  $\delta_i$  denotes the degree (= number of first neighbors) of the  $i$ -th vertex of  $G$ . The eigenvalues of the Laplacian matrix, denoted by  $\mu_1, \mu_2, \dots, \mu_n$ , are said to be the Laplacian eigenvalues of the graph  $G$  and to form its Laplacian spectrum.

The Laplacian eigenvalues are labeled so that

$$\mu_1 \geq \mu_2 \geq \dots \geq \mu_{n-1} \geq \mu_n.$$

Then for all graphs,  $\mu_n = 0$ , and for connected graphs (among which are all molecular graphs),  $\mu_{n-1} > 0$ .

\* Serbian Chemical Society active member.

The Laplacian characteristic polynomial is  $\psi(G, x) = \det[xI - L(G)]$ . It can be written in the coefficient form as:

$$\psi(G, x) = \sum_{k=0}^{n-1} (-1)^k c_k x^{n-k}$$

According to the Kel'mans theorem,<sup>3,8,16,17</sup> the  $k$ -th coefficient of the Laplacian polynomial can be computed from the structure of the graph  $G$  by means of the formula

$$c_k = \sum_F \Gamma(F)$$

where the summation goes over all spanning forests  $F$  of  $G$ , possessing  $k$  disconnected components, and where  $\Gamma(F)$  is equal to the product of the number of vertices of the components of  $F$ . In the case of a tree  $T$ , the straightforward application of the Kel'mans theorem gives:

$$\begin{aligned} c_n &= 0 \\ c_{n-1} &= n \\ c_{n-2} &= \sum_{adj} n_1 n_2 \\ c_{n-3} &= \sum_{u,v} n_1 n_2 n_3 \end{aligned} \quad (1)$$

where the notation is same as in the preceding paper.<sup>1</sup> Thus, it can immediately be realized that:

$$c_{n-2} = W(T) \quad (2)$$

$$c_{n-3} = WWW(T). \quad (3)$$

Using the Vieta identities and bearing in mind that  $\mu_n = 0$ , the coefficients  $c_{n-1}$ ,  $c_{n-2}$ , and  $c_{n-3}$  are expressed in terms of Laplacian eigenvalues as:

$$\begin{aligned} c_{n-1} &= \mu_1 \times \mu_2 \times \dots \times \mu_{n-1} \\ c_{n-2} &= \sum_i \mu_1 \times \mu_2 \times \dots \times \mu_{i-1} \times \mu_{i+1} \times \dots \times \mu_{n-1} \\ c_{n-3} &= \sum_{i < j} \mu_1 \times \mu_2 \times \dots \times \mu_{i-1} \times \mu_{i+1} \times \dots \times \mu_{j-1} \times \mu_{j+1} \times \dots \times \mu_{n-1} \end{aligned}$$

*i.e.*,

$$\begin{aligned} c_{n-1} &= \prod_k \mu_k \\ c_{n-2} &= \left( \prod_k \mu_k \right) \left( \sum_i \frac{1}{\mu_i} \right) \\ c_{n-3} &= \left( \prod_k \mu_k \right) \left( \sum_{i < j} \frac{1}{\mu_i \mu_j} \right) \end{aligned}$$

Combining the latter identities with Eqs. (1)–(3), one obtains:

$$W(T) = n \sum_{i=1}^{n-1} \frac{1}{\mu_i} \quad (4)$$

$$WWW(T) = n \sum_{i < j} \frac{1}{\mu_i \mu_j} \quad (5)$$

Formula (4), which is an expression for the Wiener index in terms of Laplacian eigenvalues, is a previously known result.<sup>3,4</sup> The analogous formula (5) is being reported here for the first time. It can be simplified as:

$$\begin{aligned} WWW(T) &= \frac{n}{2} \left( \sum_{i=1}^{n-1} \sum_{j=1}^{n-1} \frac{1}{\mu_i \mu_j} - \sum_{i=1}^{n-1} \frac{1}{(\mu_i)^2} \right) \\ &= \frac{n}{2} \left[ \left( \sum_{i=1}^{n-1} \frac{1}{\mu_i} \right) \left( \sum_{j=1}^{n-1} \frac{1}{\mu_j} \right) - \sum_{i=1}^{n-1} \frac{1}{(\mu_i)^2} \right] \\ &= \frac{n}{2} \left[ \left( \frac{W(T)}{n} \right)^2 - \sum_{i=1}^{n-1} \frac{1}{(\mu_i)^2} \right] \end{aligned}$$

which finally results in the identity:

$$WWW(T) = \frac{W(T)}{2n} - \frac{n}{2} \sum_{i=1}^{n-1} \frac{1}{(\mu_i)^2}. \quad (6)$$

Formula (6), combined with (4), is particularly suitable for computer-aided numerical calculation of the hyper-Wiener index. All the results reported in the preceding work<sup>1</sup> were obtained by means of this formula.

*Acknowledgement:* The autor thanks the Alexander von Humboldt Foundation for financial support in 2003.

#### ИЗВОД

#### ХИПЕР-ВИНЕРОВ ИНДЕКС И ЛАПЛАСОВ СПЕКТАР

ИВАН ГУТМАН

*Природно-математички факултет у Крагујевцу*

Хипер-Винеров индекс  $WWW$  хемијског стабла  $T$  дефинисан је као сума производа  $n_1 n_2 n_3$ , преко свих парова  $u, v$  чворова стабла  $T$ , где  $n_1$  и  $n_2$  означавају број чворова који леже са две стране пута који повезује  $u$  и  $v$ , а  $n_3$  је број чворова између  $u$  и  $v$ . Добивена је формула која омогућава да се  $WWW$  израчуна из Лапласових сопствених вредности стабла  $T$ .

(Примљено 7. јула 2003)

## REFERENCES

1. I. Gutman, B. Furtula, J. Belić, *J. Serb. Chem. Soc.* **68** (2003) 941
2. M. Randić, *Chem. Phys. Lett.* **211** (1993) 478
3. B. Mohar, D. Babić, N. Trinajstić, *J. Chem. Inf. Comput. Sci.* **33** (1993) 153
4. I. Gutman, S. L. Lee, C. H. Chu, Y. L. Luo, *Indian J. Chem.* **33A** (1994) 603
5. C. D. Godsil, I. Gutman, *ACH Models Chem.* **136** (1999) 503
6. I. Gutman, V. Gineityte, M. Lepović, M. Petrović, *J. Serb. Chem. Soc.* **64** (1999) 673
7. I. Gutman, D. Vidović, D. Stevanović, *J. Serb. Chem. Soc.* **67** (2002) 407
8. I. Gutman, D. Vidović, B. Furtula, *Indian J. Chem.* **42A** (2003) 1272
9. I. Gutman, *MATCH Commun. Math. Comput. Chem.* **47** (2003) 133
10. W. Xiao, I. Gutman, *MATCH Commun. Math. Comput. Chem.* **49** (2003) 67
11. W. Xiao, I. Gutman, *Theor. Chem. Acc.*, **110** (2003) 284
12. R. Grone, R. Merris, V. S. Sunder, *SIAM J. Matrix Anal. Appl.* **11** (1990) 218
13. R. Grone, R. Merris, *SIAM J. Discr. Math.* **7** (1994) 221
14. R. Merris, *Lin. Algebra Appl.* **197** (1994) 143
15. R. Merris, *Lin. Multilin. Algebra* **39** (1995) 19
16. D. Cvetković, M. Doob, H. Sachs, *Spectra of Graphs - Theory and Application*, Academic Press, New York, 1980
17. M. V. Diudea, I. Gutman, L. Jäntschi, *Molecular Topology*, Nova, Huntington, 2001.

## Influence of the synthesis conditions on the photoluminescence of silica gels

IVANA HINIĆ, GORAN STANIŠIĆ and ZORAN POPOVIĆ

*Institute of Physics, Pregrevica 118, 11000 Belgrade, Serbia and Montenegro*

(Received 2 July 2003)

**Abstract:** The photoluminescence spectra of silica xerogel samples synthesized with ethanol as solvent and xerogel where the ethanol was exchanged by water before drying are reported. In addition, the photoluminescence spectrum of a silica cryogel synthesized with *tert*-butanol as solvent was investigated. The samples were modified by formamide. Bands at 2.00, 2.20, 2.32 and 2.46 eV were identified. In the photoluminescence spectra of all samples. The band at 2.00 eV is caused by the presence of silane, and the band at 2.20 eV is connected with the nonstoichiometric composition of silica. The photoluminescence band at 2.32 eV was found to originate from the organic groups of the solvent. The origin of this band are E' defect centers, which is a prominent paramagnetic defect in conventional  $\alpha$ -SiO<sub>2</sub>.

**Keywords:** silica gel, luminescence, infrared spectroscopy.

### INTRODUCTION

The sol-gel process is a simple chemical procedure for making many different materials, among them silica gels. Silica gels are prepared by a chemical reaction employing a metal alkoxide (for example tetraethylorthosilicate (TEOS)) and water in an alcoholic solvent. The first reaction is hydrolysis which induces the substitution of OR groups linked to silicon by silanol Si–OH groups. These chemical species may react together to form Si–O–Si (siloxane) bonds which lead to silica network formation. This reaction of condensation establishes a 3D network which invades the whole volume of the container. The liquid used as solvent to perform the different chemical reactions remains within the pores of the solid network and has to be removed. Silica aerogel samples can be dried by simple evaporation at temperatures close to room temperature and atmospheric pressure, whereby so called *xerogels* (a word derived from the Greek word “xeros” which means dry) are obtained. By sublimation of frozen solvent *cryogels* are obtained. An *aerogel* results from a supercritical drying process. The drying step is performed inside an autoclave which allows the critical point ( $p_C$ ,  $T_C$ ) of the solvent to be overpassed.

A major problem during drying is cracking of the samples. Zarzycki showed that drying stress is a function of pore size and rate of evaporation of the pore liquor, which depends on the liquor vapor pressure.<sup>1</sup> Only by using supercritical extraction can large monoliths without cracks be obtained. However, because of the high costs and risk of this method, processes for preparing monolithic xerogels at ambient pressure have in recent years been developed.<sup>2,3</sup> One of these methods involves the addition of a drying control chemical additive (DCCA) to the sol. The DCCA changes the structure of the gel during gelation in such a way as to equalize the pores dimension, so the difference in the surface tension of the pores is lower and the sample can be dried under normal conditions.<sup>3</sup> The DCCA must also be removable during densification before pore closure.<sup>3</sup>

The structure of the sol-gel derived oxide networks and defects in the structure are strongly affected by the concentration of the interacting species, their ratios, the reaction medium solvent, the pH, the catalyst and the temperature during condensation. Silica gels have several microstructure defects which are responsible for the appearance of photoluminescence (PL). One such defect is a non-bridged oxygen hole center (NBOHC) described by the relation  $\text{SiOH} = \text{SiO}\cdot + \cdot\text{H}$  where the dots denote uncoupled electrons. In PL spectra of Si/O systems, this defect is connected with the bands at about 1.80 eV<sup>4</sup> or 1.90 eV.<sup>5,6</sup> The band which appears at 2.00 eV originates from the presence of silan ( $\text{SiH}$  and/or  $\text{SiH}_2$ ).<sup>7</sup> The band at 2.20 eV is caused by the non-stoichiometric structure  $\text{SiO}_x$  where  $1 < x < 2$ .<sup>7-9</sup> The origin of the PL of silica gels can be organic compounds which remain from the synthesis. Thermal treatment results in the formation and/or removal of various defect centers.<sup>10</sup>

In this work the PL spectra of silica gels synthesized and dried by different methods were investigated. First sample was a xerogel synthesized with ethanol as the solvent and DCCA-formamide modified (XG sample). The second sample was obtained by the exchange of ethanol by water in the XG sample before drying (sample XGW). Both xerogels were dried by evaporation under ambient conditions. The examined cryogel sample (CG) was synthesized using *tert*-butanol as solvent and freeze-dried. The PL spectra were compared with the PL spectra of two silica aerogels synthesized without DCCA, in ethanol solvent and dried by supercritical extraction: the first was not sintered (AG sample), and the second was sintered for 15 h at 1000 °C (AGS sample). These samples were described in a previous paper.<sup>7</sup>

#### EXPERIMENTAL

The silica gel samples were made by the sol-gel process using tetraethylorthosilicate (TEOS), water, different solvents (ethanol and *tert*-butanol), acid catalyst HCl and DCCA - formamide. The amounts of the initial compounds are presented in for each sample (Table I).

The sample XGW was washed after gelation in water for 47 days. The parameters of gelation and drying are shown in Table II.

TABLE I.

Sample	TEOS/cm <sup>3</sup>	Solvent/cm <sup>3</sup>		H <sub>2</sub> O/cm <sup>3</sup>	HCl/cm <sup>3</sup>	Formamide/cm <sup>3</sup>
		Ethanol	<i>Tert</i> -butanol			
XG	7.5	6.0	—	4.2	0.7	4.2
CG	7.5	—	6.1	6.6	0.7	4.2

TABLE II.

Sample	Gelation time/h	Gelation temperature/°C	Drying method	Drying time/days	Drying temperature/°C
XGW	1	60	Evaporation	139	20
XG	1	60	Evaporation	9	20
CG	24	40	Sublimation	1	25

The PL spectra were recorded using a Jobin-Ivon U1000 monochromator and photomultiplier as detector. The samples were excited by the 4.88 nm line of an Ar ion laser. The measurements were performed at room temperature in air. The infrared (IR) reflection spectra of all samples were measured using BOMEM DA8 spectrometer at room temperature in the spectral range from 400 to 1500 cm<sup>-1</sup>. For these measurements, the KBr pellet technique was used.

## RESULTS AND DISCUSSION

The PL spectra of the samples XGW, XG and CG are presented in Fig. 1 while the PL spectra of the samples AG and AGS are shown in Fig. 2. The PL spectra were deconvoluted using a sum of 4 or 5 pseudovoit profiles, which are also shown in Figs. 1, and 2.

The IR spectra of the same samples are shown in Fig. 3. The IR spectra were fitted using a three-parameter model of the dielectric function:

$$\varepsilon(\omega) = \varepsilon_{\infty} + \sum_j \frac{S_j}{\omega_j^2 - \omega^2 + i\gamma_j^2 \omega^3}$$

where  $S_j$ ,  $\omega_j$  and  $\gamma_j$  are respectively the oscillator strength, resonance frequency and damping parameters of  $j$ -th oscillator, and  $\varepsilon_{\infty}$  is the high frequency dielectric constant.

From the deconvolution procedure of PL spectra, the band positions, width and area below each band were obtained. The areas below the PL bands for each xerogel, cryogel and aerogel sample are shown in Fig. 4.

The PL spectra of xerogels exhibit four bands at about 2.00, 2.20, 2.32 and 2.46 eV. In the PL spectra of the aerogels an additional band at 1.80 eV appears. As was discussed in our previous work,<sup>7</sup> the band at about 1.80 eV is connected with NBOHC centers at the surface of the gel. The band at 2.00 eV is assigned to the presence of silane, while the band at 2.20 originates from the non-stoichiometric composition of the gel structure.<sup>7</sup> In the PL spectra of xerogels and cryogel, bands at 2.00 and 2.20 eV are also present. From the behavior of the band at 2.20 eV, in-



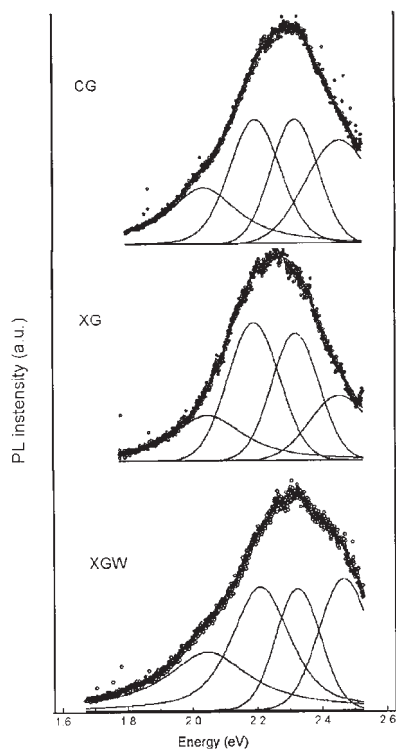


Fig. 1. PL spectra of the xerogel made with ethanol (XG), xerogel washed in water (XGW) and the cryogel made with *tert*-butanol.

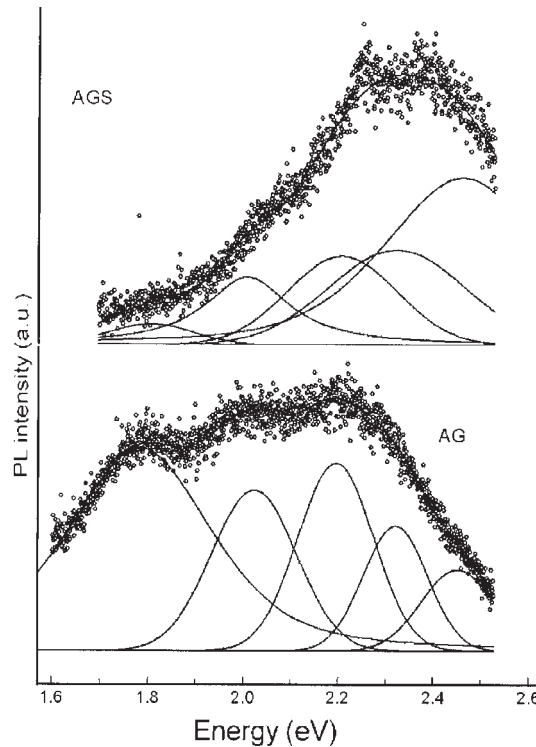


Fig. 2. PL spectra of the aerogels: non-sintered (AG) and sintered 15 h at 1000 °C.

formation about the non-stoichiometric composition of the gel structure can be obtained. The exchange of the organic solvent by water allows the polymerization reaction to go more to completion so the composition of the sample washed in water is less non-stoichiometric. The process of sintering has the same effect so the area below the 2.20 eV band is low in the case of the sintered aerogel.

After drying by evaporation or sublimation, a certain amount of solvent remains in the closed pores of the sample. The presence of the organic solvent (ethanol or *tert*-butanol) is visible in the IR spectra. The mode connected with ethanol is at about  $1050\text{ cm}^{-1}$  while the mode of *tert*-butanol is at about  $1150\text{ cm}^{-1}$ . From the fitting procedure of the IR spectra, the oscillator strengths of these modes, which are proportional to the amount of vibrating molecules or residues can be obtained. As can be seen in Fig. 5a, the area below the PL band at 2.32 eV changes in a similar manner as the oscillator strength of the organic solvents in the silica gel samples.

For example, in the sample XGW, which had been washed in water, the amount of solvent is very low, as is the case of the sintered AGS sample where the organic material had been removed by sintering at high temperature. In the case of

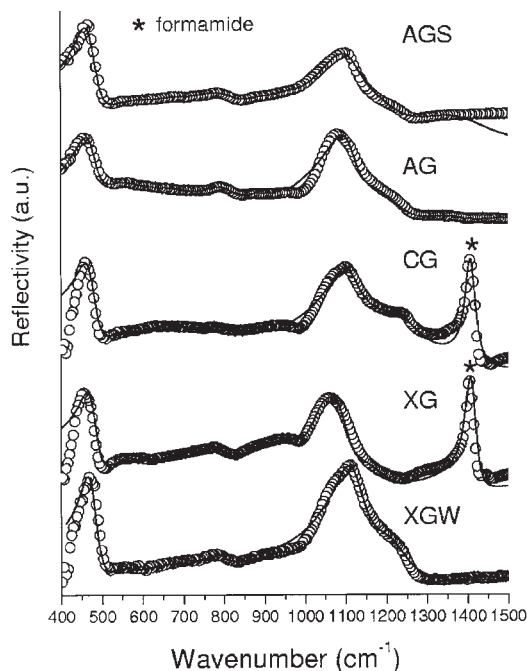


Fig. 3. IR Spectra of the xerogels, cryogel and aerogels. Experimental data are presented by circles, while the fit curve is the solid line.

these two samples the area below the band at 2.32 eV is low. It can be concluded that this band originates from the organic compounds in silica gels structure. Note that washing in water removes all the formamide. This can be seen from Fig. 3, where in the spectrum of the XGW sample the mode at about  $1400\text{ cm}^{-1}$  connected with formamide is absent.

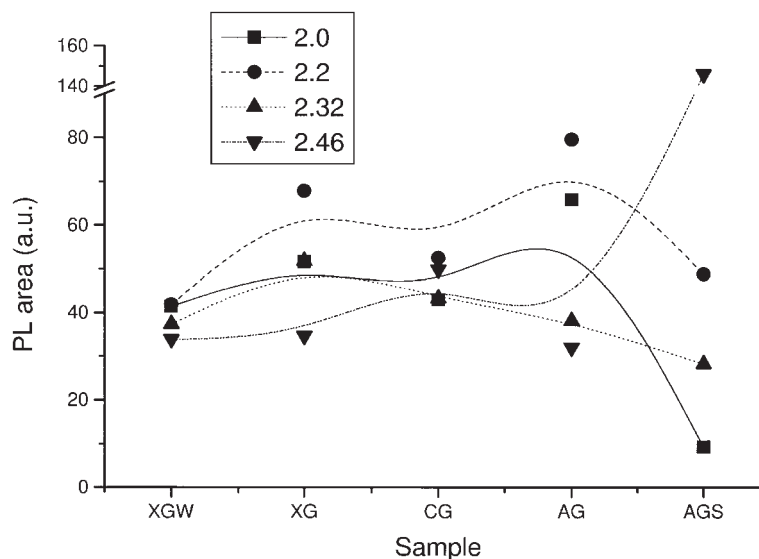


Fig. 4. Areas below the PL bands in the spectra of all the samples.

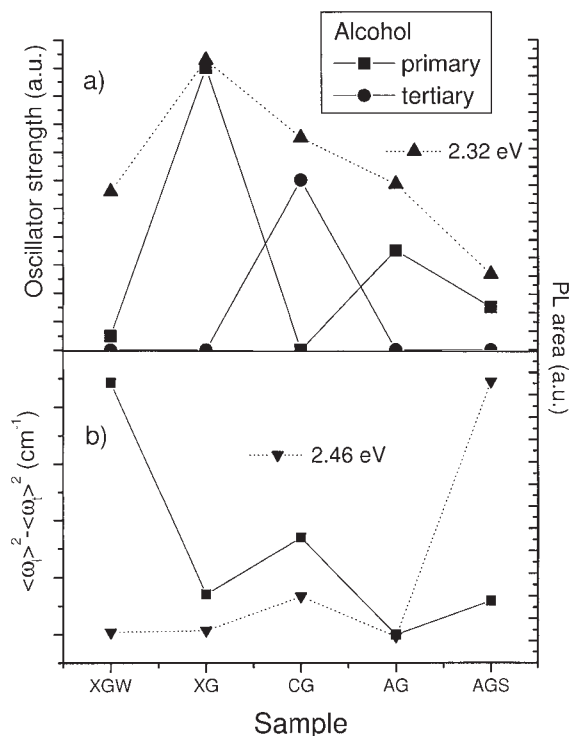


Fig. 5. a) Oscillator strengths of the alcoholic modes compared with the area below the PL mode at 2.32 eV; b) spectral activity of the IR modes connected with the antisymmetric vibration of the Si–O–Si bonds compared with the area below the PL mode at 2.46 eV.

For each sample the spectral activity in spectral range where the antisymmetric modes connected with the Si–O–Si bonds are positioned were calculated. This spectral activity increases with increasing network connectivity.<sup>11</sup>

The area below the band at 2.46 eV and the measure of spectral activity of IR spectra in the region connected with the antisymmetric vibrations of Si–O–Si are shown. The presence of water during washing (in the case of the XGW sample) allows the condensation process to continue and so the number of Si–O–Si bond increases. The sintering process affects the structure of the silica aerogel in a similar way (AGS sample). The area below the band at 2.46 eV is higher in the PL spectra of the XGW and AGS samples. It can be concluded that increasing the network connectivity increases number of defects too. There are probably E' centers which are prominent defects in conventional  $\alpha$ -SiO<sub>2</sub>.

#### CONCLUSIONS

The method of synthesis, precursors and drying procedure affect the defects which can be formed in the structure of silica gel. The PL spectra of silica xerogels and cryogels consist of four bands at 2.00, 2.20, 2.32 and 2.46 eV. The band at 2.00 eV originates from the presence of silane at the surface of the sample. The non-stoichiometric composition of the structure of the gels produces a PL band at 2.20 eV.

The band at 2.32 eV is connected with the presence of organic residues which remain in the gel pores after drying. Increasing the network density allows the formation of E' paramagnetic defect centers which produce a PL band at 2.46 eV.

*Acknowledgement:* This work was supported by the Ministry of Science, Technology and Development of the Republic of Serbia under the project No 1469.

#### ИЗВОД

#### УТИЦАЈ УСЛОВА СИНТЕЗЕ НА ФОТОЛУМИНЕСЦЕНЦИЈУ СИЛИКА ГЕЛОВА

ИВАНА ХИНИЋ, ГОРАН СТАНИШИЋ и ЗОРАН ПОПОВИЋ

*Институт за физику Пређревица 118, 11080 Београд-Земун*

Приказали смо фотолуминесцентне спектре узорка силика ксерогела синтетисаног са етанолом као растварачем и узорка ксерогела у коме је етанол замењен са водом пре сушења. Осим тога, истраживали смо фотолуминесцентни спектар силика криогела синтетисаног са *tert* бутанолом као растварачем. Узорци су модификовани формамидом. У фотолуминесцентном спектру свих узорка идентификоване су траке на 2,00, 2,20, 2,32 и 2,46 eV. Трака на 2,00 eV је узрокована присуством силана док је трака на 2,20 eV везана за нестехиометријски састав силике. Установили смо да фотолуминесцентна трака на 2,32 eV потиче од органских група из растварача. Узрок траке на 2,46 eV су E' центри који су чести парамагнетни дефекти код конвенционалног  $\alpha$ -SiO<sub>2</sub>.

(Примљено 2. јуна 2003)

#### REFERENCES

1. J. Zarzycki, in *Ultrastructure Processing and Ceramics, Glasses and Composites*, L. L. Hench and D. R. Ulrich, Eds., Wiley, New York, 1984
2. M. Einarsrud, E. Nilsen, *J. Non-Cryst. Solids* **226** (1998) 122
3. L. L. Hench in *Science of Ceramic Chemical Processing*, L. L. Hench and D. R. Ulrich, Eds., Wiley, New York, 1986
4. L. A. Balagurov, B. M. Leifertov, E. A. Petrova, A. F. Orlov, E. M. Panasencko, *J. Appl. Phys.* **79** (1996) 7143
5. H. Nishikawa, E. Watanabe, D. Ito, *J. Appl. Phys.* **80** (1996) 3513
6. N. Nishikawa, Y. Miyake, E. Watanabe, D. Ito, K. S. Seol, Y. Okhi, K. Ishii, Y. Sakurai, K. Nagasawa, *J. Non-Cryst. Sol.* **222** (1997) 221
7. I. I. Hinić, G. M. Stanišić, Z. V. Popović, *J. Sol-Gel Science and Technology* **14** (1999) 1
8. M. R. Ayers, A. J. Hunt, *J. Non-Cryst. Sol.* **217** (1997) 229
9. B. H. Augustine, E. A. Irene, *J. Appl. Phys.* **78** (1995) 4020
10. B. E. Yoldas, *J. Mater. Res.* **5** (1990) 1157
11. I. Hinić, G. M. Stanišić, Z. V. Popović, *Science of Sintering* **33** (2001) 99.

## Direct photolysis and photocatalytic degradation of 2-amino-5-chloropyridine

BILJANA F. ABRAMOVIĆ<sup>#</sup>, VESNA B. ANDERLUH<sup>#</sup>, ANDJELKA S. TOPALOV<sup>#</sup> and  
FERENC F. GAÁL<sup>#</sup>

*Department of Chemistry, Faculty of Science, Trg D. Obradovića 3, 21000 Novi Sad, Serbia and  
Montenegro (e-mail: abramovic@ih.ns.ac.yu)*

(Received 23 June 2003)

**Abstract:** The direct photolysis and photocatalytic degradation of a pyridine pesticide analogue, 2-amino-5-chloropyridine, were investigated employing different analytical techniques – potentiometry, for monitoring the pH and chloride generation, spectrophotometry, for studying the degradation of the pyridine moiety, ion chromatography, for monitoring nitrate formation, and total organic carbon analysis for investigating the efficiency of the process. The photocatalytic degradation was studied in aqueous suspensions of titanium dioxide under illumination by UV light. It was found that chloride evolution was a zero-order reaction which takes place by direct photolysis, in that way differing from the degradation of the pyridine moiety, which takes place in the presence of titanium dioxide. Changes in pH during degradation indicate the formation of acidic intermediates and nitrate in addition to chloride. The effect of the initial substrate concentration was also investigated by monitoring the reaction of chloride generation as well as the degradation reaction of the pyridine moiety. It was found that degradation of the parent compound (2.5 mmol/dm<sup>3</sup>) by direct photolysis is completed in about 20 minutes, and of the pyridine moiety by photocatalytic degradation in about nine hours. Based on the obtained data a possible reaction mechanism is proposed.

**Keywords:** direct photolysis, photocatalytic degradation, titanium dioxide, 2-amino-5-chloropyridine, water treatment.

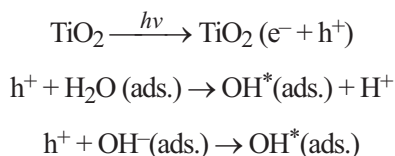
### INTRODUCTION

Pollution of waterstreams by different organic pollutants, among which pesticides are very common, represents a serious environmental problem. Several conventional methods of water treatment exist, and as such have found certain practical applications. They are, however, either slow or non-destructive for some more persistent organic pollutants. On the contrary, heterogeneous photocatalysis with titanium dioxide as catalyst under UV irradiation was proven to be an efficient method to completely mineralise organic compounds.<sup>1–12</sup> Namely, during this

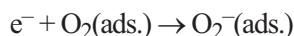
<sup>#</sup> Serbian Chemical Society active member.

process, organic carbon and hydrogen are transformed to carbon dioxide and water, while covalently bound halogen, nitrogen, sulphur and phosphorus are transformed to halide, ammonium/nitrite/nitrate, sulphate and phosphate, respectively. It is also important to point out that the inertness, low toxicity and low cost of titanium dioxide make it a good choice of semi conductor for heterogeneous photocatalysis.

When  $\text{TiO}_2$  is illuminated with UV radiation, electron-hole pairs are formed.<sup>13</sup> The thus generated holes are strong oxidizing agents ( $E = +2.8 \text{ V}$ ). In the reaction between the photogenerated holes and the water molecules and hydroxyl ions adsorbed on the  $\text{TiO}_2$  surface, hydroxyl radicals capable of the mineralization of organic compounds are formed:



To prevent electron-hole recombination, it is necessary for the illumination to take place in the presence of an electron acceptor. For this purpose, illumination is most often carried out in an oxygen stream:



In this work, the photocatalytic degradation of an analogue of pyridine pesticides,<sup>14</sup> 2-amino-5-chloropyridine, was studied by potentiometry, spectrophotometry, ion chromatography and by monitoring the change in the content of total organic carbon (TOC) in order to gain insight into the reaction kinetics and the nature of the intermediates involved and, consequently, to propose the probable mechanism of 2-amino-5-chloropyridine photodegradation. The effect of the initial concentration was also investigated.

## EXPERIMENTAL

### *Chemicals and solutions*

All chemicals used in the investigation were reagent grade and were used without further purification. 2-Amino-5-chloropyridine was purchased from Merck. The titanium dioxide used as photocatalyst was Degussa P25 (predominantly anatase,  $50 \text{ m}^2/\text{g}$ , nonporous). The solutions were prepared with doubly distilled water. Milli-Q water was used as a component of the mobile phase in the ion chromatography.

For the investigation of the effect of the initial concentration of 2-amino-5-chloropyridine, stock solutions ( $2.5$  and  $2.9 \text{ mmol/dm}^3$ ) were prepared. These solutions were diluted to prepare solutions of lower concentrations for investigation.

Standard chloride solutions for calibration were prepared by dilution of stock sodium chloride solution ( $100 \text{ mmol/dm}^3$ ) to obtain solutions in the concentration range  $0.01 - 3 \text{ mmol/dm}^3$ .

### *Photodegradation procedure*

For the irradiation experiments,  $20.0 \text{ cm}^3$  of the to be investigated compound solution were measured into a double-walled photochemical cell made of Pyrex glass, equipped with a magnetic stirring bar. Then  $40 \text{ mg}$  of titanium dioxide were added, the solution was sonicated to make the par-

ticles uniform and then thermostated at  $40 \pm 0.5$  °C in a stream of oxygen. A 125 W Philips HPL-N mercury lamp with the highest emitted intensity in the UV region at 366 nm, was used as the irradiation source.

#### *Analytical procedure*

The changes in the concentration of chloride generated during the degradation were monitored using a chloride ion selective electrode (Mettler Toledo Me-51340400) coupled to a saturated calomel electrode (Iskra K401) *via* a potassium nitrate electrolytic bridge and connected to a pH-meter (Radiometer PHM62).  $\text{KNO}_3$  ( $100 \text{ mmol/dm}^3$ ) was added to maintain the ionic strength during irradiation constant.

Changes in the pH during the degradation were monitored by continuous potentiometry using a combined glass electrode (Iskra) connected to a recorder (Goerz Electro, type Servogor SbRE 647.9) *via* a pH-meter (Iskra MA 5706).

For spectrophotometric determinations during the degradation of the substrate in the presence of  $\text{TiO}_2$ , as well as for direct photolysis experiments, aliquots of  $0.2 \text{ cm}^3$  of the reaction mixture were taken at regular time intervals and diluted to  $10.00 \text{ cm}^3$ . The solutions containing  $\text{TiO}_2$  were filtered through membrane filters (Millex-GV,  $0.22 \mu\text{m}$ ) to separate the  $\text{TiO}_2$  particles before their spectra were recorded in the wavelength range from 200 to 400 nm using a Secomam Anthelie Advanced 2 spectrophotometer. The kinetics of the degradation were monitored at 239 nm.

For ion chromatographic determinations, aliquots of  $0.25 \text{ cm}^3$  of the reaction mixture were taken at regular time intervals and diluted to  $10.00 \text{ cm}^3$ . After dilution, these solutions were filtered in the same manner as for the spectrophotometric measurements, and analysed on an ion chromatograph Dionex DX-120 equipped with a Dionex AS14 column and a conductometric detector. The eluent was a mixture of  $\text{Na}_2\text{CO}_3$  ( $3.5 \text{ mmol/dm}^3$ ) and  $\text{NaHCO}_3$  ( $1 \text{ mmol/dm}^3$ ), flow rate  $1.23 \text{ cm}^3/\text{min}$ . For TOC analysis, samples were irradiated for different time intervals and analysed using a Euroglass TOC 1200 analyzer.

## RESULTS AND DISCUSSION

The rate of 2-amino-5-chloropyridine degradation was monitored by measuring the rate of chloride formation because these two processes take place simultaneously. Since our results and the declaration of the manufacturer indicated the presence of chloride in the catalyst, for the calibration of the chloride electrode, titanium dioxide was added to the standard chloride solutions in the same amount as employed for the irradiation experiments.

The effect of the initial concentration of the substrate on the rate of chloride generation, as well as on the rate of substrate disappearance in the presence of titanium dioxide is presented in Fig. 1A. On the basis of these kinetic curves, a linear dependence of  $\ln c/c_0$  on illumination time was obtained for heterogeneous photocatalysis for all the investigated initial concentrations (insert in Fig. 1A). This suggests that over the entire investigated concentration range, the degradation reaction of the substrate is first-order. The calculated values for the rate constant ( $k$ ) are presented in Table I, together with the correlation coefficients for each of the fitted lines, and the corresponding half-life values. As can be seen, the values obtained for the rate constant are significantly higher than those found in literature, which they should be according to a mechanism involving hydroxyl radicals in the presence of titanium dioxide, independent of the type of the compound.<sup>13</sup> This would suggest that the reaction of chloride generation, *i.e.*, degradation of the initial compound, is not

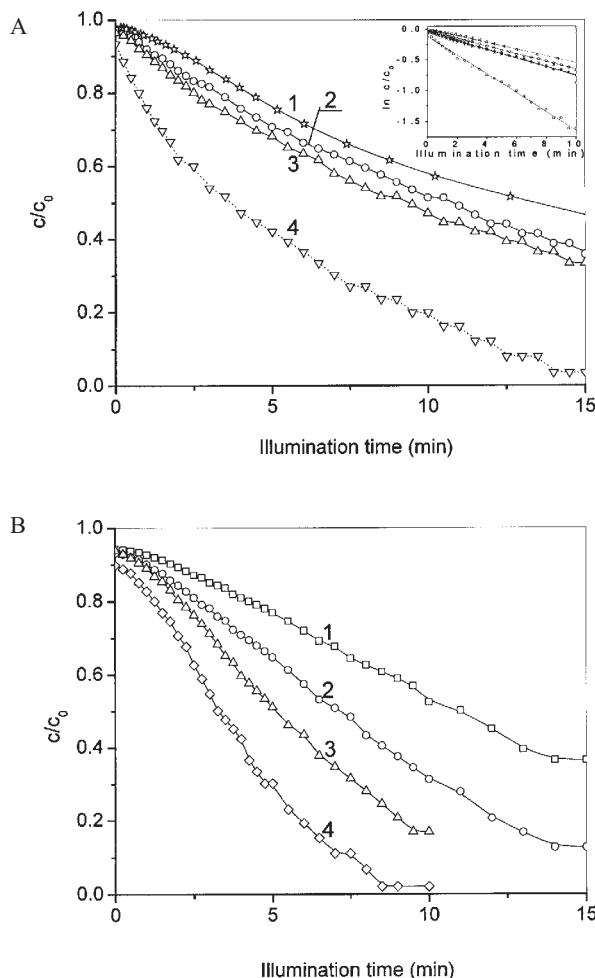


Fig. 1. Effect of the initial concentration of 2-amino-5-chloropyridine on its degradation rate monitored by potentiometry (mmol/dm<sup>3</sup>): (A) (1) 2.9; (2) 2.5; (3) 2.0; (4) 1.0; in the presence of  $\text{TiO}_2$  (2 mg/cm<sup>3</sup>); (B) (1) 2.5; (2) 2.0; (3) 1.5; (4) 1.0; in the reaction of direct photolysis.

governed by hydroxyl radical formation on titanium dioxide, but that it takes place by another mechanism. For this reason the effect of the initial substrate concentration on the kinetics of chloride generation by direct photolysis was also investigated (Fig. 1B). It was found that the reaction of chlorine elimination not only occurs in the absence of titanium dioxide, but that it is faster and of zero-order (Table II), further supporting the assumption that the reaction takes place *via* a different mechanism. In this case, the opacity and light scattering by the titanium dioxide slurry diminishes the intensity of UV light, which explains the lower values for the rate of chloride generation in the presence of titanium dioxide. This effect becomes more evident with increasing initial substrate concentration and can be explained by the fact that there are more substrate molecules at higher concentrations resulting in a lower photon efficiency.

The results represented in Table I also show that the degradation rate in the presence of titanium dioxide depends on the initial 2-amino-5-chloropyridine concentration in a



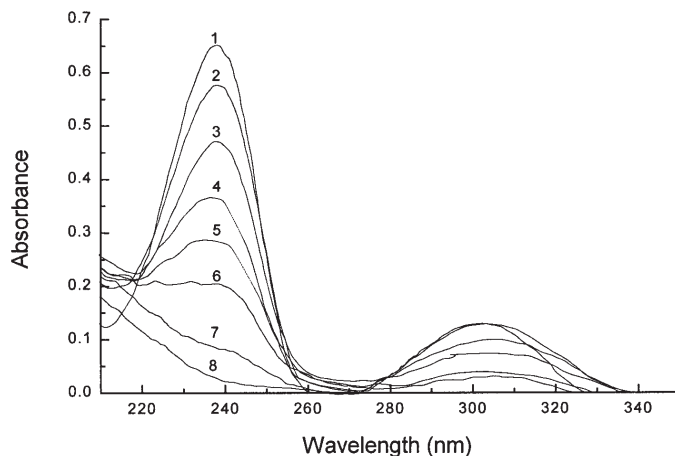


Fig. 2. UV Spectrum profiles during photocatalytic degradation of the 2-amino-5-chloropyridine ( $2.5 \text{ mmol/dm}^3$ ) in the presence of  $\text{TiO}_2$  ( $2 \text{ mg/cm}^3$ ). Illumination time (h): (1) 0; (2) 0.5; (3) 1.0; (4) 2.0; (5) 3.5; (6) 5.5; (7) 8.0; (8) 9.0.

way that the rate constant  $k$  decreases with increasing initial concentration. This finding indicates that the degradation kinetics of 2-amino-5-chloropyridine are not of simple first-order but pseudo-first-order. Furthermore, the slopes of the lines and the  $k$  values presented in Table I show that the reaction rate constant decreases rapidly at lower initial substrate concentrations, while at higher initial concentrations, it decreases more slowly.

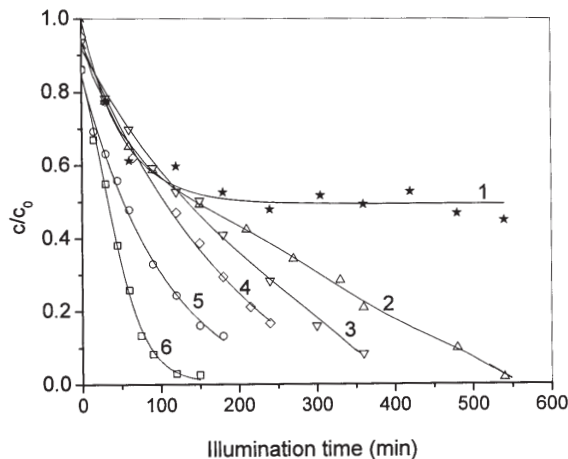


Fig. 3. Kinetic curves for the degradation of the pyridine moiety monitored by spectrophotometry ( $\text{mmol/dm}^3$ ): (1) 2.5; (2) 2.5; (3) 2.1; (4) 1.5; (5) 1.0; (6) 0.5. Curve (1) direct photolysis; curves (2)–(6) in the presence of  $\text{TiO}_2$  ( $2 \text{ mg/cm}^3$ ).

A high rate of the degradation of the initial compound does not necessarily indicate its complete mineralization. Namely, the formation of much more stable, and what is worse probably more toxic intermediates, is very common. For this reason a spectrophotometric method was used for monitoring the rate of the degradation of the pyridine moiety. It was

found that the UV spectrum of the investigated compound has two distinct absorption maxima in the range from 200 to 340 nm (Fig. 2). During illumination, Fig. 2, both the absorption maxima decrease which indicates the destruction of the pyridine moiety. The change in the concentration of the pyridine moieties during illumination are presented in Fig. 3, curves 2–6. From the obtained kinetic curves, it can be concluded that the time necessary for the elimination of chlorine (direct photolysis) is significantly lower (about 25 times) than the time necessary for the complete destruction of the pyridine moieties. This indicates that the chlorine elimination reaction dominates in the first part of the process, after which the reaction of the destruction of the pyridine moieties takes place *i.e.*, the degradation of all the pyridine intermediates.

TABLE I. Effect of the initial concentration ( $c_0$ ) of 2-amino-5-chloropyridine on the photodegradation rate

$c_0/(\text{mmol/dm}^3)$	$10^2 k/\text{min}^{-1}\text{§}$	$r^\dagger$	$t_{1/2}/\text{min}^\ddagger$
1.0	15	0.999	3.76
2.0	7.1	0.999	9.33
2.5	6.3	0.999	10.72
2.9	5.5	0.999	12.56

§First-order rate constant;  $^\dagger$ linear regression coefficient;  $^\ddagger$ half-life

The degradation of the pyridine moieties was also investigated by direct photolysis (Fig. 3, curve 1). As can be seen, complete degradation of the pyridine moieties does not occur, indicating the advantage of the application of heterogeneous photocatalysis.

TABLE II. Effect of the initial concentration ( $c_0$ ) of 2-amino-5-chloropyridine on the direct photolysis rate

$c_0/(\text{mmol/dm}^3)$	$10^4 k/(\text{mol dm}^{-3} \text{ min}^{-1})\text{§}$	$r^\dagger$	$t_{1/2}/\text{min}^\ddagger$
1.0	1.33	0.998	3.41
1.5	1.32	0.999	5.39
2.0	1.28	0.999	7.39
2.5	1.11	0.999	10.96

§Zero-order rate constant;  $^\dagger$ linear regression coefficient;  $^\ddagger$ half-life

Monitoring the kinetics of photocatalytic degradation by means of the change in the pH has mainly been employed for the investigation of simple molecules, such as chloroform, tetrachloromethane or dichloromethane, where practically no intermediates are formed, and therefore the formation of hydronium ions directly corresponds to the kinetics of the degradation of the initial compound.<sup>3</sup> This is not usually the case with more complex molecules where the change in the pH cannot be used for kinetic analysis, but, nevertheless, its monitoring during a photocatalytic process gives valuable insight into the net changes in the investigated system. Thus, the change in the pH monitored during the irradiation of a  $\approx 2.5 \text{ mmol/dm}^3$  2-amino-5-chloropyridine solution (Fig. 4, curve 3) confirms that the process of chloride generation dominates since a sudden drop of pH occurs, although its value is higher than it should be if only hydrochloric acid were formed, indicat-

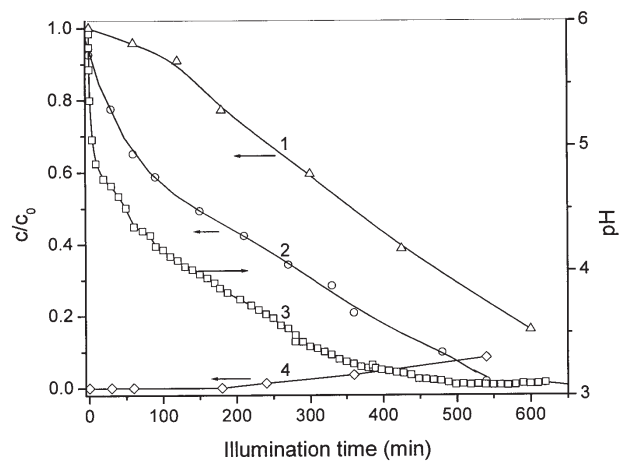


Fig. 4. Typical diagram of the degradation of 2-amino-5-chloropyridine in the presence of  $\text{TiO}_2$  ( $2 \text{ mg/cm}^3$ ): (1) TOC; (2) normalized concentration of the pyridine moiety; (3) pH; (4) normalized nitrate concentration.

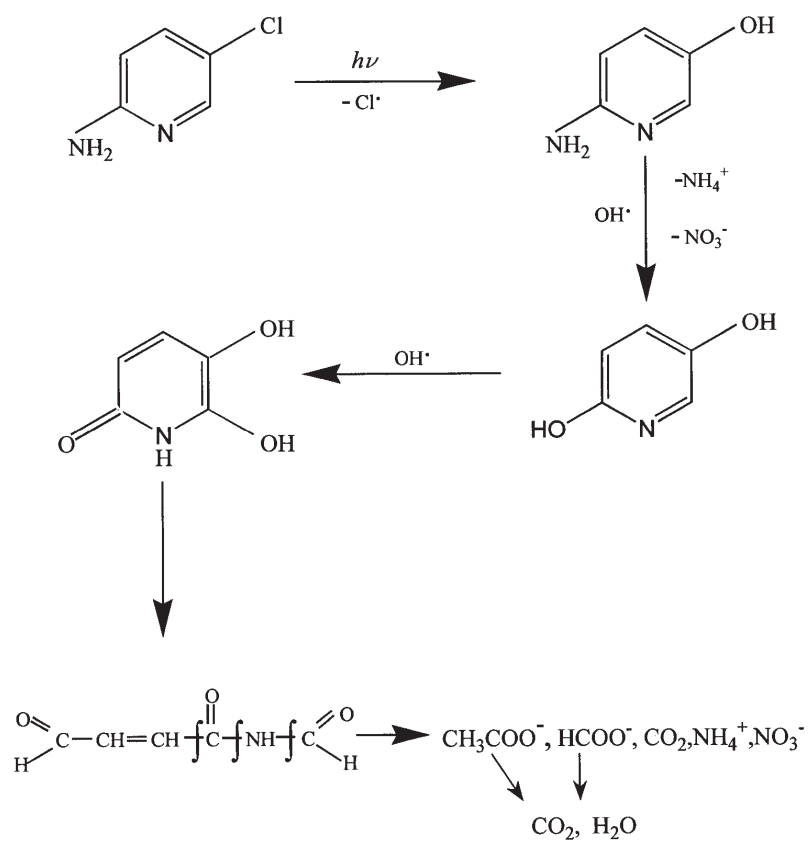


Fig. 5. Possible mechanism for the photocatalytic degradation of 2-amino-5-chloropyridine.

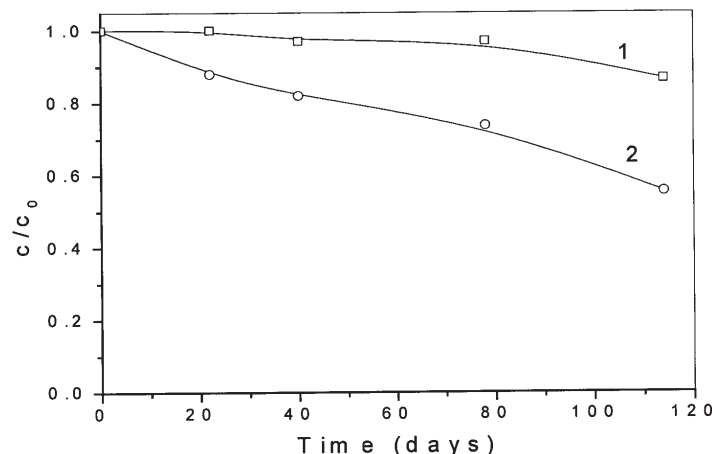


Fig. 6. Kinetics of the degradation of 2-amino-5-chloropyridine (2.5 mmol/dm<sup>3</sup>) in the absence of TiO<sub>2</sub> monitored by spectrophotometry: (1) in the dark; (2) in sunlight.

ing protonation of the pyridine nitrogen, as well as the formation of ammonium ions. The further decrease of pH is most likely due to the formation of formic, acetic and nitric acids. The evolution of nitrate was confirmed by ion chromatography (Fig. 4, curve 4), but only after three hours of illumination and in relatively low concentrations. The continuous decrease of pH value even after the complete degradation of the compound (20 h) indicates the gradual transformation of ammonium ions to nitrate.<sup>2</sup>

As it can be seen from the results of the TOC measurements (Fig. 4, curve 1), during the first part of the process, the change in TOC is small. The subsequent steady decrease of the TOC with time confirms the complete mineralization of the initial compound, as well as the intermediates formed during the process. After 9 h of irradiation (when all the pyridine moieties had been degraded, Fig. 4, curve 2), the initial TOC had been reduced by about 80 %, indicating possible presence of formic and acetic acids.

Taking into account the nature of some of the observed species and the rate of their disappearance, as well as literature data,<sup>2,3,12,15–17</sup> the probable mechanism of the photocatalytic degradation of 2-amino-5-chloropyridine is shown in Fig. 5. As can be seen, in the first stage substitution of the Cl atom by an OH group takes place.<sup>3,12,16</sup> After that the NH<sub>2</sub> group and one of the ring H atoms are substituted by OH radicals.<sup>17</sup> The substituted amino group is further transformed to nitrogen containing inorganic ions (predominantly in the form of NH<sub>4</sub><sup>+</sup>).<sup>17</sup> The parent compound, after transformation into a polyhydroxylic pyridine readily undergoes ring opening and further degradation to acetic and formic acid, carbon dioxide and nitrogen containing inorganic ions (predominantly in the form of NH<sub>4</sub><sup>+</sup>).<sup>2,15</sup> By a further action of OH radicals, the acetic and formic acid are decomposed into CO<sub>2</sub> and H<sub>2</sub>O.

In order to confirm the efficiency of the photocatalytic degradation, the degradation kinetics were monitored in the absence of TiO<sub>2</sub> in both the presence and absence of sunlight. It was found that the substrate decomposes spontaneously under sunlight but at a lower rate (Fig. 6, curve 2). After 115 days of exposition of substrate solutions to daily sunlight about 40 % of the

substrate had been degraded. The solutions protected from sunlight showed no change even after 80 days (Fig. 6, curve 1). These results indicate that, as was expected, the most efficient method for the destruction of the substrate is irradiation in the presence of  $\text{TiO}_2$ .

*Acknowledgement:* The work is financed by the Ministry of Science, Technology and Development of the Republic of Serbia (Project: "Development of New and Improvement of the Existing Analytical Methods and Techniques for Monitoring the Quality of the Environment", No 1622). The authors are grateful to the Department of Inorganic and Analytical Chemistry of the Faculty of Sciences, University of Szeged, for making the TOC measurements possible.

#### ИЗВОД

#### ДИРЕКТНА ФОТОЛИЗА И ФОТОКАТАЛИТИЧКА РАЗГРАДЊА 2-АМИНО-5-ХЛОРПИРИДИНА

БИЉАНА Ф. АБРАМОВИЋ, ВЕСНА Б. АНДЕРЛУХ, АНЂЕЛКА С. ТОПАЛОВ и ФЕРЕНЦ Ф. ГАЛ

*Департаман за хемију, Природно-математички факултет, Трг Д. Обрадовића 3, 21000 Нови Сад*

Испитиване су директна фотолиза и фотокаталитичка разградња 2-амино-5-хлорпиридина, као модел једињења за пестициде који у свом молекулу имају пиридински прстен. Примењене су различите аналитичке технике – потенциометрија, за праћење рН и за настајање хлорида, спектрофотометрија за праћење разградње пиридинског прстена, јонохроматографија за праћење настајања нитрата и анализа укупног органског угљеника ради испитивања ефикасности процеса. Фотокаталитичка разградња је проучавана у воденим суспензијама титан(IV)-оксида уз озрачивање ултраљубичастом светлошћу. Нађено је да је реакција настајања хлорида нултог реда и да се одвија директном фотолизом, те се на тај начин разликује од процеса разградње пиридинског прстена, до ког долази у присуству титан(IV)-оксида. Промена рН у току разградње указује на настајање киселих интермедијера и нитрата поред хлорида. Такође је испитан и утицај почетне концентрације супстрата праћењем како реакције настајања хлорида, тако и реакције разградње пиридинског прстена. Нађено је да је разградња полазног једињења ( $2,5 \text{ mmol/dm}^3$ ) директном фотолизом потпуна за око 20 минута, а пиридинског прстена применом фотокаталитичке разградње за око девет сати. На основу добијених података предложен је могућ механизам реакције.

(Примљено 23. јуна 2003)

#### REFERENCES

1. D. F. Ollis, C. -Y. Hsiao, L. Budiman, C. -L. Lee, *J. Catal.* **88** (1984) 89
2. C. Maillard-Dupuy, C. Guillard, H. Courbon, P. Pichat, *Environ. Sci. Technol.* **28** (1994) 2176
3. J. Theurich, M. Lindner, D. W. Bahnemann, *Langmuir* **12** (1996) 6368
4. A. Bianco Prevot, E. Pramauro, *Talanta* **48** (1999) 847
5. K. -H. Wang, Y. -H. Hsieh, M. -Y. Chou, C. -Y. Chang, *Appl. Catal. B: Environ.* **21** (1999) 1
6. J. -M. Herrmann, C. Guillard, *C. R. Acad. Sci. Paris, Série IIc, Chimie/Chemistry* **3** (2000) 417
7. A. Topalov, D. Molnár-Gábor, M. Kosanić, B. Abramović, *Wat. Res.* **34** (2000) 1473
8. A. Piscopo, D. Robert, J. V. Weber, *Appl. Catal. B: Environ.* **35** (2001) 117
9. A. Topalov, B. Abramović, D. Molnár-Gábor, J. Csanádi, O. Arcson, *J. Photochem. Photobiol. A: Chem.* **140** (2001) 249
10. S. Malato, J. Blanco, J. Cáceres, A. R. Fernández-Alba, A. Agüera, A. Rodríguez, *Catal. Today* **76** (2002) 209
11. S. Parra, J. Olivero, C. Pulgarin, *Appl. Catal. B: Environ.* **36** (2002) 75

12. I. Ilisz, A. Dombi, K. Mogyorósi, A. Farkas, I. Dékány, *Appl. Catal. B: Environ.* **39** (2002) 247
13. C. S. Turchi, D. F. Ollis, *J. Catal.* **122** (1990) 178
14. C. Tomlin, (Ed.), *The Pesticide Manual*, 10<sup>th</sup> Ed., Crop Protection Publications, 1995.
15. G. K. – C. Low, S. R. McEvoy, R. W. Matthews, *Environ. Sci. Technol.* **25** (1991) 460
16. L. Meunier, P. Boule, *Pest Manag. Sci.* **56** (2000) 1077
17. E. Brillas, E. Mur, R. Sauleda, L. Sánchez, J. Peral, X. Doménech, J. Casado, *Appl. Catal. B: Environ.* **16** (1998) 31.

## Normal-phase high performance liquid chromatography of estradiol derivatives on amino- and diol- columns

MARIJANA M. AČANSKI

*Department of General and Inorganic Chemistry, Faculty of Technology, University of Novi Sad, Bulevar cara Lazara 1, 21000 Novi Sad, Serbia and Montenegro (e-mail: marijana@tehnol.ns.ac.yu)*

(Received 7 April, revised 13 August 2003)

**Abstract:** The retention behaviour of estradiol derivatives was studied by HPLC on chemically bonded polar stationary phases: commercially available amino- and diol- columns, as a function of the heptane-propan-1-ol as the mobile phase, when the volume fraction of propan-1-ol in the binary mobile phase was low, even less than 5 %. The relationship between the logarithm of the retention constant ( $\log k$ ) and the logarithm of the volume fraction of propan-1-ol ( $-\log \varphi$ ) in the eluent was linear for all solutes studied. The results are discussed in terms of the solute and stationary phase properties and compared with the results of the same derivatives obtained in earlier investigations.

**Keywords:** HPLC, amino- and diol- columns, non-aqueous eluent, estradiol derivatives, retention behaviour.

### INTRODUCTION

Estrogens<sup>1</sup> are important physiologically active substances produced by the ovaries. Among the most important estrogens is estradiol. Some simple chemical modification of the basic structure of the steroid can have a direct effect on the activity, in particular on the binding activity, of estradiol.

In our previous papers<sup>2–6</sup> the retention behaviour and retention mechanism of some estradiol and estrone derivatives chromatographed on silica gel, alumina, chemically bonded polar phases and C-18 bonded silica gel in normal and reversed phase, using several non-aqueous and aqueous eluents, was described. The type of the stationary and mobile phases, as well as the nature, number, and position of substituents in the molecule of the steroids were observed to have significant and distinct effects on the retention.

Non-aqueous mobile phases are more often used with chemically bonded polar stationary phases<sup>7–10</sup> than are aqueous mobile phases. Amino- and diol- stationary phases bonded on a silica gel support, comprising three carbon atoms (aminopropyl and 1,2-dihydroxypropylether), are less polar than non-modified silica gel or alumina adsorbents. The bonded chains are not long enough to provide efficient shielding of the residual silanol

groups, which could not be modified in the silanization procedure because of steric reasons. As a result of this, chemically bonded polar stationary phases provide for more specific interaction at the surface and have operating advantages over traditional silica gel columns.

Several studies have reported that the competitive model of adsorption can be used to describe retention on chemically bonded polar phases in normal-phase chromatography.<sup>4,11–13</sup> This model yields, with some simplification, Eq. (1) describing the dependence of the retention (capacity factor,  $k$ ) on the mole fraction of the polar solvent,  $N_b$ , in a binary mobile phase comprised of a polar solvent and a none-polar one<sup>14</sup>:

$$\log k = \log k_0 - n \log N_b \quad (1)$$

In this exponential equation,  $n$  is a constant giving the ratio of the molecular area on the adsorbent surface occupied by one molecule of the sample solute to that occupied by one molecule of the polar solvent. The concentration can often be expressed as the volume fraction,  $\varphi$ , instead of the mole fraction:<sup>15</sup>

$$\log k = \log k_0 - n \log \varphi \quad (2)$$

In addition, the competitive model does not take into account so-called secondary solvent effects. These effects, resulting from solute–solvent interactions in both the mobile and adsorbed phases, give rise to some of the most useful changes in retention and are often the source of chromatographic selectivity.

Although Eq. (2) is widely known in the chromatographic literature, Jandera and Churaček<sup>15</sup> have shown that for normal phase liquid–liquid chromatography the relationship between logarithm retention constant  $\log k$  and volume fraction of the more polar component,  $\varphi$ , in a binary eluent is better represented by the quadratic expression:

$$\log k = a\varphi^2 + b\varphi + c \quad (3)$$

Assuming that the quadratic term can be ignored, to a first approximation, they obtained Eq. (4):

$$\log k = \log k_0 - m\varphi \quad (4)$$

This model<sup>15</sup> interprets that the retention and retention mechanism are governed by a partitioning process.

This paper investigates the retention behaviour and retention mechanism of estradiol derivatives on amino- (aminopropyl) and diol- (1,2-dihydroxypropylether) columns using heptane-propan-1-ol eluents. The volume fraction of propan-1-ol in the binary mobile phases was low, even less than 5 %.

The compounds and their molecular structures are listed in Table I.

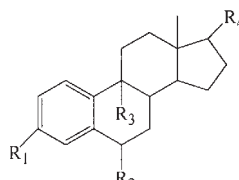
#### EXPERIMENTAL

The separations were performed with a Milton Roy (Riviera Beach, FL, USA) Consta Metric 3000 pump and a Milton Roy Spectro Monitor 3160 variablewavelength UV-vis detector set at 254 nm. The samples were injected using a Rheodyne 7125 valve (Cotati, CA, USA) fitted with a 20  $\mu$ L loop. The columns



used were commercially available 5  $\mu\text{m}$  LiChrosorb  $\text{NH}_2$  and LiChrosorb DIOL, 250 $\times$ 4 mm i.d. (E. Merck, Darmstadt, Germany).

TABLE I. IUPAC names and chemical structures of the studied compounds



No.	IUPAC Name	R <sub>1</sub>	R <sub>2</sub>	R <sub>3</sub>	R <sub>4</sub>
1	3,17 $\beta$ -Dihydroxyestra-1,3,5(10)-triene (estradiol)	OH			OH
2	3-Methoxy-17 $\beta$ -hydroxyestra-1,3,5(10)-triene	<sup>a</sup> )OMe			OH
3	3-Acetoxy-17 $\beta$ -hydroxyestra-1,3,5(10)-triene	<sup>b</sup> )OAc			OH
4	3,17 $\beta$ -Diacetoxyestra-1,3,5(10)-triene	OAc			OAc
5	3-Propionyloxy-17 $\beta$ -hydroxyestra-1,3,5(10)-triene	<sup>c</sup> )OPr			OH
5a	3-Hydroxy-17 $\beta$ -propionyloxy estra-1,3,5(10)-triene	OH			OPr
6	3,17 $\beta$ -Dipropionyloxyestra-1,3,5(10)-triene	OPr			OPr
7	3-Benzoyloxy-17 $\beta$ -propionyloxy estra-1,3,5(10)-triene	<sup>d</sup> )OBz			OH
8	3,17 $\beta$ -Dibenzoyloxyestra-1,3,5(10)-triene	OBz			OBz
9	3-Acetoxy-17 $\beta$ -benzoyloxyestra-1,3,5(10)-triene	OAc			OBz
10	3,17 $\beta$ -Dihydroxyestra-1,3,5(10)-triene-6-one	OH	=O		OH
11	3-Methoxy-17 $\beta$ -hydroxyestra-1,3,5(10)-triene-6-one	OMe	=O		OH
12	3-Hydroxy-17 $\beta$ -propionyloxy estra-1,3,5(10)-triene-6-one	OH	=O		OPr
13	3,17 $\beta$ -Dipropionyloxy-1,3,5(10)-triene-6-one	OPr	=O		OPr
14	3,9 $\alpha$ -Dihydroxy-17 $\beta$ -propionyloxyestra-1,3,5(10)-triene-6-one	OH	=O	$\alpha$ -OH	OPr
15	3,17 $\beta$ -Dipropionyloxy-9 $\alpha$ -hydroxyestra-1,3,5(10)-triene-6-one	OPr	=O	$\alpha$ -OH	OPr

<sup>a</sup>)OMe-OCH<sub>3</sub>, <sup>b</sup>)OAc-OCOCH<sub>3</sub>, <sup>c</sup>)OPr-OCOCH<sub>2</sub>CH<sub>3</sub>, <sup>d</sup>)OBz-OCOC<sub>6</sub>H<sub>5</sub>

The estradiol derivatives (Table I), synthesized by original reactions or according to literature methods,<sup>16</sup> were dissolved (0.005 mg mL<sup>-1</sup>) in methanol and the solutions prefiltered through a 0.2  $\mu\text{m}$  Chromafil filter (Macherey-Nagel, Düren, Germany).

One binary solvent system, heptane–propan-1-ol was used as the mobile phase with varying contents of the more polar component; propan-1-ol 1–20 %; increments 2 and 5 %. The solvents used to prepare the mobile phases were of analytical grade and were filtered through a 0.45  $\mu\text{m}$  filter and degassed before use. The flow rate was 1 mL min<sup>-1</sup> at room temperature.

The retention factor,  $k$ , was calculated from  $k = (t_r - t_0)/t_0$ , where  $t_r$  is the retention time of the solute and  $t_0$  the column void time measured using the solvent disturbance peak obtained when trace amounts of methanol were injected into the column. Each  $t_r$  value was measured in triplicate and averaged.

## RESULTS AND DISCUSSION

The logarithmic relationship between the retention factor,  $k$ , of the investigated compounds and the volume fraction,  $\varphi$ , of the propan-1-ol as the stronger solvent in the binary

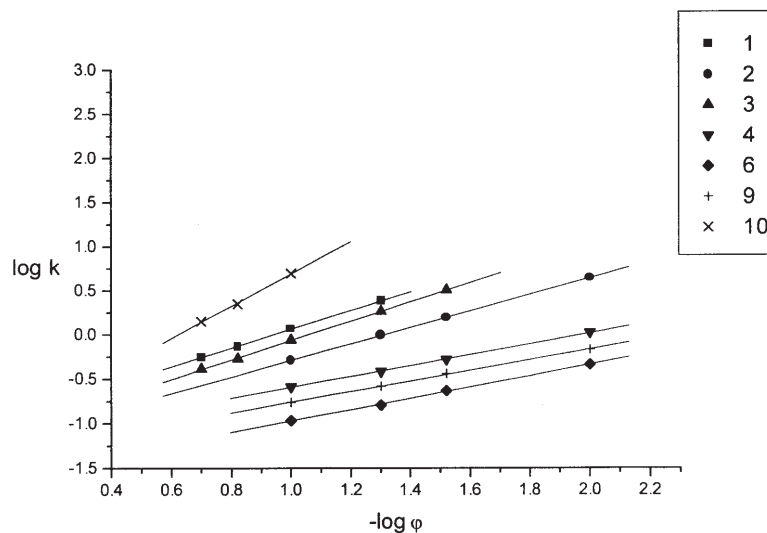


Fig. 1. Correlation lines of Eq. (2) for the amino column and eluent heptane–propan-1-ol; compound designation as in Table I.

eluent, for both columns was linear. This behaviour suggests that the model based on Eq. (2) is suitable to describe the experimental behaviour of estradiol derivatives on both columns. The numerical data for  $\log k$  and the constants  $n$  and  $\log k_0$  for each studied compound for the amino- and diol- column with heptane–propan-1-ol as the eluent are presented in Tables II and III, respectively. The correlation coefficients from linear regression analysis of the experimental  $\log k$  values varied from 0.9959 to 1. The linear relationship between the logarithm of the retention constant and the logarithm of the volume fraction of

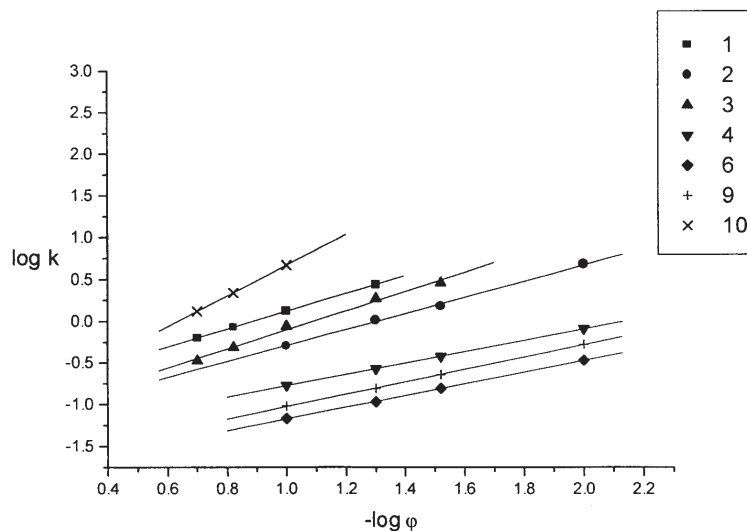


Fig. 2. Correlation lines of Eq. (2) for the diol column and eluent heptane–propan-1-ol; compound designation as in Table I.

propan-1-ol in the eluent for compounds 1, 2, 3, 4, 6, 9 and 10 on the amino- and diol- columns are presented in Figs. 1 and 2, respectively.

TABLE II. Retention data and constants  $n$  and  $\log k_0$  of Eq. (2) of the estradiol derivatives for the amino column;  $r$ -correlation coefficient;  $\varphi$  is the concentration of propan-1-ol % (v/v) in the binary mobile phase heptane–propan-1-ol

$\varphi$	0.2	0.15	0.1	0.05	0.03	0.01			
$-\log \varphi$	0.7	0.82	1	1.3	1.52	2			
Comp.	$\log k$						$n$	$\log k_0$	$r$
1	-0.25	-0.134	0.065	0.383	—	—	1.06	-0.998	0.9999
2	—	—	-0.291	-0.004	0.191	0.643	0.93	-1.221	0.9999
3	-0.386	-0.271	-0.06	0.265	0.506	—	1.1	-1.159	0.9999
4	—	—	-0.586	-0.412	-0.28	0.002	0.59	-1.176	0.9999
5	-0.526	-0.381	-0.18	0.158	0.41	—	1.14	-1.317	0.9999
5a	-0.468	-0.313	-0.098	0.313	0.529	—	1.24	-1.328	0.9988
6	—	—	-0.966	-0.78	-0.63	-0.34	0.63	-0.1599	0.9944
7	-0.468	-0.318	-0.131	0.2	0.44	—	1.1	-1.229	0.9998
8	—	—	-0.852	-0.676	-0.53	-0.24	0.61	-1.469	0.9998
9	—	—	-0.762	-0.58	-0.44	-0.17	0.59	-1.35	0.9996
10	0.153	0.35	0.698	—	—	—	1.83	-1.133	0.9991
11	-0.177	-0.029	0.257	0.63	—	—	1.36	-1.129	0.9991
12	-0.294	-0.163	0.1	0.454	—	—	1.26	-1.182	0.9999
13	—	—	-0.278	-0.043	0.131	0.504	0.78	-1.06	0.9999
14	0.112	0.301	0.646	—	—	—	1.79	-1.151	0.9986
15	-0.267	-0.082	0.217	0.62	—	—	1.48	-1.294	0.9988

The retention behaviour of the estradiol derivatives on both columns were very similar and in accordance with the general retention behaviour in normal phase liquid chromatography. The retention sequence obtained with the eluent heptane–propan-1-ol is that predicted on the basis of the polarity of the compounds; the more polar solutes, compounds 1, 10 and 14 were more strongly retained and *vice versa*.

All the studied estradiol derivatives are more strongly retained on the amino column than on the diol column. Namely, both functions can form hydrogen bonds using both their own hydrogen atoms and hydrogen originating from the solute or solvent molecules, but only the amino function can be protonated.

The adsorption characteristics of the stationary phase of both columns are the consequence of proton acceptor-donor behaviour.

The slopes for the same compounds on the different columns (Tables II and III) were very similar. Because of this it was possible to average the values. Slope  $n$  in Eq. (2) is the change of the retention constant  $\log k$  with the change of the volume fraction,  $\varphi$ , in the eluent and can be expressed as:

$$n = \frac{d(\log k)}{d(\log \varphi)} \quad (5)$$

TABLE III. Retention data and constants  $n$  and  $\log k_0$  of Eq. (2) of the estradiol derivatives for the diol column;  $r$ -correlation coefficient;  $\varphi$  is the concentration of propan-1-ol % (v/v) in the binary mobile phase heptane–propan-1-ol

$\varphi$	0.2	0.15	0.1	0.05	0.03	0.01			
$-\log \varphi$	0.7	0.82	1	1.3	1.52	2			
Comp.	$\log k$						$n$	$\log k_0$	$r$
1	-0.199	-0.069	0.13	0.44	—	—	1.07	-0.942	0.9999
2	—	—	-0.289	0.018	0.185	0.676	0.96	-0.243	0.9994
3	-0.474	-0.313	-0.058	0.272	0.458	—	1.14	-1.245	0.9959
4	—	—	-0.769	-0.568	-0.42	-0.088	0.68	-1.453	0.9999
5	-0.535	-0.435	-0.169	0.156	0.354	—	1.16	-1.38	0.9960
5a	-0.568	-0.364	-0.082	0.277	0.51	—	1.31	-1.439	0.9961
6	—	—	-1.165	-0.966	-0.805	-0.468	0.7	-1.869	0.9999
7	-0.56	-0.41	-0.145	0.176	0.383	—	1.16	-1.346	0.9969
8	—	—	-1.12	-0.896	-0.736	-0.388	0.73	-1.849	0.9999
9	—	—	-1.018	-0.805	-0.639	-0.276	0.74	-1.767	0.9999
10	0.123	0.343	0.67	—	—	—	1.82	-1.152	1
11	-0.201	-0.051	0.17	0.535	—	—	1.32	-1.173	0.9999
12	-0.363	-0.195	0.063	0.411	—	—	1.29	-1.253	0.9985
13	—	—	-0.482	-0.24	0.078	0.274	0.75	-1.227	0.9997
14	0.081	0.296	0.641	—	—	—	1.87	-1.232	0.9998
15	-0.375	-0.195	0.091	0.479	—	—	1.43	-1.362	0.9988

From Eq. (5) it is clear that the retention of a compound which has a slope decreases faster with increasing  $\varphi$  in comparison with a compound which has a lower values of the constant  $n$ . With increasing  $\varphi$ , the interactions solute-stationary phase are reduced but the interactions solute-mobile phase are increased. On silica gel,<sup>2,17-19</sup> the retention and slope are strictly a function of the polarity of compound. More polar compounds have larger retentions and a bigger slope. However, in this and in earlier investigations<sup>4</sup> on chemically bonded phases, this rule was not confirmed. The retention order of the estradiol derivatives on both columns for  $\varphi = 0.1$  and order of the average values of constant  $n$  are as follows:

Amino 10>14>11>.15>12>1>3>5a>7>5>13>2>4>9>8>6

Diol 10>14>11>1>15>12>3>5a>7>5>2>13>4>9>8>6

$n^-$  10 = 14> 15> 7>3>11>12=5a>5>1>2>13>9=9=6>4

As the slopes of the solutes were not in accordance with their retention values there was no correlation between  $n$  and  $\log k_0$  of the compounds.

## ИЗВОД

## ВИСОКО ПРИТИСНА ТЕЧНА ХРОМАТОГРАФИЈА ДЕРИВАТА ЕСТРАДИОЛА НА АМИНО- И ДИОЛ- КОЛОНИ СА НЕВОДЕНОМ ПОКРЕТНОМ ФАЗОМ

МАРИЈАНА М. АЧАНСКИ

Одељење за општу и неорганску хемију, Технолошки факултет, Универзитет у Новом Саду,  
Булевар цара Лазара 1, 21000 Нови Сад

У раду је применом високо притисне течне хроматографије испитано ретенционо понашање деривата естрадиола на аминок- и диол- хемијски везаној фази. Као покретна фаза коришћена је смеша хептан-1-пропанола, у различитим односима. Удео 1-пропанола био је низак, у неким покретним фазама мањи од 5 %. Ретенционо понашање испитиваних деривата је дискутовано са аспекта природе растворка, непокретне и покретне фазе. За све испитане деривате добијена је линеарна зависност између логаритма ретенционе константе и логаритма запреминског удела поларније компоненте покретне фазе тј., 1-пропанола. Иако су ретенциона времена деривата естрадиола дужа на аминок колони, ефикасност раздвајања на различитим колонама је веома слична. Добијени резултати су упоређени и са ретенционим подацима истих једињења добијених у ранијим испитивањима на силика гелу.

(Примљено 7. априла, ревидирано 13. августа 2003)

## REFERENCES

1. E. Palomino, in E. J. Parish, W. D. Nes, Eds., *Biochemistry and Function of Sterols*, CRC Press, Boca Raton, FL, 1997, p. 245, Chapter 18
2. S. M. Petrović, M. Ačanski, V. Pejanović, J. Petrović, *J. Planar Chromatogr.* **6** (1993) 29
3. S. M. Petrović, M. Ačanski, Lj. Kolarov, E. Lončar, *J. Planar Chromatogr.* **8** (1995) 200
4. S. M. Petrović, M. Ačanski, V. Pejanović, J. Petrović, *Chromatographia* **43** (1996) 551
5. M. M. Ačanski, S. M. Petrović, V. M. Pejanović, J. A. Petrović, *J. Serb. Chem. Soc.* **65** (2000) 811
6. M. M. Ačanski, *J. Serb. Chem. Soc.* **68** (2003) 163
7. M. Prošek, M. Pukl, *Kvantitativna planarna kromatografija*, Хемијски институт Борис Кидрич, Завод Републике Словеније за шолство и спорт, 1991, p. 30 (in Serbian)
8. ChromBook Merck 2nd Edition, Darmstadt, Germany, p. 45
9. D. Milojković-Opsenica, *Chem. Review* **41** (2000) 38
10. J. G. Dorsey, W. T. Copper, *Anal. Chem.* **66** (1994) 857
11. J. Fischer, P. Jandera, *J. Chromatogr. A* **684** (1994) 77
12. S. Hara, S. Ohnishi, *J. Liq. Chromatogr.* **7** (1984) 59
13. S. Hara, S. Ohnishi, *J. Liq. Chromatogr.* **2** (1984) 69
14. L. R. Snyder, *Anal. Chem.* **46** (1981) 1384
15. P. Jandera, J. Churaček, *J. Chromatogr.* **91** (1974) 207
16. V. Pejanović, *Ph. D. Thesis*, Faculty of Science, Novi Sad, 1991
17. S. M. Petrović, Lj. A. Kolarov, E. S. Traljić, J. A. Petrović, *Anal. Chem.* **54** (1982) 934
18. S. M. Petrović, Lj. A. Kolarov, J. A. Petrović, *Chromatographia* **18** (1984) 145
19. S. M. Petrović, M. Ačanski, *J. Planar. Chromatogr.* **2** (1989) 214.

## The role of titanium oxide concentration profile of titanium oxide of RuO<sub>2</sub>-TiO<sub>2</sub> coatings obtained by the sol-gel procedure on its electrochemical behavior

VLADIMIR V. PANIĆ<sup>1\*#</sup>, ALEKSANDAR B. DEKANSKI<sup>1#</sup>, VESNA B. MIŠKOVIĆ-STANKOVIĆ<sup>2#</sup>,  
SLOBODAN K. MILONJIĆ<sup>3#</sup> and BRANISLAV Ž. NIKOLIĆ<sup>2#</sup>

<sup>1</sup>ICTM–Center of Electrochemistry, University of Belgrade, Njegoševa 12, P.O. Box 473, 11001 Belgrade,

<sup>2</sup>Faculty of Technology and Metallurgy, University of Belgrade, Karnegijeva 4, P.O. Box 3503, 11120 Belgrade and <sup>3</sup>Vinča Institute of Nuclear Sciences, P.O. Box 522, 11001 Belgrade, Serbia and Montenegro

(Received 1 August 2003)

**Abstract:** In order to understand the role of TiO<sub>2</sub> in the deactivation mechanism of an active RuO<sub>2</sub>-TiO<sub>2</sub> coating, an additional TiO<sub>2</sub> layer was introduced in the support/coating inter-phase of regular Ti/[RuO<sub>2</sub>-TiO<sub>2</sub>] anode in one case and on the surface of the coating in the other. The electrochemical behavior of these, with TiO<sub>2</sub> enriched, anodes was compared with the behavior of anodes with regular RuO<sub>2</sub>-TiO<sub>2</sub> coatings, which were subjected to an accelerated stability test. A high-frequency semicircle in the complex plane plot, obtained by electrochemical impedance spectroscopy, for a regular RuO<sub>2</sub>-TiO<sub>2</sub> coating corresponds to TiO<sub>2</sub> enrichment in the coating as a consequence of anode corrosion. In the case of the coatings with additional TiO<sub>2</sub> layers, a high-frequency semicircle was not observed. The additional TiO<sub>2</sub> layers increase the coating overall resistance and influence the coating impedance behavior at low frequencies. Similar equivalent electrical circuits were used to analyze the impedance behavior of coatings having an additional TiO<sub>2</sub> layer at different position within RuO<sub>2</sub>-TiO<sub>2</sub> coating.

**Keywords:** RuO<sub>2</sub>-TiO<sub>2</sub> coating, corrosion stability, oxide sols, sol-gel procedure, electrochemical impedance spectroscopy.

### INTRODUCTION

Dimensionally stable anodes lose their electrocatalytic activity during long-term electrolysis, which leads to the end of their service life of an anode. Corrosion stability, *i.e.*, anode service life, can be monitored by an accelerated stability test (AST),<sup>1–4</sup> which is based on the galvanostatic electrolysis of a dilute chloride solution at relatively high current density. In the AST, the end of the service life of an anode is seen as a sudden increase of the potential at constant current, which is caused by an increase in the coating resistance. The increase in resistance could be a consequence of the growth of an insulating TiO<sub>2</sub> layer in

\* Corresponding author.

# Serbian Chemical Society active member.

the substrate|coating interphase, caused by the oxidation of the Ti substrate, and/or by the anodic dissolution of catalytically active Ru species, which enriches the coating surface with insulating  $\text{TiO}_2$ . An erosion of the coating can also be involved in this deactivation pathway.<sup>1,5</sup> The anode deactivation mechanism depends on the coating morphology. In earlier works,<sup>4,6</sup>  $\text{Ti}/[\text{RuO}_2\text{--TiO}_2]$  anodes with considerably different service life were obtained by changing the conditions in the sol-gel procedure for the coating preparation, which resulted in oxide particles of different size and, consequently, differences in the coating morphology. Also, sol-gel prepared anodes have considerably longer service life than corresponding anodes prepared by the thermal decomposition of ruthenium and titanium chloride.<sup>3,4</sup>

Electrochemical impedance spectroscopy (EIS) can provide useful information on the deactivation mechanism of oxide coatings.<sup>2,7–9</sup> The appearance of a semicircle in the high frequency domain of a complex plane plot indicates the loss of the electrocatalytic activity of the  $\text{RuO}_2\text{--TiO}_2$  coating.<sup>9</sup> The resistance related to this semicircle does not depend on the electrode potential at which the EIS data were collected, but does depend on the employed electrolyte and its conductivity.<sup>9</sup> Boots and co-workers<sup>2,7</sup> registered similar impedance behavior for corroded  $\text{RuO}_2\text{--IrO}_2$  and  $\text{RuO}_2\text{--Co}_3\text{O}_4$  coatings.

From our earlier results<sup>9</sup> and literature data,<sup>2,7</sup> it is not clear whether the insulating  $\text{TiO}_2$  layer, which causes the appearance of a semicircle, grows in the Ti substrate|coating interphase and/or on the surface of the corroded coating. The aim of this work was to investigate the influence of the concentration profile of titanium oxide in the  $\text{RuO}_2\text{--TiO}_2$  coating on the electrochemical behavior of the anode, which should provide useful information about the anode deactivation mechanism.

## EXPERIMENTAL

### *Preparation of anodes*

The forced hydrolysis of chloride salts in extremely acid aqueous solutions at boiling temperature was used to prepare  $\text{RuO}_2$  and  $\text{TiO}_2$  sols.<sup>3,4</sup> The solutions were aged for 46 h ( $\text{RuO}_2$  sol preparation) and 30 h ( $\text{TiO}_2$  sol preparation), in order to obtain the coating with the best characteristics.<sup>4</sup> The oxide sols were mixed in amounts to produce a coating composition of 40 % at. Ru–60 %at. Ti. To prepare the regular  $\text{RuO}_2\text{--TiO}_2$  coating, an appropriate amount of the mixture of sols, which would produced an amount of coating of  $0.5 \text{ mg cm}^{-2}$  counted to the binary oxide, was applied onto titanium plates ( $2 \text{ cm} \times 2 \text{ cm} \times 1 \text{ mm}$ ). After drying at  $70^\circ\text{C}$  in air, whereby a gel phase is formed on the surface, the sample was calcined at  $450^\circ\text{C}$  in air. The additional  $\text{TiO}_2$  layer in the substrate|coating interphase of a regular  $\text{Ti}/[\text{RuO}_2\text{--TiO}_2]$  anode was obtained by application of the appropriate amount of  $\text{TiO}_2$  sol (to produce an amount of  $0.3 \text{ mg cm}^{-2}$  of  $\text{TiO}_2$ ) and thermal treatment under the same temperature regime. A  $\text{TiO}_2$  layer on the coating surface was obtained in the same manner. Consequently, the notations of the investigated anodes are:  $\text{Ti}/[\text{RuO}_2\text{--TiO}_2]$ ,  $\text{Ti}/\text{TiO}_2/[\text{RuO}_2\text{--TiO}_2]$  and  $\text{Ti}/[\text{RuO}_2\text{--TiO}_2]/\text{TiO}_2$ . In some experiments, two  $\text{TiO}_2$  layers were formed on the active  $\text{RuO}_2\text{--TiO}_2$  coating surface.

### *Accelerated stability test of $\text{Ti}/[\text{RuO}_2\text{--TiO}_2]$ anode*

The AST of the  $\text{Ti}/[\text{RuO}_2\text{--TiO}_2]$  anode was performed by electrolysis of  $0.5 \text{ mol dm}^{-3}$  NaCl, pH 2, at a constant current density of  $400 \text{ mA cm}^{-2}$  and a temperature of  $25^\circ\text{C}$ , in a cell with a Pt plate counter electrode. The changes in the anode potential were recorded during the AST. A sudden increase of the potential implies that the anode can no longer be used in practice (the end of service life). Illustration of an AST is given in Fig. 1.

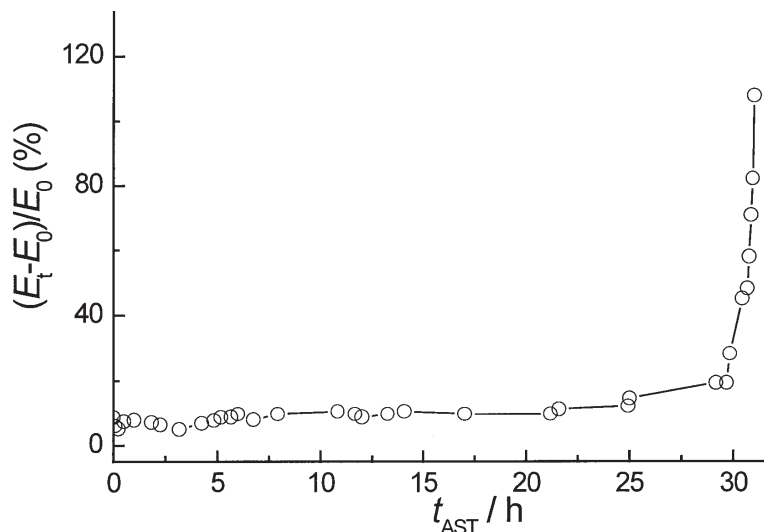


Fig. 1. Accelerated stability test of a regular Ti/RuO<sub>2</sub>-TiO<sub>2</sub> anode. Electrolyte: 0.5 mol dm<sup>-3</sup> NaCl, pH 2; temperature: 25 °C; current density: 400 mA cm<sup>-2</sup>.

#### Investigation of anode properties

The electrochemical properties of Ti//TiO<sub>2</sub>/[RuO<sub>2</sub>-TiO<sub>2</sub>] and Ti//[RuO<sub>2</sub>-TiO<sub>2</sub>]/TiO<sub>2</sub> anode as well as the properties of Ti//[RuO<sub>2</sub>-TiO<sub>2</sub>] anode before and after AST were investigated by cyclic voltammetry (CV) and EIS in 1 mol dm<sup>-3</sup> HClO<sub>4</sub> and by polarization measurements in 0.5 mol dm<sup>-3</sup> NaCl, pH 2. The cell was equipped with a magnetic stirrer, a Pt plate as counter electrode and a saturated calomel electrode (SCE) as the reference electrode. All potentials are expressed on the SCE scale. The impedance data were recorded using a 5 mV amplitude of sinusoidal voltage around the potential of 1.25 V over a frequency range of 100 kHz to 50 mHz and analyzed using a suitable fitting procedure.<sup>10</sup> The experiments were performed at room temperature.

## RESULTS AND DISCUSSION

#### Cyclic voltammetry

The cyclic voltammograms of a fresh (before AST) Ti//[RuO<sub>2</sub>-TiO<sub>2</sub>] anode, a corroded (after AST) Ti//[RuO<sub>2</sub>-TiO<sub>2</sub>] anode, a Ti//TiO<sub>2</sub>/[RuO<sub>2</sub>-TiO<sub>2</sub>] and a Ti//[RuO<sub>2</sub>-TiO<sub>2</sub>]/TiO<sub>2</sub> anode are shown in Fig. 2. Within the potential window of electrolyte stability, the voltammograms are of similar shape, which is characteristic for the pseudocapacitive behavior of this type of electrode material.<sup>11</sup> The anodes with an additional TiO<sub>2</sub> layer seem to be more active for hydrogen evolution than the regular Ti//[RuO<sub>2</sub>-TiO<sub>2</sub>] anode. The voltammogram of the corroded anode and of the anodes containing an additional TiO<sub>2</sub> layer are tilted due to the considerable resistance of the coating, indicating the greater resistance of the Ti//TiO<sub>2</sub>/[RuO<sub>2</sub>-TiO<sub>2</sub>] compared to the Ti//[RuO<sub>2</sub>-TiO<sub>2</sub>]/TiO<sub>2</sub> anode. This means that a more compact TiO<sub>2</sub> layer is formed in the interphase than on the coating surface. The insulating TiO<sub>2</sub> layer on the coating surface covers the active sites on the surface, but the inner active sites (in pores and cracks) are still active. The capacitive behavior is related to the inner active sites



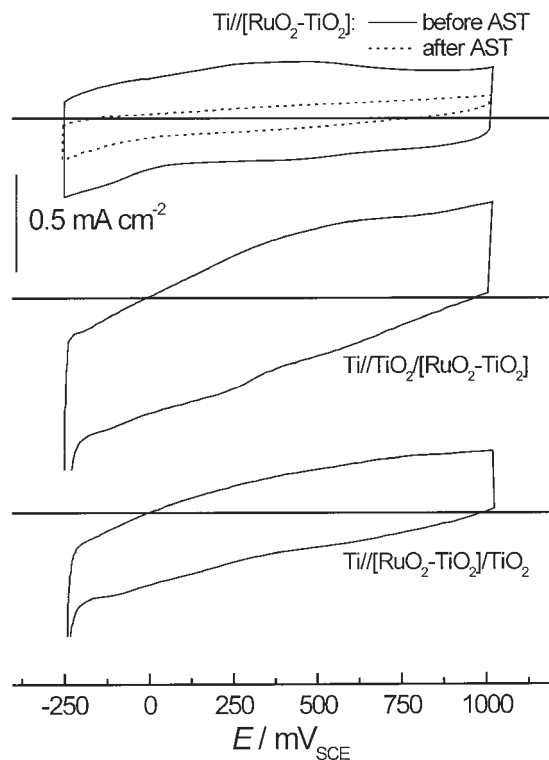


Fig. 2. Cyclic voltammograms of the Ti//[RuO<sub>2</sub>-TiO<sub>2</sub>] anode recorded before and after AST and of the Ti/TiO<sub>2</sub>/[RuO<sub>2</sub>-TiO<sub>2</sub>] and Ti//[RuO<sub>2</sub>-TiO<sub>2</sub>]/TiO<sub>2</sub> anode. Electrolyte: 1 mol dm<sup>-3</sup> HClO<sub>4</sub>, room temperature. Sweep rate: 20 mV s<sup>-1</sup>.

with capacitance and pore resistance in series. The number of active sites accessible to the electrolyte, *i.e.*, the electrochemically active surface area,<sup>4</sup> corresponds to the surface area under the anodic part of the voltammetric curves. The apparent anodic charge densities, in mC cm<sup>-2</sup>, obtained from the voltammograms for fresh Ti//[RuO<sub>2</sub>-TiO<sub>2</sub>], corroded Ti//[RuO<sub>2</sub>-TiO<sub>2</sub>], Ti/TiO<sub>2</sub>/[RuO<sub>2</sub>-TiO<sub>2</sub>] and Ti//[RuO<sub>2</sub>-TiO<sub>2</sub>]/TiO<sub>2</sub> anode are 12.25, 3.05, 13.10 and 8.72, respectively. A considerably smaller anodic charge is registered for the corroded Ti//[RuO<sub>2</sub>-TiO<sub>2</sub>] anode when compared to the others. This indicates a decrease in the number of active sites due to the continuous dissolution of Ru species during the AST. The additional TiO<sub>2</sub> layer in the substrate|coating interphase does not significantly affect the anodic charge, but a lower value is registered for the anode with the TiO<sub>2</sub> layer on the coating surface. These effects are expected, since insulating TiO<sub>2</sub> on the surface covers the active RuO<sub>2</sub> species but does not affect those species if it is placed in the interphase.

#### Polarization measurements

$E$ - $\log j$  plots of the investigated anodes are shown in Fig. 3. The plots have been corrected for the pseudo-ohmic voltage drop by the IR compensation procedure given for the PAR 273A potentiostat, used for the CV and polarization measurements. It should be mentioned that the resistance values required for the IR compensation followed the order:

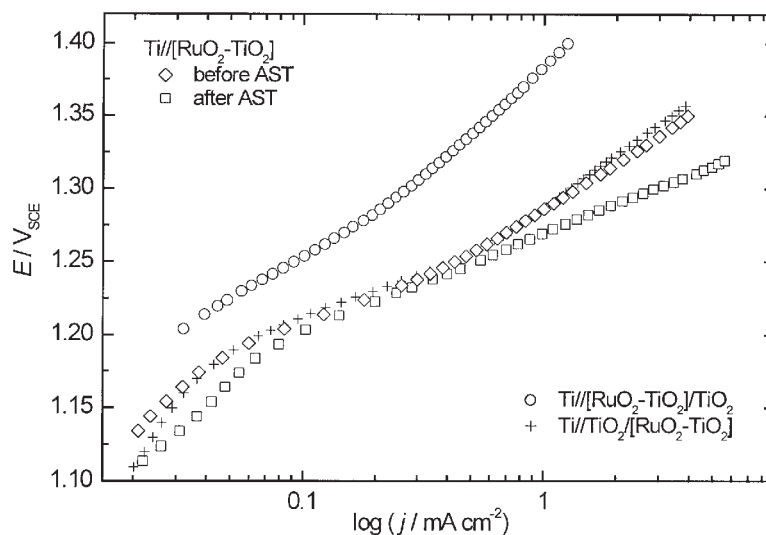


Fig. 3.  $E$ - $\log j$  characteristics of the Ti//[RuO<sub>2</sub>-TiO<sub>2</sub>] anode recorded before and after AST, and of the Ti//TiO<sub>2</sub>/[RuO<sub>2</sub>-TiO<sub>2</sub>] and Ti//[RuO<sub>2</sub>-TiO<sub>2</sub>]/TiO<sub>2</sub> anode. Electrolyte: 0.5 mol dm<sup>-3</sup> NaCl, pH 2; room temperature.

Ti//[RuO<sub>2</sub>-TiO<sub>2</sub>] < corroded Ti//[RuO<sub>2</sub>-TiO<sub>2</sub>] < Ti//[RuO<sub>2</sub>-TiO<sub>2</sub>]/TiO<sub>2</sub> << Ti/TiO<sub>2</sub>/[RuO<sub>2</sub>-TiO<sub>2</sub>], indicating the increased value of the coating resistance after the AST and by addition of the TiO<sub>2</sub> layers, particularly by the layer in the substrate/coating interphase.

Regardless the kinetics and mechanism of the processes occurring on the anode, it is obvious that the Ti//[RuO<sub>2</sub>-TiO<sub>2</sub>]/TiO<sub>2</sub> anode shows the worst polarization characteristics, while the Ti//TiO<sub>2</sub>/[RuO<sub>2</sub>-TiO<sub>2</sub>] and Ti//[RuO<sub>2</sub>-TiO<sub>2</sub>] anode behave similarly. It seems strange that the corroded Ti//[RuO<sub>2</sub>-TiO<sub>2</sub>] anode shows good polarization characteristics, even better than the others in the region of higher current density. Although most of the electrocatalytically active RuO<sub>2</sub> species were dissolved during the AST, there are still enough active sites for a current (considerably smaller than the current used in the AST) to pass. The coating is more porous after the AST, the surface area is large and this effect overcomes the effect of RuO<sub>2</sub> dissolution. This statement can be supported by the fact that the overpotential decreases exponentially with the thickness of the porous layer, which is a feature known from the theory of porous electrodes.<sup>12</sup> Since the dissolution of Ru species during the AST produces a coating with a more porous structure, the active sites of the corroded Ti//[RuO<sub>2</sub>-TiO<sub>2</sub>] anode situated deeper in the bulk of the coating became involved in the reaction. On the contrary, the polarization data of the Ti//[RuO<sub>2</sub>-TiO<sub>2</sub>] anode before the AST should relate to the active sites situated closer to the surface of the coating. It was found earlier that the number of active sites in the bulk of the coating is greater than on the coating surface due to surface enrichment in TiO<sub>2</sub> during the thermal formation of the coating.<sup>1</sup>

*Electrochemical impedance spectroscopy*

The complex plane plots shown in Fig. 4 illustrate the impedance behavior of the prepared anodes in the oxygen evolution reaction. Figure 4a shows the EIS data collected over the whole frequency range (100 kHz–50 mHz), while Fig. 4b shows the high-frequency part of the plots from Fig. 4a. The lines in Fig. 4 give the results of the fitting procedure.

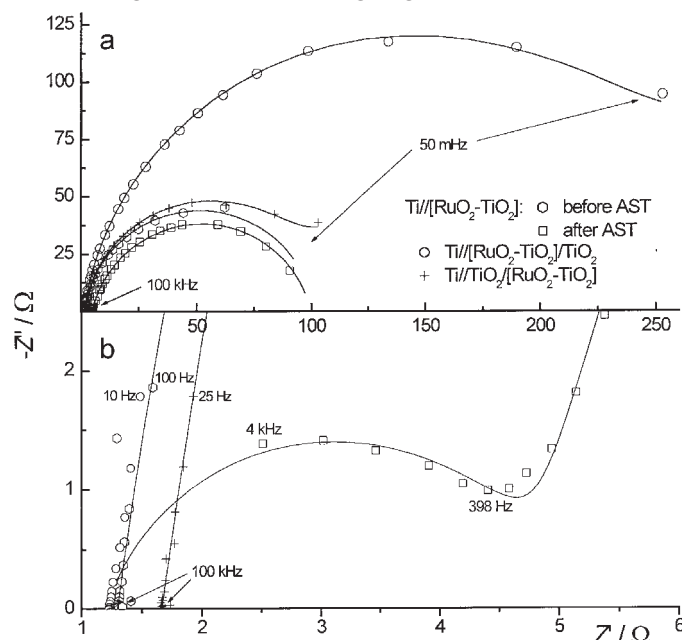


Fig. 4. The impedance complex plane plots of the  $\text{Ti}/[\text{RuO}_2\text{-TiO}_2]$  anode recorded before and after AST, and of the  $\text{Ti}/\text{TiO}_2/[\text{RuO}_2\text{-TiO}_2]$  and  $\text{Ti}/[\text{RuO}_2\text{-TiO}_2]/\text{TiO}_2$  anode over the whole frequency range (a) and in the high frequency range (b). Potential: 1.25 V, electrolyte:  $1 \text{ mol dm}^{-3} \text{ HClO}_4$ , room temperature.

The anode deactivation by the AST is manifested by the appearance of high-frequency semicircle in the EIS plot for the corroded  $\text{Ti}/[\text{RuO}_2\text{-TiO}_2]$  anode (Fig. 4b). Similar behavior was observed in an earlier work,<sup>9</sup> and also by other authors.<sup>7,8</sup> It was shown that the coating pore resistance, related to the high-frequency semicircle, depends on the electrolyte conductivity but not on the electrode potential.<sup>9</sup> Figure 4a also shows that anode corrosion results in no significant changes in the characteristics of the semicircle related to charge transfer across the solution/coating interphase at lower frequencies.

Differences in the EIS behavior of the  $\text{Ti}/\text{TiO}_2/[\text{RuO}_2\text{-TiO}_2]$  and  $\text{Ti}/[\text{RuO}_2\text{-TiO}_2]$  anode are seen at high and low frequencies. Since the somewhat higher value of the electrolyte resistance of  $\text{Ti}/\text{TiO}_2/[\text{RuO}_2\text{-TiO}_2]$  anode should rather be ascribed to experimental error, the main difference in their EIS behavior is registered at low frequencies. A considerably greater charge transfer semicircle is obtained for the  $\text{Ti}/[\text{RuO}_2\text{-TiO}_2]/\text{TiO}_2$  anode, which again confirms the considerably smaller number of active sites that exchange charge with the electrolyte.

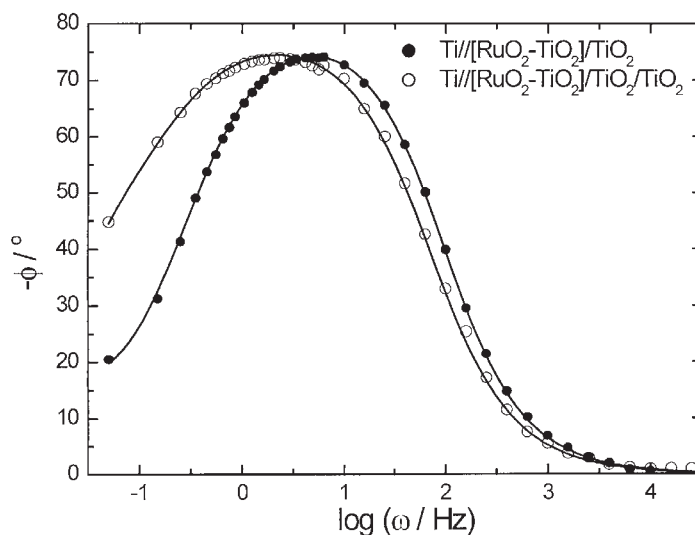


Fig. 5. Bode phase angle plots of the anodes with different amount of TiO<sub>2</sub> inserted at the coating surface. EIS data recorded in 1 mol dm<sup>-3</sup> HClO<sub>4</sub> at a potential of 1.25 V.

As can be seen in Fig. 4b, there is no evidence of a well-pronounced high-frequency semicircle in the plots of the EIS data for the anodes with an additional TiO<sub>2</sub> layer. This indicates that the morphology of the additional layer is different to that formed during anode deactivation. Also, the morphology of the additional TiO<sub>2</sub> layer depends on the position of the layer with respect to the RuO<sub>2</sub>-TiO<sub>2</sub> coating, which causes a difference in the anode impedance behavior. Concerning the anode with the TiO<sub>2</sub> layer on the coating surface, there is no significant difference in impedance behavior at high frequencies if the amount of TiO<sub>2</sub> on the coating surface is doubled (two additional layers: Ti/[RuO<sub>2</sub>-TiO<sub>2</sub>]/TiO<sub>2</sub>/TiO<sub>2</sub>), as illustrated by the Bode phase angle plots in Fig. 5. On the contrary, the differences in the low-frequency domain became more pronounced with increased amount of TiO<sub>2</sub> at the coating surface.

#### Equivalent electrical circuits

The simple equivalent electrical circuit (EEC) with the inscription  $R_{\Omega}(R_{ct}Q)$ ,<sup>10</sup> where  $R_{\Omega}$  is the solution resistance,  $R_{ct}$  is the charge transfer resistance across the active site/solution interphase, and  $Q$  is a constant phase element related to the coating capacitance, was sufficient to describe the impedance behavior of a freshly prepared Ti/[RuO<sub>2</sub>-TiO<sub>2</sub>] anode. In order to describe the anode impedance behavior after AST, additional elements, which represent the pore resistance,  $R_p$ , of TiO<sub>2</sub> layer formed during anode deactivation and  $Q_L$ , related to the TiO<sub>2</sub> layer capacitance, were included in the EEC:  $R_{\Omega}(R_pQ_L)(R_{ct}Q)$ .

The values of the parameters of the EEC elements are given in Table I. There are no considerable changes in the  $R_{ct}$  values, nor in the values of the parameters  $Y_0$  and  $n$  for  $Q$ , which is consistent with the results and conclusions from polarization

measurements. The charge transfer resistance is lower for the corroded anode, while the capacitance is higher. This is opposite to the CV results, which indicates that EIS “can see” deeper into the coating bulk than CV at the applied sweep rate. The unique feature caused by anode deactivation is the appearance of the  $R_p Q_L$  combination.

The EECs which describe the impedance behavior of the anodes with an additional  $\text{TiO}_2$  layer in the substrate|coating interphase and two  $\text{TiO}_2$  layers on the coating surface are similar to the EEC of the corroded  $\text{Ti}/[\text{RuO}_2\text{--TiO}_2]$  anode. The same elements as in the case of the corroded anode constitute the EEC for  $\text{Ti}/[\text{RuO}_2\text{--TiO}_2]/\text{TiO}_2/\text{TiO}_2$ , where  $R_p$  is the pore resistance of the additional  $\text{TiO}_2$  layers. The circuit inscription for  $\text{Ti}/\text{TiO}_2/[\text{RuO}_2\text{--TiO}_2]$  anode is  $R_\Omega(R_L Q_L)(R_{ct}Q)$ , where  $R_L$  is the resistance of the  $\text{TiO}_2$  layer instead of  $R_p$ . Contrary to the corroded anode, the semicircles related to the additional  $\text{TiO}_2$  layers and that related to charge transfer are highly overlapped and cannot be separately seen in the plots in Fig. 4. In the case of the  $\text{Ti}/[\text{RuO}_2\text{--TiO}_2]/\text{TiO}_2$  anode, there is no evidence of the formation of a separate  $\text{TiO}_2$  layer, and EEC is  $R_\Omega(Q_{dl}(R_{ct}(Q_p)))$ , where  $Q_p$  is a constant phase element related to the pseudocapacitance of  $\text{RuO}_2$ . This EEC indicates that the addition of  $\text{TiO}_2$  on the coating surface enables the pseudocapacitance to be distinguished from the double layer capacitance, which is a known impedance feature of  $\text{RuO}_2\text{--TiO}_2$  coatings with low  $\text{RuO}_2$  content.<sup>11</sup> The obtained  $Y_0$  value of  $Q_p$  (Table I) is of the same order of magnitude as the capacitance that can be calculated from the voltammogram shown in Fig. 2 ( $10^{-2} \text{ F cm}^{-2}$ ). This consideration indicates that the  $\text{TiO}_2$  on the coating surface is highly doped with  $\text{RuO}_2$  migrating from the neighboring  $\text{RuO}_2\text{--TiO}_2$  layer during thermal treatments.

The values of the EEC parameters for the anodes with additional  $\text{TiO}_2$  can be seen in Table I. The  $R_L$  value obtained for  $\text{Ti}/\text{TiO}_2/[\text{RuO}_2\text{--TiO}_2]$  is considerably higher than the  $R_p$  value obtained for the corroded  $\text{Ti}/[\text{RuO}_2\text{--TiO}_2]$  anode, while the  $Y_0$  value of  $Q_L$  for the latter is considerably lower. Even so, the  $Y_0$  value of  $Q_L$  for  $\text{Ti}/\text{TiO}_2/[\text{RuO}_2\text{--TiO}_2]$  is quite similar to the  $Y_0$  value of  $Q$  obtained for fresh and corroded  $\text{Ti}/[\text{RuO}_2\text{--TiO}_2]$  anodes, which indicates the doping effect from the neighboring  $\text{RuO}_2\text{--TiO}_2$  layer, like in the case of the  $\text{Ti}/[\text{RuO}_2\text{--TiO}_2]/\text{TiO}_2$  anode. This consideration leads to the conclusion that the  $R_L$  value should not be considerably higher than the value of  $R_p$  for the corroded anode, which suggests the formation of  $\text{TiO}_2$  in the substrate|coating interphase as the cause for deactivation of sol-gel prepared anodes is less probable. On the other hand, the  $Y_0$  value of  $Q_L$  obtained for the  $\text{Ti}/[\text{RuO}_2\text{--TiO}_2]/\text{TiO}_2/\text{TiO}_2$  anode is closer to the value obtained for the corroded anode than to the value for  $\text{Ti}/\text{TiO}_2/[\text{RuO}_2\text{--TiO}_2]$  anode, while the  $R_p$  value is three orders of magnitude higher than for the corroded anode. This is due to the considerably greater compactness of the additional  $\text{TiO}_2$  layers in the  $\text{Ti}/[\text{RuO}_2\text{--TiO}_2]/\text{TiO}_2/\text{TiO}_2$  anode. The high compactness of the  $\text{TiO}_2$  layer is also seen through the  $R_{ct}$  value registered for the  $\text{Ti}/[\text{RuO}_2\text{--TiO}_2]/\text{TiO}_2/\text{TiO}_2$  anode being the highest, since the active sites are hardly accessible for the species involved in the charge transfer process.

TABLE I. The values of the equivalent electrical circuit parameters for the investigated anodes

Parameter	Anode				
	Ti//[RuO <sub>2</sub> -TiO <sub>2</sub> ]		Ti/TiO <sub>2</sub> [RuO <sub>2</sub> -TiO <sub>2</sub> ]	Ti//[RuO <sub>2</sub> -TiO <sub>2</sub> ]/TiO <sub>2</sub>	Ti//[RuO <sub>2</sub> -TiO <sub>2</sub> ]/TiO <sub>2</sub> /TiO <sub>2</sub>
	Before AST	After AST			
EEC:	$R_{\Omega}(R_{ct}Q)$	$R_{\Omega}(R_pQ_L)(R_{ct}Q)$	$R_{\Omega}(R_LQ_L)(R_{ct}Q)$	$R_{\Omega}(Q_{dl}(R_{ct}(Q_p))$	$R_{\Omega}(R_pQ_L)(R_{ct}Q)$
$R_{\Omega}/\Omega$	1.7	1.8	1.8	1.6	2.0
$R_p/\Omega$	—	3.9	—	—	1283
$R_L/\Omega$	—	—	168	—	—
$Q_L$ $Y_0/\Omega^{-1}$	—	$1.6 \times 10^{-5}$	$3.2 \times 10^{-3}$	—	$4.1 \times 10^{-4}$
$n$	—	0.77	0.82	—	0.91
$R_{ct}/\Omega$	103	96	150	264	347
$Q$ $Y_0/\Omega^{-1}$	$3.5 \times 10^{-3}$	$4.7 \times 10^{-3}$	$4.8 \times 10^{-3}$	—	$3.8 \times 10^{-3}$
$n$	0.91	0.87	0.96	—	0.87
$Q_{dl}$ $Y_0/\Omega^{-1}$	—	—	—	$2.4 \times 10^{-3}$	—
$n$	—	—	—	0.91	—
$Q_p$ $Y_0/\Omega^{-1}$	—	—	—	$4.6 \times 10^{-2}$	—
$n$	—	—	—	0.63	—

The impedance behavior of the investigated anodes indicates that the loss of electro-catalytic activity of sol-gel prepared anodes is due to the formation of a TiO<sub>2</sub> layer on the coating surface rather than to the growth of a TiO<sub>2</sub> layer at the substrate|coating interphase.

## CONCLUSION

Regular Ti//[RuO<sub>2</sub>-TiO<sub>2</sub>] anodes and anodes with additional TiO<sub>2</sub> layers in the substrate|coating interphase and on the coating surface were investigated by cyclic voltammetry, polarization measurements and electrochemical impedance spectroscopy. Cyclic voltammetry experiments showed a decrease in the electrochemically active surface area during corrosion of the RuO<sub>2</sub>-TiO<sub>2</sub> coating and an increase in the coating resistance. The coating resistance is also increased by additional TiO<sub>2</sub> layers, particularly by a layer in the substrate|coating interphase. Similar conclusions about the coating resistance resulted from polarization measurements, but they indicated an increase in the porosity of the coating during anode corrosion. The mechanism of the deactivation of the Ti//[RuO<sub>2</sub>-TiO<sub>2</sub>] anode during long-term electrolysis is seen in its impedance behavior as the appearance of a high-frequency semicircle, as the consequence of TiO<sub>2</sub> enrichment in the coating. The data obtained by EIS measurements for the anode with two additional TiO<sub>2</sub> layers on the coating surface show similarity to the EIS data of the corroded Ti//[RuO<sub>2</sub>-TiO<sub>2</sub>] anode. The conclusion appears to be that the loss of anode activity of sol-gel prepared Ti//[RuO<sub>2</sub>-TiO<sub>2</sub>] anode is dominantly due to an enrichment of the coating surface with TiO<sub>2</sub> which remains after RuO<sub>2</sub> dissolution.

*Acknowledgements:* This research is financially supported by the Ministry of Science, Technology and Development, Republic of Serbia, Project No. 1230.

## ИЗВОД

УЛОГА КОНЦЕНТРАЦИОНОГ ПРОФИЛА ТИТАН-ОКСИДА У  
ЕЛЕКТРОХЕМИЈСКОМ ПОНАШАЊУ  $\text{RuO}_2\text{--TiO}_2$  ПРЕВЛАКА ДОБИЈЕНИХ  
СОЛ-ГЕЛ ПОСТУПКОМ

ВЛАДИМИР В. ПАНИЋ<sup>1</sup>, АЛЕКСАНДАР Б. ДЕКАНСКИ<sup>1</sup>, ВЕСНА Б. МИШКОВИЋ-СТАНКОВИЋ<sup>2</sup>,  
СЛОБОДАН К. МИЛОЊИЋ<sup>3</sup> и БРАНИСЛАВ Ж. НИКОЛИЋ<sup>2</sup>

<sup>1</sup>ИХТМ - Центар за електрохемију, Њеђошева 12, ђ. ђр. 815, 11000 Београд,

<sup>2</sup>Технолошко-металуришки факултет, Карнегијева 4, ђ. ђр. 3503, 11120 Београд и

<sup>3</sup>Институт за нуклеарне науке "Винча", ђ. ђр. 522, 11001 Београд

У циљу испитивања улоге титан-оксида у деактивацији  $\text{RuO}_2\text{--TiO}_2$  превлаке на титанској подлози, испитиване су особине анода са додатним слојем  $\text{TiO}_2$  у међуфази подлога/превлака, односно на површини превлаке. Електрохемијско понашање ових упоређено је са понашањем анода са уобичајеном  $\text{RuO}_2\text{--TiO}_2$  превлаком, као и са онима које су биле подвргнуте убрзаном тесту стабилности. Појава полукруга у високо-фреквентној области у дијаграмима у комплексној равни, која је регистрована спектроскопијом електрохемијске импеданције за уобичајене  $\text{RuO}_2\text{--TiO}_2$  превлаке, а која је последица обогаћивања превлаке са  $\text{TiO}_2$  током њене деактивације, није уочена код анода са додатим  $\text{TiO}_2$  слојем. Додати  $\text{TiO}_2$  слојеви повећавају омску отпорност превлаке и утичу на импеданцијско понашање при ниским фреквенцијама. За анализу импеданцијског понашања превлака са додатим  $\text{TiO}_2$  слојевима као и уобичајених  $\text{RuO}_2\text{--TiO}_2$  превлака које су деактивирани коришћена су слична еквивалентна електрична кола.

(Примљено 1. августа 2003)

## REFERENCES

1. V. M. Jovanović, A. Dekanski, P. Despotov, B. Nikolić, R. T. Atanasoski, *J. Electroanal. Chem.* **339** (1992) 147
2. V. A. Alves, L. A. Silva, J. F. C. Boodts, *J. Appl. Electrochem.* **28** (1998) 899
3. V. Panić, A. Dekanski, S. Milonjić, R. Atanasoski, B. Nikolić, *Colloids Surfaces A* **157** (1999) 259
4. V. Panić, A. Dekanski, S. Milonjić, R. Atanasoski, B. Nikolić, *Electrochim. Acta* **46** (2000) 415
5. A. Dekanski, V. M. Jovanović, P. Despotov, B. Nikolić, R. T. Atanasoski, *J. Serb. Chem. Soc.* **56** (1991) 167
6. D. Mitrović, V. Panić, A. Dekanski, S. Milonjić, R. Atanasoski, B. Nikolić, *J. Serb. Chem. Soc.* **66** (2001) 847
7. L. M. Da Silveira, L. A. De Faria, J. F. C. Boodts, *J. Electroanal. Chem.* **532** (2002) 141
8. T. A. F. Lassali, J. F. C. Boodts, L. O. S. Bulhões, *J. Appl. Electrochem.* **30** (2000) 625
9. V. Panić, V. Mišković-Stanković, A. Dekanski, S. Milonjić, B. Nikolić, *The European Corrosion Congress, EUROCORR 2001*, Riva del Garda, Lake Garda, Italy, October 2001, CD-ROM, Paper No. 097
10. B. Boucamp, *Equivalent Circuit (EQUIVCRT.PAS) Users Manual*, Univ. Twente, Enschede, The Netherlands, 1989
11. B. Conway, *Electrochemical Supercapacitors – Scientific Fundamentals and Technological Applications*, Plenum Publishers, New York, 1999, p. 259
12. Yu. Chizmadzev, Yu. Chirkov in *Comprehensive Treatise of Electrochemistry Vol. 6*, E. Yeager, J. Bockris, B. Conway, S. Sarangapani, Eds., Ch. 5, Plenum Press, New York, 1983.



## Comparative electrochemical study of some cobalt(III) and cobalt(II) complexes with azamacrocycles and $\beta$ -diketonato ligands

K. BABIĆ-SAMARDŽIJA<sup>1</sup>, S. P. SOVILJ<sup>1</sup> and V. M. JOVANOVIĆ<sup>2\* #</sup>

<sup>1</sup>Faculty of Chemistry, University of Belgrade, P. O. Box 158, 11001 Belgrade, (e-mail: ssovilj@chem.bg.ac.yu) and <sup>2</sup>ICTM, Department of Electrochemistry, Njegoševa 12, P. O. Box 815, 11000 Belgrade, Serbia and Montenegro (e-mail: vlad@elab.tmf.bg.ac.yu)

(Received 16 May, revised 21 August 2003)

**Abstract:** The electrochemical properties of eight mixed-ligand cobalt(III) and cobalt(II) complexes of the general formulas  $[\text{Co}^{\text{III}}(\text{Rac})\text{cyclam}](\text{ClO}_4)_2$  (**1**)–(**4**) and  $[\text{Co}_2^{\text{II}}(\text{Rac})\text{tpmc}](\text{ClO}_4)_3$  (**5**)–(**8**) were studied. The substances were investigated in aqueous  $\text{NaClO}_4$  solution and non-aqueous  $\text{LiClO}_4/\text{CH}_3\text{CN}$  solution by cyclic voltammetry at a glassy carbon electrode. In aqueous solution, *cyclam* and *Rac* ligands being soluble in water undergo anodic oxidation. Coordination to Co(III) in complexes **1**–**4**, stabilizes these ligands but reversible peaks in cathodic region indicate the redox reaction  $\text{Co}^{\text{III}}/\text{Co}^{\text{II}}$  ion. In the case of the binuclear Co(II) complexes **5**–**8**, peaks recorded on the CVs represent oxidation of the bridged *Rac* ligand. The complexes examined influence the cathodic reaction of hydrogen evolution in aqueous solutions by shifting its potential to more negative values and its current is increased. In non-aqueous solution the CVs of the ligands show irreversible anodic peaks for *cyclam*, *tpmc* and for the *Rac* ligands soluble in acetonitrile. The absence of any peaks in the case of the investigated complexes **1**–**4** indicates that coordination to Co(III) stabilizes both the *cyclam* and *Rac* ligands. Cyclic voltammograms of the complexes **5**–**8** show oxidation processes of the *Rac* ligand and Co(II) ions but the absence of a highly anodic peak of the coordinated macrocycle *tpmc* shows its stabilization. Contrary to in aqueous solution, the redox reaction  $\text{Co}(\text{III})/\text{Co}(\text{II})$  does not occur in acetonitrile indicating a higher stability of the complexes **1**–**4** in this media in comparison with the binuclear cobalt(II)-*tpmc* complexes **5**–**8**.

**Keywords:** cobalt(III) and cobalt(II) complexes, azamacrocycles and  $\beta$ -diketonato ligands, cyclic voltammetry, glassy carbon.

### INTRODUCTION

Complexes with macrocyclic polyamines might serve as convenient building blocks for the construction of mixed-ligand mono- and polynuclear complexes.<sup>1</sup> Tetraamine [14]and- $\text{N}_4$  *cyclam* (1,4,8,11-tetraazacyclotetradecane) as a macro-

\* Corresponding author.

# Serbian Chemical Society active member.



cyclic flexible ring can exist in the *cis* and *trans* configurations<sup>2</sup> but only *cis* complexes have been observed in the presence of additional bidentate co-ligands.<sup>3–7</sup> The N<sub>4</sub>-2-pyridylmethyl-substituted octaamine ligand *tpmc* (*N,N',N'',N'''*-tetrakis(2-pyridyl methyl)-1,4,8,11-tetraazacyclotetradecane) through coordination provides interesting structural and chemical properties, *i.e.*, invariable formation of binuclear molecules with strong affinity towards various anions to form bridged complexes<sup>8–10</sup> and unusual stabilization of the divalent state of cobalt ion against oxidation to the trivalent state.<sup>10</sup> Macrocyclic ligands such as *cyclam* and *tpmc* are very useful to form and stabilize mixed-ligand complexes with additional exocyclic ligand(s).

In this context,  $\beta$ -diketones are suitable to combine with other ligands of comparable ligating ability, especially because of their ability to form keto-enolate structures and a few different coordination modes.<sup>11</sup> The chelating “pseudoaromatic” ring of  $\beta$ -diketones have found extensive application in the study of the formation of various types of metal complexes,<sup>12</sup> as well as giving the opportunity to investigate them in terms of different  $\beta$ -diketones R-groups.<sup>7</sup>

Therefore, these types of complexes could be interesting not only from aspects of molecular structures but from the electrochemical point of view as well, because structural and electronic factors may simultaneously affect the multi-redox peak potentials and catalytic features of the complexes.<sup>3,8,13</sup> For example, cyclic voltametric data for the cobalt(III)-*cyclam* oxalato complex<sup>3</sup> suggest large electrochemical stability, as well as its possible catalytic effect on the electrochemical reduction of CO<sub>2</sub>. In the case of the binuclear cobalt(II)-*tpmc* oxalato complex<sup>8</sup> multi-redox reactions of the metal centers and high electrochemical stability up to the potential of cobalt reduction were observed. The fact that the potential of hydrogen evolution is shifted to the anodic side in the presence of the complex indicates possible catalytic properties as well.<sup>8</sup> Electrochemical examination of mixed-ligand cobalt(III)-*cyclam* complexes with heterocyclic dithiocarbamates (*Rdtc*)<sup>13</sup> show redox reactions of the Co(III) ion at potentials the position of which are influenced by the presence of different heterocyclic rings in the *Rdtc* ligand, while the preliminary results in acidic media show their inhibition of iron corrosion and influence on hydrogen evolution in acidic media.

For the above-mentioned reasons, eight new mixed-ligand cobalt complexes were synthesized and characterized elsewhere,<sup>6,7</sup> *i.e.*, cobalt(III) complexes with macrocyclic ligand *cyclam* or *tpmc* in binuclear cobalt(II) complexes with R-symmetric bidentate  $\beta$ -diketones (*Rac*), *i.e.*, *acac* (2,4-pentanedionato), *dibzac* (1,3-diphenyl-1,3-propanedionato), *hfac* (1,1,1,5,5,5-hexafluoro-2,4-pentanedionato) or *tmhd* (2,2,6,6-tetramethyl-3,5-heptanedionato) ions, of the general formulas [Co<sup>III</sup>(*Rac*)*cyclam*](ClO<sub>4</sub>)<sub>2</sub> (**1**)–(**4**) and [Co<sup>II</sup>(*Rac*)*tpmc*](ClO<sub>4</sub>)<sub>3</sub> (**5**)–(**8**), respectively. The aim of this work was a comparative study of the electrochemical behavior of these compounds and corresponding ligands in aqueous and non-aqueous solutions by

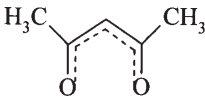
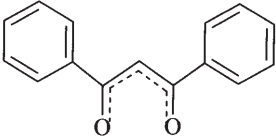
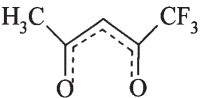
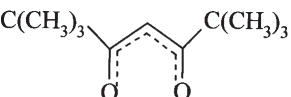
cyclic voltammetry (CV) and their possible influence on hydrogen evolution and oxygen reduction.

### EXPERIMENTAL

A glassy carbon (GC) disc electrode (Sigardur-Sigri Electrographite, GmbH, Germany) was used as the working electrode. The electrode was mechanically refreshed with emery paper of decreasing grain size, polished with alumina (0.5  $\mu$  particle size) and cleaned in 18 M $\Omega$  water in an ultrasonic bath. For each experiment, the prepared electrode was first examined in the basic electrolyte by CV before the substance was added to the solution. The counter electrode was a platinum wire. A saturated calomel electrode (SCE) was used as the reference in aqueous solution and a bridged SCE in CH<sub>3</sub>CN.

All the complexes **1–8**, macrocyclic *cyclam* and *tpmc* as well as the corresponding *Rac* ligands were examined in the concentration range of 10<sup>–6</sup> to 10<sup>–4</sup> M, in 0.1 M NaClO<sub>4</sub> aqueous solution and in 0.1 M LiClO<sub>4</sub> in CH<sub>3</sub>CN. The solutions were prepared from analytical grade reagents and were maintained oxygen-free by purging with nitrogen.

TABLE I.  $\beta$ -Diketonato ligands in the complexes **1–8**

Structure of <i>Rac</i> ion	Abbreviations and name of <i>Rac</i>	Coordinate d <i>Rac</i> in complexes
	<i>acac</i> 2,4-Pentanedionato ion	(1) (5)
	<i>dibzac</i> 1,3-Diphenyl-1,3-propanedionato ion	(2) (6)
	<i>hfac</i> 1,1,1,5,5,5-Hexafluoro-2,4-pentanedionato ion	(3) (7)
	<i>tmhd</i> 2,2,6,6-Tetramethyl-3,5-heptanedionato ion	(4) (8)

Cyclic voltammetry was performed at sweep rates of 25, 50 and 100 mV/s. The potential range examined was between –0.5 V to 2.0 V in aqueous and –1.5 V to 1.5 V in non-aqueous solution. All the potentials are given *versus* the SCE electrode.

The [Co<sup>III</sup>(*hfac*)*cyclam*](ClO<sub>4</sub>)<sub>2</sub> complex (at a concentration of 10<sup>–4</sup> M) was examined in 0.1 M HClO<sub>4</sub> solution by cyclic voltammetry (potential range from –1.2 V to 1.2 V *vs.* SCE, sweep rate 25, 50, 100 mV/s) as well. Also, the possible influence of this complex on the reduction of oxygen was tested in 0.1 M HClO<sub>4</sub> solution saturated with O<sub>2</sub> at a rotating GC electrode at a sweep rate of 5 mV/s in the potential range 0.2 V to –1.1 V *vs.* SCE.

All of the experiments were performed at room temperature in a three electrodes – three-compartment electrochemical cell. The electronic equipment in all of the experiments consisted of a Pine Instrument, Model RDE4 Potentiostat and a Philips Model 8033 X-Y recorder.

## RESULTS AND DISCUSSION

The series of eight complexes, with general formulas  $[\text{Co}^{\text{III}}(\text{Rac})\text{cyclam}](\text{ClO}_4)_2$  (**1**)–(**4**) (Fig. 1A) and  $[\text{Co}_2^{\text{II}}(\text{Rac})\text{tpmc}](\text{ClO}_4)_3$  (**5**)–(**8**) (Fig. 1B) and the corresponding

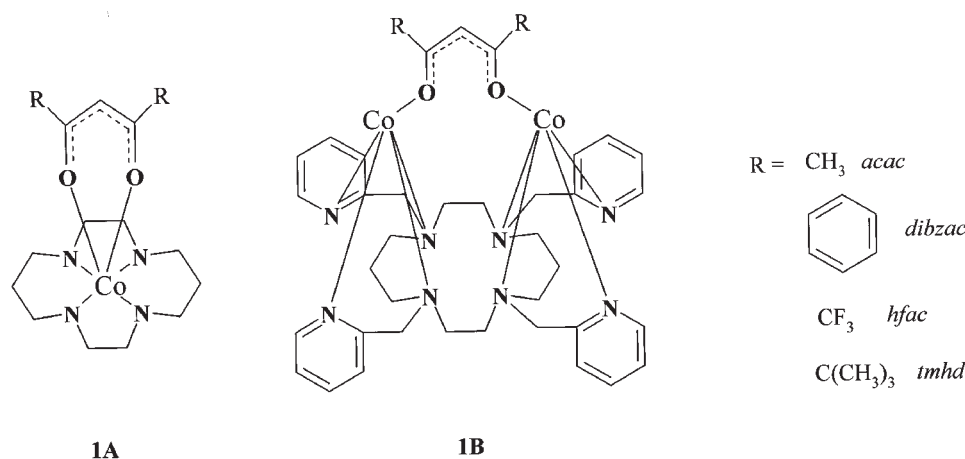


Fig. 1. Structures of the  $[\text{Co}^{\text{III}}(\text{Rac})\text{cyclam}](\text{ClO}_4)_2$  complexes **1–4** (1A) and of the  $[\text{Co}_2^{\text{II}}(\text{Rac})\text{tpmc}](\text{ClO}_4)_3$  complexes **5–8** (1B).

macrocyclic *cyclam* and *tpmc* as well as *Rac* (Table I) ligands were electrochemically characterized both in aqueous and non-aqueous solutions. The peak potentials for all of the ligands examined and for the complexes **1–8** are listed in Table II and the selected cyclic voltammograms are presented in Figs. 2–4.

#### Aqueous solution

The cyclic voltammogram of the GC electrode in aqueous ( $\text{NaClO}_4$ ) solution in the absence of any compound shows no electron exchange occurred. With the addition of the macrocyclic ligands *cyclam* and *tpmc* one irreversible anodic peak appears at 0.95 V vs. SCE for the tetraaza amine only (Table II).<sup>13,8</sup> The CVs for the *Rac* ligands soluble in water (*Hacac* and *Hhfac* – Table II and Fig. 2A) indicate the existence of an irreversible anodic peak at 1.05 V and 1.40 V vs. SCE, respectively, which should correspond to oxidation processes of the organic species.

Two anodic peaks in the 0.65–0.90 V and 1.50–1.60 V vs. SCE regions for the cobalt(III)-*cyclam* complexes **1–3** can be identified only at the beginning of the cyclization (Fig. 2A – insert). During continued scanning, these anodic peaks are no longer observed, which might point to the low stability of the complex species. The number of cycles before the stabilization depends on the *Rac* ligand in the order of *hfac* > *acac* > *dibzac* in the complexes **1–3**. In the case of complex **4** with a coordinated *tmhd* ligand (Fig. 2B), the steady state was established already at the first cycle, which can contribute to the higher stabilization of this complex ion. However, the steady-state CVs of the complexes **1–4** exhibit a reverse peak in the

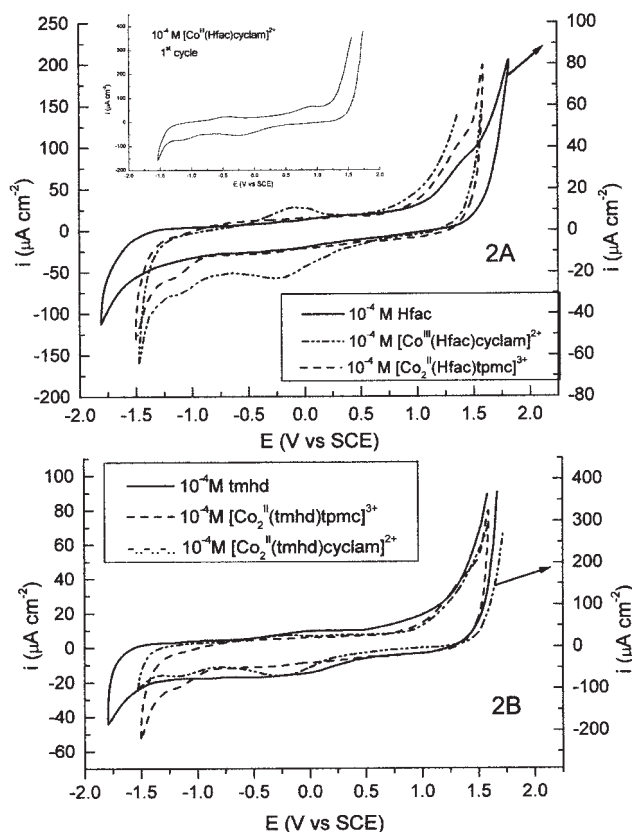


Fig. 2. Cyclic voltammograms at GC electrode in 0.1 M NaClO<sub>4</sub> and: A)  $10^{-4}$  M *dibzac* ligand,  $10^{-4}$  M  $[\text{Co}^{\text{III}}(\text{dibzac})\text{cyclam}](\text{ClO}_4)_2$  complex,  $10^{-4}$  M  $[\text{Co}_2^{\text{II}}(\text{dibzac})\text{tpmc}](\text{ClO}_4)_3$  complex. B)  $10^{-4}$  M *tmhd* ligand,  $10^{-4}$  M  $[\text{Co}^{\text{III}}(\text{tmhd})\text{cyclam}](\text{ClO}_4)_2$  complex,  $10^{-4}$  M  $[\text{Co}_2^{\text{II}}(\text{tmhd})\text{tpmc}](\text{ClO}_4)_3$  complex, (sweep rate 100 mV/s).

cathodic region (Table II and Fig. 2) in the region  $-0.25$  V to  $-0.4$  V depending on the *Rac* ligand. This pair of peaks probably indicates the redox reaction  $\text{Co}^{\text{III}}/\text{Co}^{\text{II}}$  from the complexes **1–4** as other previously characterized  $\text{Co}(\text{III})$ -*cyclam* complexes (with dithiocarbamate and oxalato ligands) also display a similar redox pair at potentials influenced by the additional ligand.<sup>3,13</sup> In relation with these peaks, the highly cathodic peak at  $-1.15$  V probably represent reduction to metal cobalt.

Peaks recorded on the CVs of the cobalt(II)-*tpmc* complex **5–8** between about 0.90 V to 1.40 V vs. SCE correspond to oxidation processes of the electroactive *Rac* ligands, exhibiting almost the same potential values for the free and coordinated  $\beta$ -diketonato ligands (Fig. 2A). The absence of any peak for the complex **6** with a coordinated *dibzac* ligand indicates its higher stability in aqueous media under the given electrochemical conditions. Only in the case of the complexes **5** and **8**, with coordinated *acac* and *tmhd* ligand, respectively, a poorly defined cathodic peak at  $-1.15$  V vs. SCE points to the reduction process to metal cobalt (Table II

and Fig. 2B).<sup>8</sup> The dependence of the peak current on the sweep rate indicates that all of the reactions are surface localized and not diffusion controlled, which should mean that the complexes are adsorbed on the electrode surface.

TABLE II. The peak potentials of the ligands and the corresponding complexes in aqueous (NaClO<sub>4</sub>) and non-aqueous (LiClO<sub>4</sub>/CH<sub>3</sub>CN) solutions vs SCE

Compound	Aqueous solution		Non-aqueous solution
	$E_{pa}$	$E_{pc}$	$E_{pa}$
<i>tpmc</i>	—	—	1.82
<i>cyclam</i>	0.95	—	1.75
<i>acac</i>	1.05	—	—
<i>dibzac</i>	—	—	1.30
<i>hfac</i>	1.40	—	1.40
<i>tmhd</i>	—	—	—
[Co(acac)cyclam] <sup>2+</sup> (1)	0.70*	1.50*	—1.15
	—0.30	—0.40	
[Co(dibzac)cyclam] <sup>2+</sup> (2)	0.65*	1.53*	—1.15
	—0.25	—0.30	
[Co(hfac)cyclam] <sup>2+</sup> (3)	0.90*	1.60*	—1.15
	—0.25	—0.30	
[Co(tmhd)cyclam] <sup>2+</sup> (4)	—0.25	—0.30	—1.15
[Co <sub>2</sub> (acac)tpmc] <sup>3+</sup> (5)		0.95	—1.15
			1.48
[Co <sub>2</sub> (dibzac)tpmc] <sup>3+</sup> (6)		—	
			1.30
[Co <sub>2</sub> (hfac)tpmc] <sup>3+</sup> (7)		1.4	
			1.30
[Co <sub>2</sub> (tmhd)tpmc] <sup>3+</sup> (8)		0.9	—1.15
			1.25

\* Peaks recorded at the beginning of cyclization;  $E_{pa}$  = anodic peak;  $E_{pc}$  = cathodic peak

In aqueous NaClO<sub>4</sub> solutions, the CVs demonstrate that the presence of any of the Co(III)-*cyclam* and Co(II)-*tpmc* complexes **1–8** examined influence the cathodic reaction of hydrogen evolution by slightly shifting the potential to more negative values in the order coordinated *tmhd* > *acac* > *dibzac* > *hfac* ligands, increasing its current in the opposite order (Fig. 3a). The effect of the Co(III)-*cyclam* complexes **1–4**, regarding this reaction, is more pronounced, especially in the increase of the current, compared with the Co(II)-*tpmc* compounds **5–8**. Furthermore, the cathodic shift of potential occurred only in the presence of the complexes **6** and **8** characterized with cathodic peak at –1.15 V (possible reduction to Co), in which the current of the H<sub>2</sub> reduction slightly decreased. The other two Co(II)-*tpmc* complexes **5** and **7** negligibly affect the current of H<sub>2</sub> evolution and have practically no influence on the potential. Regarding the cathodic shift of hydrogen evolution, the Co(III)-*cyclam* complexes **1–4** are similar to Co(III)-*cyclam* oxalate complex<sup>3</sup> which, however, has

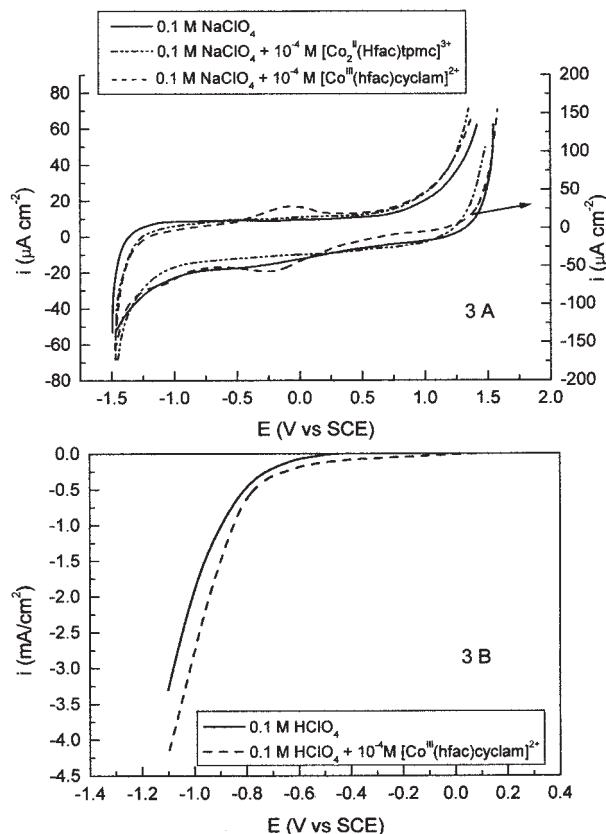


Fig. 3. A) Cyclic voltammograms at GC electrode in 0.1 M  $\text{NaClO}_4$ , 0.1 M  $\text{NaClO}_4 + 10^{-4}$  M  $[\text{Co}^{\text{III}}(\text{hfac})\text{cyclam}](\text{ClO}_4)_2$  complex and 0.1 M  $\text{NaClO}_4 + 10^{-4}$  M  $[\text{Co}^{\text{II}}(\text{hfac})\text{tpmc}](\text{ClO}_4)_3$ , (sweep rate 100 mV/s). B) Oxygen reduction curves for GC electrodes in 0.1 M  $\text{HClO}_4$  saturated with  $\text{O}_2$  and 0.1 M  $\text{HClO}_4 + 10^{-4}$  M  $[\text{Co}^{\text{III}}(\text{hfac})\text{cyclam}](\text{ClO}_4)_2$  complex saturated with  $\text{O}_2$  (sweep rate 5 mV/s, 900 rpm).

the opposite effect on the reaction current, namely increasing it. This difference could be ascribed to the structural factor of the enlarged chelate rings of the O,O'- $\beta$ -diketone ligand in comparison with the oxalato one. On the other hand, the binuclear  $\text{Co}(\text{II})$ -*tpmc* oxalato complex<sup>8</sup> when present in the solution leads to an anodic shift of hydrogen evolution and a remarkable increase of the reaction current, which is completely contrary to the  $\text{Co}(\text{II})$ -*tpmc*  $\beta$ -diketone complexes 5–8.

Complexes of transition metals (like Co or Fe) of the  $\text{MN}_4$  chromophore appear to be a promising class of materials for the reduction of oxygen.<sup>14,15</sup> According to Chang *et al.*,<sup>16</sup> *cis* and *trans* configuration of the complex favor different paths of oxygen reduction. Complexes with *cyclam*, as a macrocycle that can exist in both of these configurations, can be interesting from this point of view. Therefore, we were interested to test the influence of the  $[\text{Co}^{\text{III}}(\text{hfac})\text{cyclam}](\text{ClO}_4)_2$  complex on oxygen reduction in acidic solution. The complex was first examined in 0.1 M  $\text{HClO}_4$  by cyclic voltammetry and the recorded CV displayed only the  $\text{Co}(\text{III})/\text{Co}(\text{II})$  redox peaks at the same potentials as in 0.1 M  $\text{NaClO}_4$ . The reduction of oxygen was examined at a GC rotating electrode in  $\text{O}_2$  saturated 0.1 M  $\text{HClO}_4$  in the potential range from 0.2 V to -1.1 V at a sweep rate of 5 mV/s and at 4 different rotation rates. As shown in Fig. 3B the pres-

ence of the  $[\text{Co}^{\text{III}}(\text{hfac})\text{cyclam}](\text{ClO}_4)_2$  complex caused a shift in of the potential of this reaction in the anodic direction and an increase of its current to some extent. Also, it can be seen that both curves for  $\text{O}_2$  reduction are without a limiting current density plateau. Furthermore, the curve recorded for the GC electrode is similar to the one presented by Sundberg *et al.*<sup>17</sup> for the same material (GC Sigradur) in 0.1 M HCl and according to the authors shows the reduction of  $\text{O}_2$  to  $\text{H}_2\text{O}_2$  as the major final product. The rather small difference in the current of this reaction in the presence of the complex probably means that the same mechanism is operative as on a pure GC electrode. As this complex is in the *cis* conformation these results are contrary to the conclusion Chang *et al.*<sup>16</sup> that the *cis* conformation rather than the *trans* one favors the 4-electron path in the reduction of oxygen. However, more about the exact influence of the  $[\text{Co}^{\text{III}}(\text{Rac})\text{cyclam}](\text{ClO}_4)_2$  complex on the reduction of  $\text{O}_2$  can be said after completion of the detailed examinations that are in progress.

#### Non-aqueous solution

Electrochemical characterization of the macrocyclic ligands *cyclam* and *tpmc*,  $\beta$ -diketonato ligands and all of the complexes **1–8** was also performed in non-aqu-

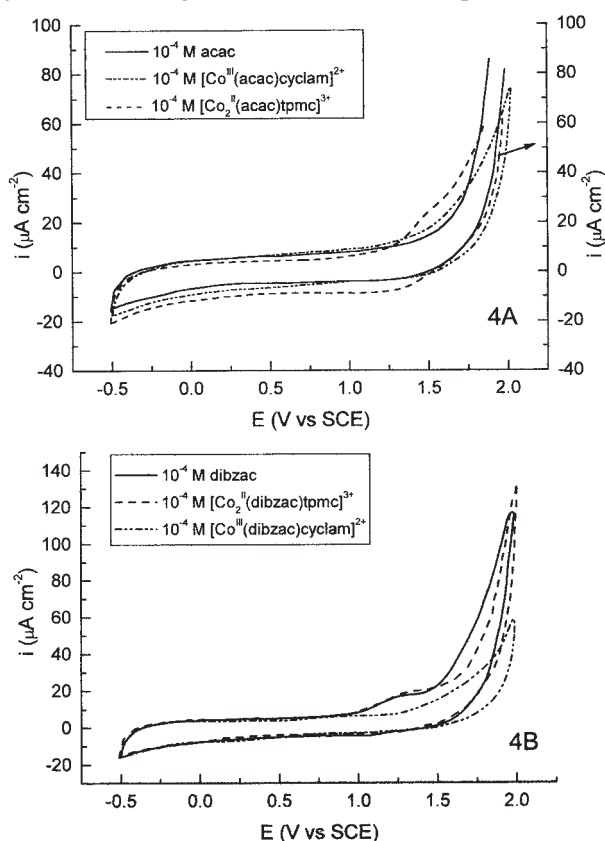


Fig. 4. Cyclic voltammograms at GC electrode in 0.1 M  $\text{LiClO}_4/\text{CH}_3\text{CN}$  and: A)  $10^{-4}$  M *acac* ligand,  $10^{-4}$  M  $[\text{Co}^{\text{III}}(\text{acac})\text{cyclam}](\text{ClO}_4)_2$  complex,  $10^{-4}$  M  $[\text{Co}_2^{\text{II}}(\text{acac})\text{tpmc}](\text{ClO}_4)_3$  complex. B)  $10^{-4}$  M *dibzac* ligand,  $10^{-4}$  M  $[\text{Co}^{\text{III}}(\text{dibzac})\text{cyclam}](\text{ClO}_4)_2$  complex,  $10^{-4}$  M  $[\text{Co}_2^{\text{II}}(\text{dibzac})\text{tpmc}](\text{ClO}_4)_3$  complex, (sweep rate 100 mV/s).



eous ( $\text{LiClO}_4$  in  $\text{CH}_3\text{CN}$ ) solution. Selected cyclic voltammograms are presented in Fig. 4 and the peak potentials are listed in Table II. CVs of macrocyclic ligands<sup>8,13</sup> show their irreversibly oxidation at potentials of 1.75 V for *cyclam* and 1.82 V for *tpmc* vs. SCE. One irreversible anodic peak at 1.30 V and 1.40 V vs. SCE (Table II and Fig. 4) were recorded on each CVs of  $\beta$ -diketonato ligands soluble in acetonitrile (*Hdibzac* and *Hhfac*).

The absence of any peaks of the investigated Co(III)-*cyclam* **1–4** complexes ruled out the redox reactions, indicating the stabilization both of *cyclam* and *Rac* ligands through the coordination to cobalt(III) (Fig. 4). Electrochemical inactivity of acetylacetonate ligand being in coordination sphere of Co(III) was found in other non-aqueous solutions too.<sup>18</sup> The solvent polarities might have a strong influence on forming intermolecular hydrogen bonds, due to electronic properties of both ligands, thus producing the corresponding difference in the bond stability between cobalt ion and nitrogen/oxygen atoms of the respective ligands.<sup>19</sup>

The absence of highly anodic peak of coordinated macrocycle *tpmc* in the Co(II)-*tpmc* **5–8** complexes means stabilization of this ligand in non-aqueous solution. It is probably due to the fact that the *tpmc* is very flexible ligand, adapting itself to both cobalt(II) ions with the bridging ligand. Anodic peaks at high positive potentials recorded on CVs of the binuclear **5–8** complexes (Table II and Fig. 4) correspond to oxidation processes of bidentate *Rac* ligand as well as metal ions. Actually, if the  $\beta$ -diketonato ligand is electrochemically non-active (as *Hacac* and *Htmhd*) the anodic peak in 1.25–1.48 V region origins only from Co(II) ions oxidation (Fig. 4A), contrary to electroactive *Rac* ligands (as *Hdibzac* and *Hhfac*) where in the same range the process of oxidation both for the metal and *Rac* ligand probably proceeds simultaneously (Fig. 4B). Therefore, potential values are in correlation with combined electronic and steric effects of coordinated  $\beta$ -diketones and they are characteristic for the binuclear penta-coordinated cobalt(II) complexes.<sup>20</sup>

#### Correlation with IR and NMR/EPR data

All of the ligands as well as their **1–8** complexes were also examined by spectroscopy methods. According to the earlier results<sup>6,7</sup> R-groups on the  $\beta$ -diketone largely influence the frequencies shifting  $\nu(\text{C}\cdots\text{C})$  and  $\nu(\text{C}\cdots\text{O})$  bands in IR spectra of the all complexes, as a consequence of different resonance and inductive effects along conjugated double bonds through the *Rac* anion. Influence of R-groups exhibits movement of important bands in  $^{13}\text{C}$ -NMR spectra of the **1–4** complexes as well as *g* factor values in EPR spectra of the **5–8** complexes, following from much positive to high negative inductive effect, in order of complexes with coordinated *tmhd* > *acac* > *dibzac* > *hfac* ligands.

The powerful efficacy of six fluorine atoms, of the *hfac* ligand in the **3** and **7** complexes, is especially expressed in all spectral characteristics through movement to higher wave numbers of important IR bands. In NMR<sup>7</sup> and EPR spectra (at



temperatures of 4 K and 11 K) the effect is quite opposite. In both series of complexes, electrochemical examinations in aqueous and non-aqueous solutions, display the anodic peaks at higher potential values for the corresponding **3** and **7** complexes with coordinated *hfac* ligand. On the other side, opposite electronic effect of  $-\text{C}(\text{CH}_3)_3$  groups of *tmhd* ligand in **4** and **8** complexes gave anodic peaks at lowest potential values.

From available results for the **1–8** complexes, it is evident that the same effects *i.e.*, structural and electronic, affect on spectral and electrochemical behavior, which were transmitted due to delocalised bands of coordinated *Rac* as a bidentate ligand in the Co(III)-*cyclam* **1–4** (Fig. 1A) or bridged bidentate ligand in the Co(II)-*tpmc* **5–8** complexes (Fig. 1B).

#### CONCLUSION

Based on the data obtained, some conclusions and comparison can be made about the influence of the structure of the **1–8** complexes and their electrochemical characteristics. Furthermore, the ability to influence these behavior seems to be related closely to the electronic properties of the *Rac* ligand as a whole, not just the oxygen atoms bonded to cobalt ions.

Consequently, Co(III) ions from the **1–4** and Co(II) ions from the **5–8** complexes undergo redox reactions in aqueous solution at the potentials, which are affected by the presence of different *Rac* ligands. The peak potentials of the mononuclear complexes **1–4** demonstrate reactions, which continuously proceed from  $\text{Co}^{\text{III}}/\text{Co}^{\text{II}}$  to  $\text{Co}^0$  reduction while in the binuclear **5–8** complex species in aqueous solution only reduction to metal Co occurs. Those behaviors could indicate different influence of coordinated *Rac* ligand besides folded tetraamine (*cyclam*) than in the presence of macrocyclic octamine (*tpmc*) in *boat* conformation. On the other side, in correlation to the former binuclear Co(II)-*tpmc* oxalato complex<sup>8</sup> where electronic exchange – antiferromagnetic coupling between the two metal ions is presented, in the case of the complexes **5–8** particularly pronounced electronic effect of the *Rac* bridging unit subsists to produce additional stabilization.

Preliminary examinations of oxygen reduction in the presence of  $[\text{Co}^{\text{III}}(\text{hfac})\text{cyclam}](\text{ClO}_4)_2$  complex shows possible catalytic effect on the reaction in acidic media.

Contrary to the aqueous solution, in acetonitrile, Co(III) redox reaction does not occur, indicating a higher stability of the complexes **1–4** in this media as well as their greater electrochemical stability in comparison with the binuclear cobalt(II)-*tpmc* complexes **5–8**. The influence of solvent polarities might be of importance on different redox behavior of the complexes in aqueous and non-aqueous solutions.<sup>15</sup>

*Acknowledgements:* The financial support was provided by the Ministry of Science, Technology and Development of the Republic Serbia, Grant Nos. 1796 and 1318.

## ИЗВОД

КОМПАРАТИВНО ЕЛЕКТРОХЕМИЈСКО ИСПИТИВАЊЕ НЕКИХ КОБАЛТ(III) И КОБАЛТ(II) КОМПЛЕКСА СА АЗАМАКРОЦИКЛИЧНИМ И  $\beta$ -ДИКЕТОНАТО ЛИГАНДИМАК. БАБИЋ-САМАРЏИЈА<sup>1</sup>, С. П. СОВИЉ<sup>1</sup> И В. М. ЈОВАНОВИЋ<sup>2</sup><sup>1</sup>Хемијски факултет, Универзитет у Београду, бр. 158, 11001 Београд и <sup>2</sup>ИХТМ Институт за електрохемију, Универзитет у Београду, бр. 473, 11001 Београд

Цикличном волтаметријом испитано је осам комплекса кобалта(III) и кобалта(II) са мешовитим лигандима, опште формуле  $[\text{Co}^{\text{III}}(\text{Rac})\text{cyclam}](\text{ClO}_4)_2$  (**1**)–(**4**) и  $[\text{Co}^{\text{II}}(\text{Rac})\text{tpmc}](\text{ClO}_4)_3$  (**5**)–(**8**), у воденој ( $\text{NaClO}_4$ ) и неводеној ( $\text{LiClO}_4/\text{CH}_3\text{CN}$ ) средини. У воденој средини *cyclam* и *Rac* лиганди подлежу анодној оксидацији. Координација са  $\text{Co}(\text{III})$  у комплексима (**1**)–(**4**) стабилизује ове лиганде али долази до редокс реакције  $\text{Co}(\text{III})/\text{Co}(\text{II})$ . У случају бинукларних  $\text{Co}(\text{II})$  комплекса (**5**)–(**8**) долази до оксидације *Rac* лиганда. Испитивани комплекси у воденом раствору утичу на реакцију издвајања водоника катодно померајући потенцијал и повећавајући струју. У неводеним растворима анодно се оксидују оба макроциклична (*cyclam* и *tpmc*) и *Rac* лиганди растворни у ацетонитрилу. Међутим, у овим растворима  $\text{Co}(\text{III})$  комплекса не долази до електрохемијских реакција што значи не само да и овде координација са кобалтом стабилизује лиганде већ нема ни редокс реакције за кобалт. Са друге стране, у  $\text{Co}(\text{II})$  комплексима стабилизован је *tpmc* али се оксидују *Rac* лиганди и  $\text{Co}(\text{II})$  па су тако у неводеним растворима комплекси  $\text{Co}(\text{III})$  стабилнији од бинукларних  $\text{Co}(\text{II})$ -*tpmc* комплекса.

(Примљено 16. маја, ревидирано 21. августа 2003)

## REFERENCES

1. J. Costamagna, G. Ferraudi, B. Matsuhira, M. Campos-Vallete, J. Canales, M. Villagran, J. Vargas, M. J. Aguirre, *Coord. Chem. Rev.* **196** (2000) 125
2. B. Bosnich, C. K. Poon, M. L. Tobe, *Inorg. Chem.* **4** (1965) 1102
3. S. P. Sovilj, G. Vučković, K. Babić, N. Matsumoto, M. Avramov-Ivić, V. M. Jovanović, *J. Coord. Chem.* **31** (1994) 167
4. S. P. Sovilj, G. Vučković, K. Babić, T. J. Sabo, S. Macura, N. Juranić, *J. Coord. Chem.* **41** (1997) 19
5. S. P. Sovilj, K. Babić-Samardžija, *Synth. React. Inorg. Met.-org. Chem.* **29** (1999) 1655
6. S. P. Sovilj, K. Babić-Samardžija, D. M. Minić, *J. Serb. Chem. Soc.* **63** (1998) 979
7. S. P. Sovilj, K. Babić-Samardžija, D. Stojić, *Spectroscopy Lett.* **35** (2002)
8. S. P. Sovilj, G. Vučković, K. Babić-Samardžija, N. Matsumoto, V. M. Jovanović, J. Mrozinski, *Synth. React. Inorg. Met.-org. Chem.* **29** (1999) 785
9. G. Vučković, D. Opsenica, S. P. Sovilj, D. Poletti, M. Avramov-Ivić, *J. Coord. Chem.* **42** (1997) 241
10. G. Vučković, D. Opsenica, S. P. Sovilj, D. Poletti, *J. Coord. Chem.* **47** (1999) 334
11. M. Seco, *J. Chem. Edu.* **66** (1989) 779
12. J. P. Facler, Jr., *Prog. Inorg. Chem.* **7** (1966) 361
13. V. M. Jovanović, K. Babić-Samardžija, S. P. Sovilj, *Electroanal.* **13** (2001) 1129
14. J. Jiang, A. Kucernak, *Electrochim. Acta* **47** (2002) 1967
15. P. Gouerec, A. Biloul, O. Contamin, G. Scarbeck, M. Savy, J. Riga, L. T. Weng, P. Bertand, *J. Electroanal. Chem.* **422** (1997) 61
16. H.-Y. Liu, I. Abdalmuhdi, C. K. Chang, F. C. Anson, *J. Phys. Chem.* **89** (1985) 665
17. K. M. Sundberg, Lj. Atanasoska, R. Atanasoski, W. H. Smyrl, *J. Electroanal. Chem.* **220** (1987) 161
18. E. Simon, P. L'Haridon, R. Pichon, M. L'Her, *Inorg. Chim. Acta.* **282** (1998) 173
19. J. Charette, G. Falthanse, Ph. Teyssie, *Spectrochim. Acta* **20** (1964) 597
20. H. Harada, M. Kodera, G. Vučković, N. Matsumoto, S. Kida, *Inorg. Chem.* **30** (1991) 1190.

## The growth of Nd:CaWO<sub>4</sub> single crystals

ALEKSANDAR GOLUBOVIĆ<sup>1\*</sup>#, SLOBODANKA NIKOLIĆ<sup>1</sup>, RADOŠ GAJIĆ<sup>1</sup>,  
STEVAN ĐURIĆ<sup>2</sup> and ANDREJA VALČIĆ<sup>3</sup>

<sup>1</sup>*Institute of Physics, Pregrevica 118, P. O. Box 57, 11001 Belgrade,* <sup>2</sup>*Faculty of Mining and Geology, Đušina 7, P. O. Box 162, 11000 Belgrade and* <sup>3</sup>*Faculty of Technology and Metallurgy, Karnegijeva 4, 11000 Belgrade, Serbia and Montenegro (galek@Eunet.yu)*

(Received 25 March 2003)

**Abstract:** CaWO<sub>4</sub> doped with 0.8 % at. Nd (Nd:CaWO<sub>4</sub>) single crystals were grown from the melt in air by the Czochralski technique. The critical diameter  $d_c = 1.0$  cm and the critical rate of rotation  $\omega_c = 30$  rpm were calculated from hydrodynamic equations for buoyancy-driven and forced convection. The rate of crystal growth was experimentally obtained to be 6.7 mm/h. For chemical polishing, a solution of 1 part saturated chromic acid (CrO<sub>3</sub> in water) and 3 parts conc. H<sub>3</sub>PO<sub>4</sub> (85 %) at 433 K with an exposure time of 2 h was found to be adequate. A mixture of 1 part concentrated HF and 2 parts chromic acid at room temperature after exposure for 30 min was found to be a suitable etching solution. The lattice parameters  $a = 0.52404$  (6) nm,  $c = 1.1362$  (6) nm and  $V_0 = 0.312$  (2) nm<sup>3</sup> were determined by X-ray powder diffraction. The obtained results are discussed and compared with published data.

**Keywords:** Czochralski technique, single crystal, Nd:CaWO<sub>4</sub>, growth, etching.

### INTRODUCTION

Calcium tungstate (CaWO<sub>4</sub>) belongs to the group of AWO<sub>4</sub> compounds, where A is a second group metal. AWO<sub>4</sub> compounds are important materials due to their use as scintillate detectors, photoanodes, solid-state laser hosts and in optical fibre applications.<sup>1–6</sup> Calcium tungstate has been proved to be an efficient laser host material with a number of lanthanide ions.<sup>7</sup> It is a uniaxial crystal with a tetragonal scheelite structure and the space group C<sub>4h</sub>. The trivalent lanthanide ions are known to occupy divalent calcium ion sites, the point symmetry of which is S<sub>4</sub>, making the host lattice an interesting system to study. The scheelite structure<sup>8</sup> may be regarded as a cubic close-packed array of Ca<sup>2+</sup> and [WO<sub>4</sub>]<sup>2–</sup> units with the coordination numbers of 8 and 4 oxygen atoms for the Ca and W cations, respectively.

\* Corresponding author.

# Serbian Chemical Society active member.

Various techniques, such as the Czochralski technique,<sup>9,10</sup> the flux method,<sup>11,12</sup> and solid-state reactions<sup>13</sup> have been used to synthesize single crystals, whiskers and powder of  $\text{CaWO}_4$ . Some attempts were made to prepare single crystal films,<sup>14–16</sup> but these experiments had limited success because of the high vaporization pressure of  $\text{WO}_3$  and obtained films were not of uniform structure. In our previous work,<sup>10</sup> we obtained  $\text{CaWO}_4$  single crystals taking some hydrodynamic equations into account, but the crystals were of nonuniform quality. Applying both theoretical and experimental investigations, we successfully obtained many oxide single crystals ( $\text{Bi}_{12}\text{SiO}_{20}$ ,<sup>17</sup>  $\text{Bi}_{12}\text{GeO}_{20}$ ,<sup>18</sup> sapphire,<sup>19</sup> Nd:YAG,<sup>20</sup> *etc.*). The aim of this work was to produce and characterize Nd:CaWO<sub>4</sub> single crystals by applying both theoretical and experimental treatment. The Nd atomic percentage was 0.8, as is usually the case for laser materials.

### EXPERIMENTAL

Calcium tungstate doped neodymium single crystals (Nd:CaWO<sub>4</sub>) were grown by the Czochralski technique using a MSR 2 crystal puller, as described previously.<sup>21</sup> The atmosphere used was air. The starting materials were powdered CaWO<sub>4</sub> (Koch&Light, Colnbrook, Buckinghamshire, England), and Nd<sub>2</sub>O<sub>3</sub> (Koch&Light, Colnbrook, Buckinghamshire, England) both of 4N purity. Powdered ZrO<sub>2</sub> (Koch&Light, Colnbrook, Buckinghamshire, England) of 4N purity was used for isolation. The rhodium crucible (4.12 cm diameter, 3.6 cm high and 0.2 cm thickness) was placed into an alumina vessel surrounded by ZrO<sub>2</sub> wool isolation. Double walls were used to protect the high radiation. To decrease the radial temperature gradient in the melt, alumina was mounted all around the system. The pull rates were generally in the range 0.54–12 mm/h, and the best results were obtained with a pull rate of 6.7 mm/h. The crystal rotation rates were between 22 and 40 rpm. The best results were obtained with a crystal rotation of 30 rpm. The diameters of the crystals were between 3 and 20 mm. The crucible was not rotated during the growth. After the growth run, the crystal boule was cooled at a rate of about 50 K/h down to room temperature.

Various solutions of H<sub>3</sub>PO<sub>4</sub> at different temperatures and for various exposure times were tried for chemical polishing. A solution of 1 part saturated chromic acid (CrO<sub>3</sub> in water) and 3 parts conc. H<sub>3</sub>PO<sub>4</sub> (85 %) (Merck, Darmstadt, Germany) at 433 K after exposure for 2 h was found to be suitable for chemical polishing. Various water solutions of HCl (Merck, Darmstadt, Germany) at different temperatures, and various solutions of concentrated HF (Merck, Darmstadt, Germany) and chromic acid, and for various exposure times were tried for etching. A mixture of 1 part concentrated HF and 2 parts chromic acid at room temperature after exposure for 30 minutes was found to be a suitable etching solution.

All the obtained crystal plates were observed in polarised light to reveal striations.

The chemical compositions of the products were determined by the XRD powder technique. All the samples were examined under the same conditions, using a Philips PW 1729 X-ray generator, a Philips 1710 diffractometer and the original APD software. The radiation source was an X-ray LLF tube with copper radiation and a graphite monochromator. The radiations were  $\lambda\text{CuK}\alpha_1 = 0.154060$  nm and  $\lambda\text{CuK}\alpha_2 = 0.154438$  nm. The anode tube load was 40 kV and 30 mA. Slits of 1.0 and 0.1 mm were fixed. Samples were pressed into standard aluminium frames and measured in the  $2\theta$  ranges from 10° to 80°. Each 1/50° (0.02°) was measured for 0.5 s. For product identification, the MPDS program and JCPDS (ASTM) card files were used.

### RESULTS AND DISCUSSION

The pulling of a crystal from a melt by the Czochralski method is a process essentially governed by the shape of the melt meniscus near the solid-liquid-vapour

junction and the thermal gradients on both sides of the growth interface. It is a well-known practical fact that in order to produce a crystal in the shape of a right cylinder some kind of regulation of the external conditions, like the supplied heating power or the pulling speed,<sup>22</sup> has to be applied. In principle, this requirement can be due to the process being inherently unstable, or simply that the heat transfer conditions are changing as the crystal is grown longer, *i.e.*, batch-induced variations. Surek<sup>23</sup> first addressed the fundamental question of inherent stability in an analysis where only the capillary effect was taken into account. That classical argument showed that a purely surface-tension-controlled process is unstable. Subsequently, some authors<sup>24</sup> investigated the dynamics of the crystal radius in response to variations in the temperature at the base of the meniscus, and they concluded that the pulling process (Ge was, in this case, the example) is linearly stable during Czochralski growth of crystals except in the case of very small diameters. Others<sup>25–27</sup> analytically or experimentally investigated the coupling to the thermal conditions, but the conclusions were conflicting. In our case we predicted that the growing crystal process was linearly stable for single crystals grown to about 1 cm in diameter.

The hydrodynamics of a melt are governed by buoyancy-driven convection of free convection, by forced convection due to crystal rotation and by thermo-capillary surface convection. Three dimensionless numbers can describe all these flows: the Grashof ( $Gr$ ), Reynolds ( $Re$ ) and Marangoni ( $Ma$ ) numbers. It can be said that the depth of the melt influences the Grashof number, the rotation rate of the crystal modifies the Reynolds number, and the temperature gradients over the surface of the melt acts on the Marangoni number.<sup>28</sup> The  $Ma$  number will not change significantly if a small temperature gradient exists over the surface of the melt, and so the hydrodynamics will be governed mainly by the  $Re$  and  $Gr$  numbers.

$$Re = \omega r^2 \nu^{-1}, \quad (1)$$

$$Gr = g \beta \Delta T R^3 \nu^{-2}, \quad (2)$$

where  $\omega$  – rotation rate;  $r$  – crystal radius,  $\nu$  – kinematic viscosity;  $g$  – acceleration due to gravity;  $\beta$  – volumetric expansion coefficient of the melt;  $\Delta T$  – temperature difference ( $T_{\text{crucible}} - T_{\text{mp}}$ ), and  $R$  – radius of the crucible. It was presumed, as did Carruthers,<sup>29</sup> that there was no change in the kinematic viscosity at the interface melt/crystal during the process of growth and that there was equilibrium  $Gr = Re^2$ . There is during this time, a flat melt/crystal interface at a critical rotation rate  $\omega_c$  and a critical diameter  $d_c$ . It was decided to use the relations derived by Carruthers in the calculations for our experimental system. These relations are in a good agreement with the experimental system. These relations are in a good agreement with the experimental data of many authors<sup>30,31</sup> and it was assumed that they could also be useful in our case. In this way, by applying the hydrodynamic forms, the values of the critical rate of rotation  $\omega_c = 30$  rpm, and the critical diameter  $d_c = 10$  mm were obtained. The rate of crystal growth was experimentally obtained to be 6.7 mm/h. A picture of an obtained Nd:CaWO<sub>4</sub> single crystal plate is shown in Fig. 1.

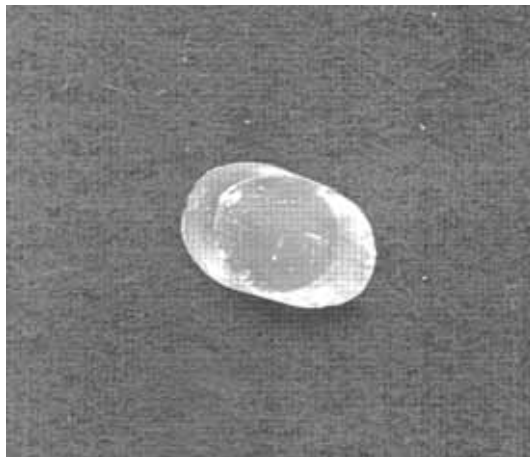


Fig. 1. A view of a chemically polished (001) cleavage plane of a Nd:CaWO<sub>4</sub> single crystal plate.

The widely known etch pit technique is very suitable for the study of crystalline solids. For such studies, cleavage planes are often preferred to the mature surface, because the former are free from the usual growth features and the characteristic surface marking which affect each pattern produced. Natural scheelite (CaWO<sub>4</sub>) is known to have (101), (112) and (001) cleavages.<sup>32</sup> On the other hand, synthetic CaWO<sub>4</sub> crystals, both pure and doped, grown by the Czochralski technique from the melt have been reported to exhibit (001) cleavages.<sup>33</sup> CaWO<sub>4</sub> is not a very hard material, with a hardness of 5 degrees on the Mohs scale.<sup>34</sup> It was found that a suitable solution for chemical polishing a mixture of 1 part saturated chromic acid (CrO<sub>3</sub> in water) and 3 parts conc. H<sub>3</sub>PO<sub>4</sub> (85 %) at 433–473 K was a suitable solution for chemical polishing after exposure times between 1.5 and 2 h. The best results were obtained at 433 K and an exposure time of 2 h. An etching solution is usually reported for the (001) cleavage plane.<sup>35</sup> It was found<sup>36</sup> that a mixture of 1 part concentrated HF and 2 parts saturated chromic acid (CrO<sub>3</sub> in water) is a suitable etching solution (etchant), which produces sizable pits (about 6 μm) in about



Fig. 2. A view of an etched (001) cleavage plane of a Nd:CaWO<sub>4</sub> single crystal plate after an etching exposure time of 30 min. Dislocation density 638 cm<sup>-2</sup>. Magnification 270×.



Fig. 3. A view of an etched (001) cleavage plane of a Nd:CaWO<sub>4</sub> single crystal plate after an etching exposure time of 15 min. Dislocation density 3200 cm<sup>-2</sup>. Magnification 270×.



20 min at room temperature. Many experiments were performed with various exposure times, and the best results were obtained with an exposure time of 30 minutes. Pictures of etch-pit specimens are presented in Figs. 2 and 3.



Fig. 4. A view of a small angle boundary in the (001) cleavage plane of a Nd:CaWO<sub>4</sub> single crystal plate. Magnification 270 $\times$ .

Figure 2 presents the sample after an exposure time of 30 min with a dislocation density of 638 cm<sup>-2</sup> (pulling speed was 6.7 mm/h,  $\omega_c = 30$  rpm,  $d_c = 10$  mm), and Fig. 3 presents the sample after an exposure time of 15 min with a dislocation density of 3200 cm<sup>-2</sup> (the pulling speed was 6.7 mm/h,  $\omega_c = 30$  rpm,  $d_c = 10$  mm). It should be noted that the obtained single crystal had a much smaller dislocation density ( $5 \times 10^2$ – $2 \times 10^3$  cm<sup>-2</sup>) than those reported in literature<sup>9,10</sup> where values of about  $10^5$  cm<sup>-2</sup> were cited. Figure 4 shows what could occur with an inappropriate pulling speed (11.4 mm/h) although the critical diameter  $d_c = 1.0$  cm and the critical rate of rotation  $\omega_c = 30$  rpm were applied. The low angle boundary is clearly seen.

A solution of conc. H<sub>3</sub>PO<sub>4</sub> at 593–603 K and exposure times between 1.5 and 2 h was also tested as a solution for chemical polishing, but better results were obtained with the above mentioned one. An aqueous solution of HCl at various temperatures was tested as an etchant, but better results were obtained with the men-

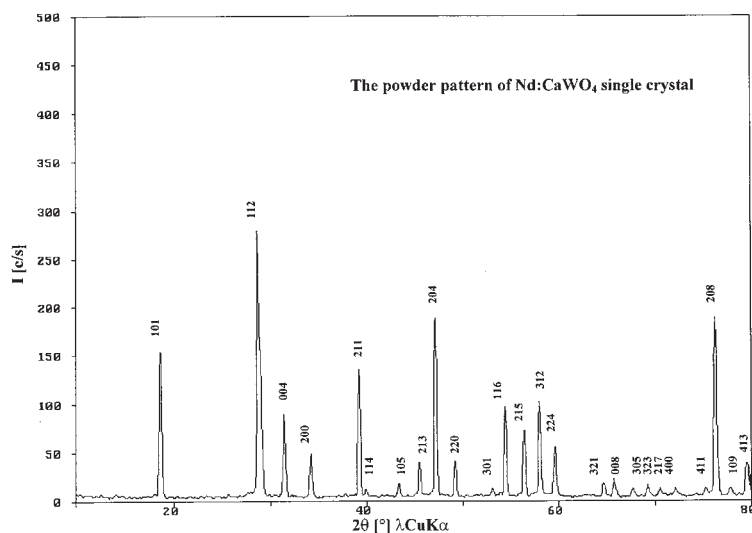
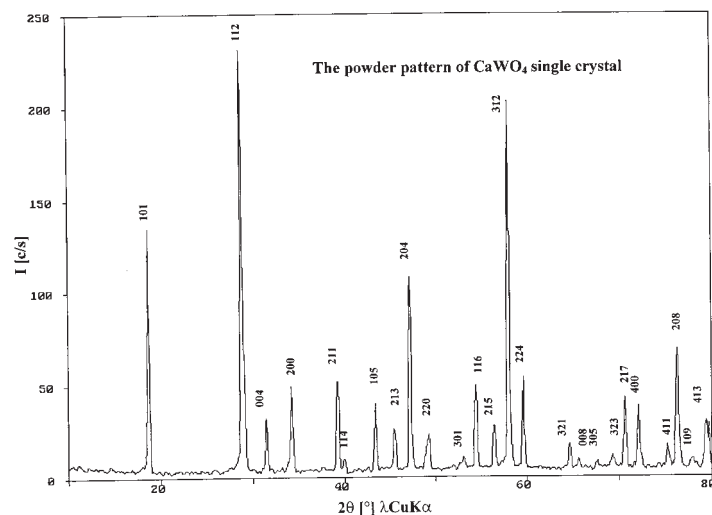


Fig. 5. X-Ray pattern of a powdered Nd:CaWO<sub>4</sub> single crystal.

Fig. 6. X-Ray pattern of a powdered  $\text{CaWO}_4$  single crystal.

tioned mixture of HF and saturated chromic acid. When examined under polarised light, the polished crystal plates showed the absence of bubbles, entrapments, non-homogeneous impurity concentrations and striations.

TABLE I. Table of spacing ( $d$ ), intensities ( $I$ ) and indices ( $hkl$ ) of an  $\text{Nd:CaWO}_4$  single crystal in comparison to literature data.<sup>37</sup>

$d_{\text{lit}}/\text{nm}$	$d_{\text{cal.}}/\text{nm}$	$I_{0\text{lit}}/\%$	$I_{0\text{cal.}}/\%$	( $hkl$ )	$d_{\text{lit}}/\text{nm}$	$d_{\text{cal.}}/\text{nm}$	$I_{0\text{lit}}/\%$	$I_{0\text{cal.}}/\%$	( $hkl$ )
0.47645	0.47437	84	60.90	101	0.15528	0.15518	13	18.89	224
0.31049	0.31024	100	100	112		0.15474		9.80	
0.30714	0.30660	30	50.45	103	0.14426	0.14419	5	6.13	321
0.28425	0.28404	39	35.78	004	0.14218	0.14210	4	7.09	008
0.26213	0.26187	19	16.91	200		0.14179		4.04	
0.23803	0.24041	1	2.24	202	0.13860	0.13857	3	4.04	305
0.22962	0.22958	18	50.45	211		0.13818		2.67	
0.22562	0.22539	3	2.24	114	0.13577	0.13576	4	6.61	323
0.20865	0.20858	6	4.04	105		0.13537		3.85	
0.19943	0.19945	10	15.41	213	0.13356	0.13353	4	3.85	217
0.19276	0.19256	36	76.36	204	0.13109	0.13092	2	2.24	400
0.18536	0.18533	15	13.96	220	0.12637	0.12636	2	3.85	411
0.18536	0.18541	15	7.79	301	0.12497	0.12478	7	78.83	208
0.16877	0.16869	17	34.67	116		0.12446		32.50	
	0.16823		16.15		0.12285	0.12271	2	2.24	109
0.16326	0.16317	8	40.39	215	0.12076	0.12074	4	6.37	332
	0.16274		16.91		0.12055	0.12050	2	16.91	413
0.15921	0.15914	23	40.98	312		0.12019		5.90	
0.15873	0.15572	4	24.53	303					



The structural properties of the obtained crystals were obtained using X-ray analysis of powdered samples. A Philips PW 1710 diffractometer was used in the  $2\theta$  ranges from  $10^\circ$  to  $80^\circ$ . The unit cell of calcium tungstate was calculated by the least square method using 29 reflections, including more  $K\alpha_2$  for 8 reflections. All the reflections correspond to  $\text{CaWO}_4$  crystals with the parameters of the tetragonal unit cell  $a = 0.524294$  (6) nm,  $c = 1.1373$  (7) nm and  $V_0 = 0.31263$  nm<sup>3</sup>.<sup>37</sup> Some divergence of the compared results can be explained by the fact that X-ray powder diffraction analysis gives a statistical result. The calculated results for the lattice parameters are  $a = 0.52404$  (6) nm,  $c = 1.1362$  (6) nm, and  $V_0 = 0.312$  (2) nm<sup>3</sup>, which are in good agreement with the published data.<sup>2,9,13</sup> The X-ray diffractogram for powdered Nd:CaWO<sub>4</sub> is given in Fig. 5, in which the weak reflections are not marked with Mueller indices. The X-ray diffractogram of a powdered CaWO<sub>4</sub> single crystal,<sup>38</sup> which can be used to show that the small amount of dopant has not influence on the diffractogram, is presented in Fig. 6. The Nd concentration is 0.8 atomic percentages and this amount did not change the unit cell. It can be seen from Figs. 5 and 6 that the positions of the peaks are at the same place. The intensities are changed as could be expect because they show statistical values. It

TABLE II. Table of angles ( $\theta$ ), intensities ( $I$ ) and indices ( $hkl$ ) of a Nd:CaWO<sub>4</sub> single crystal in comparison to literature data<sup>37</sup>

$\theta_{\text{lit.}}/^\circ$	$\theta_{\text{cal.}}/^\circ$	$I_{0\text{lit.}}/\%$	$I_{0\text{cal.}}/\%$	( $hkl$ )	$\theta_{\text{lit.}}/^\circ$	$\theta_{\text{cal.}}/^\circ$	$I_{0\text{lit.}}/\%$	$I_{0\text{cal.}}/\%$	( $hkl$ )
18.608	18.685	84	60.90	101	59.477	59.525	13	18.89	224
28.729	28.770	100	100	112		59.710		9.80	
29.049	29.065	30	50.45	103	64.544	64.585	5	6.13	321
31.445	31.480	39	35.78	004	65.605	65.650	4	7.09	008
34.178	34.195	19	16.91	200		65.815		4.04	
37.763	37.795	1	2.24	202	67.516	67.545	3	4.04	305
39.201	39.230	18	50.45	211		67.760		2.67	
39.925	39.995	3	2.24	114	69.132	69.140	4	6.61	323
43.329	43.375	6	4.04	105		69.365		3.85	
45.442	45.480	10	15.41	213	70.422	70.465	4	3.85	217
47.106	47.160	36	76.36	204	71.970	72.085	2	2.24	400
49.110	49.120	15	13.96	220	75.111	75.120	2	3.85	411
52.973	53.045	15	7.79	301	76.104	76.240	7	78.83	208
54.311	54.340	17	34.67	116		76.475		32.50	
	54.500		16.15		77.658	77.765	2	2.24	109
56.302	56.340	8	40.39	215	79.266	79.285	4	6.37	332
	56.500		16.91		79.431	79.470	2	16.91	413
57.869	57.900	23	40.98	312		79.715		5.90	
58.061	58.065	4	24.53	303					

has been reported<sup>39</sup> that only almost perfect single crystals can split X-ray reflections into  $K\alpha_1$  and  $K\alpha_2$  and the presence of doublets is one more confirmation of the quality of the produced crystals.

The intensities of the reflections for some crystal planes, together with their Mueller indices and distances between the planes of the reflections are given in Table I. The intensities of the reflections from Fig. 5 are given together with published intensities for the same planes in JCPDS ("Joint Committee on Powder Diffraction Standards"). Table II represents the intensities of the reflections for some crystal planes, together with their Mueller indices and the angles of the reflections. Some divergences between the experimentally obtained  $2\theta$  values and these in the literature could be explained as being the consequence of the employed wavelength  $\text{CuK}\alpha_1$  (0.154178 nm) and  $\text{CuK}\alpha_1$  cited in the literature<sup>37</sup> (0.1540598 nm).

#### CONCLUSIONS

The conditions for growing  $\text{Nd:CaWO}_4$  single crystals were calculated using a combination of Reynolds and Grashof numbers. From the hydrodynamics of the melt the critical crystal diameter  $d_c = 1.0$  cm and the critical rate of rotation  $\omega_c = 30$  rpm were calculated. The value of the rate of crystal growth was experimentally found to be 6.7 mm/h.

A mixture of 1 part saturated chromic acid ( $\text{CrO}_3$  in water) and 3 parts conc.  $\text{H}_3\text{PO}_4$  (85 %) at 433 K after exposure for 2 h was shown to be suitable for chemical polishing. A mixture of 1 part concentrated HF and 2 parts chromic acid at room temperature after exposure for 30 min was shown to be a suitable etching solution.

#### ИЗВОД

##### РАСТ МОНОКРИСТАЛА $\text{Nd:CaWO}_4$

АЛЕКСАНДАР ГОЛУБОВИЋ<sup>1</sup>, СЛОБОДАНКА НИКОЛИЋ<sup>1</sup>, РАДОШ ГАЈИЋ<sup>1</sup>, СТЕВАН ЂУРИЋ<sup>2</sup> и  
АНДРЕЈА ВАЛЧИЋ<sup>3</sup>

<sup>1</sup>Институт за физику, Предревуца 118, бр. 57, 11001 Београд, <sup>2</sup>Рударско-геолошки факултет, Бушина 7, бр. 162, 11000 Београд и <sup>3</sup>Технолошко-металуршки факултет, Карнегијева 4, 11000 Београд

Монокристали  $\text{CaWO}_4$  допирани са 0,8 атомских % Nd ( $\text{Nd:CaWO}_4$ ) расли су у ваздуху теником раста кристала по Чохралском. Вредности критичног пречника  $d_c = 1,0$  cm и критичне брзине ротације  $\omega_c = 30$  o/min су одређене помоћу једначина динамике флуида. Брзина извлачења кристала од 6,7 mm/h је одређена експериментално. Као средство за хемијско полирање је одређена смеша 1 дела засићене хромне киселине (водени раствор  $\text{CrO}_3$ ) и 3 дела conc.  $\text{H}_3\text{PO}_4$  (85 %) на 433 K при излагању од 2 сата. Смеса 1 дела концентроване HF и 2 дела хромне киселине на собној температуре при излагању од 30 минута се показала као погодно средство за нагризање. Одређени су параметри решетке  $a = 0,52404$  (6) nm,  $c = 1,1362$  (6) nm и  $V_0 = 0,312$  (2) nm<sup>3</sup> помоћу рендгенске дифракционе анализе праха. Добијени резултати су дискутовани и упоређени са литературним подацима.

(Примљено 25. марта 2003)

## REFERENCES

1. H. Wang, F. D. Medina, Y. D. Zhou, Q. N. Zhang, *Phys. Rev. B* **45** (1992) 10356
2. A. Kuzmin, J. Purans, *Rad. Measur.* **33** (2001) 583
3. V. Muerk, B. Namozov, N. Yaroshevich, *Rad. Measur.* **24** (1995) 371
4. V. Nagirnyi, E. Feldbach, L. Jonsson, M. Kirm, A. Lushchik, Ch. Lushchik, L. L. Nagornaya, V. D. Ryzhikov, F. Savikhin, G. Svensson, I. A. Tupitsina, *Rad. Measur.* **29** (1998) 247
5. J. Hulliger, A. Caprez, P. Meyer, P. Mikhail, *Mat. Res. Bull.* **32** (1997) 1045
6. A. Lushchik, E. Feldbach, R. Kink, Ch. Lushchik, M. Kirm, I. Martinson, *Phys. Rev. B.* **53** (1996) 5379
7. A. G. Page, S. V. Godbole, M. D. Sastry, *J. Phys. Chem. Solids* **50** (1989) 571
8. E. Guermen, E. Daniels, J. S. King, *J. Chem. Phys.* **55** (1971) 1093
9. P. S. Porto, J. F. Scott, *Phys. Rev.* **157** (1967) 716
10. A. Valčić, R. Roknić, S. Nikolić, *Proc. 23 Chem. of SR Serbia Symp.*, Belgrade, Yugoslavia, 1981, p. 627 (in Serbian)
11. S. Oishi, M. Hirao, *J. Mater. Sci. Lett.* **8** (1989) 1397
12. S. Oishi, M. Hirao, *Bull. Chem. Soc. Jpn.* **63** (1990) 984
13. G. Blasse, L. H. Brixner, *Chem. Phys. Lett.* **173** (1990) 409
14. C. Feldman, *J. Soc. Motion Pict. Eng.* **67** (1958) 455
15. W.-S. Cho, M. Yashima, M. Kakihana, A. Kudo, T. Sakata, M. Yoshimura, *Appl. Phys. Lett.* **66** (1995) 1027
16. N. Saito, A. Kudo, T. Sakata, *Bull. Chem. Soc. Jpn.* **69** (1996) 1241
17. A. Golubović, S. Nikolić, R. Gajić, S. Đurić, A. Valčić, *J. Serb. Chem. Soc.* **64** (1999) 553
18. A. Golubović, S. Nikolić, R. Gajić, S. Đurić, A. Valčić, *Hem. ind.* **53** (1999) 227 (in Serbian)
19. A. Golubović, S. Nikolić, S. Đurić, A. Valčić, *J. Serb. Chem. Soc.* **66** (2001) 411
20. A. Golubović, S. Nikolić, R. Gajić, S. Đurić, A. Valčić, *J. Serb. Chem. Soc.* **67** (2002) 291
21. A. Golubović, R. Gajić, S. Nikolić, S. Đurić, A. Valčić, *J. Serb. Chem. Soc.* **65** (2000) 391
22. M. A. Gevelber, G. Stephanopoulos, M. J. Wargo, *J. Crystal Growth* **91** (1988) 199
23. T. Surek, *J. Appl. Phys.* **47** (1976) 4384
24. D. T. Hurler, G. C. Joyce, G. C. Wilson, M. Ghassempoory, A. B. Crowley, E. J. Stern, *J. Crystal Growth* **100** (1990) 111
25. T. Surek, S. R. Coriell, B. Chalmers, *J. Crystal Growth* **50** (1980) 21
26. A. B. Crowley, *J. Appl. Math.* **30** (1983) 173
27. J. J. Derby, R. A. Brown, *J. Crystal Growth* **83** (1988) 137
28. M. T. Santos, J. C. Rojo, L. Arizmendi, E. Dieguez, *J. Crystal Growth* **142** (1994) 103
29. J. R. Curruthers, *J. Crystal Growth* **36** (1976) 212
30. R. A. Brown, *Advances in Crystal Growth*, P. M. Dryburgh Ed., Prentice-Hall, Englewood Cliffs, New York, 1987, p. 41
31. R. Ristorcelli, J. L. Lumley, *J. Crystal Growth* **116** (1992) 647
32. C. Palache, H. Berman, C. Frondel, *Dana's System of Mineralogy Vol. 2*, 7<sup>th</sup> edn., Wiley, New York, 1951, pp. 1073–1089
33. K. Nassau, A. M. Broyer, *J. Appl. Phys.* **33** (1962) 3064
34. A. R. Patel, S. K. Arora, *J. Phys. D: Appl. Phys.* **7** (1974) 2301
35. H. J. Levinstein, A. M. Broyer, *J. Appl. Phys.* **33** (1962) 3064
36. A. R. Patel, S. K. Arora, *J. Phys. D: Appl. Phys.* **7** (1974) 1485
37. JCPDS 41–1431
38. A. Golubović, S. Nikolić, S. Đurić, A. Valčić, *Metallurgija* **9** (2003) (in press) (in Serbian)
39. S. Đurić, *Nauka Tehnika Bezbednost* **1** (1995) 45 (in Serbian).

BOOK REVIEW

**COMPREHENSIVE ENZYME KINETICS**  
**by Vladimir Leskovac**

*Published by Kluwer Academic/Plenum Publisher New York, March 2003-11-17*

Pages: ii + 438, 125 Figures, 50 Tables, 900 Equations, EURO 118.00/USD 125.00/GBP 77.50,  
ISBN: 0-306-46712-7 Hardbound

Today, in the post-genomic era, no fundamental or applied work can be thought about in biochemistry and its related molecular biology, and in life sciences in general without considering enzymes. Above all, enzymes are becoming powerful reagents and tool in all other fields of chemistry too, but also an integral part of everyday life. Biotechnology, as one of the branches of science, and its applications, which shall determine the trends in civilization in the forthcoming century, are inconceivable without enzymes and their activity. These are only some of the reasons why the book “*Comprehensive Enzyme Kinetics*” by Professor Vladimir Leskovac from the Faculty of Technology, University of Novi Sad (Serbia & Montenegro) is welcome.

Through 18 chapters, the author takes the user of the Book systematically, simply and clearly, in a modern and an expert way into the complex kinetic relations of the interactions of enzymes and substrates, starting from the introduction which relates to the structure of enzymes and their active sites, through the bases of chemical kinetics, indispensable for an understanding of enzyme kinetics, in order to reach the basic topic. The next 11 chapters are dedicated to a gradual survey of monosubstrate, bisubstrate and trisubstrate reactions, including nonhyperbolic rate equations and allosteric and cooperative effects. Simple but also complex kinetic models are explained in this Book. Sections 14 and 15 are dedicated to the effect of pH and temperature on enzyme catalysis.

The Author emphasizes the importance of the graphic presentation of kinetic models owing to which the Book abounds in graphs – such a way of presenting results. Mathematical models are often in the form of double-reciprocal plots.

In the last 3 chapters, special attention is paid to isotope exchange, kinetic isotope effects and statistical analysis of the initial rate and binding data, which relate to enzyme reactions. The Book also contains a Subject Index.

The Book is of special value due to the numerous examples which illustratively support a simpler understanding of the reported contents.

Pertaining references (almost 600 in total) are cited after each chapter and with the exception of 3 places (chapters 1, 7 and 11) are systematized as books, review articles and specific references which facilitate their utilization. A certain number of examples are from the Author's and associates' references.

The Book is a modern textbook but also a contemporary handbook intended for students of Biochemistry first and foremost, but also for all those who meet enzymes in their research work. "*Comprehensive Enzyme Kinetics*" by Professor Leskovac is a novelty written in a "scholarly fashion", as stated in the Preface by the Author himself, which exceeds the limits of textbook literature and makes up the shortage among a large number of books dedicated to this topic since it presents understandably and concisely, free from unneeded details and excessive explanations, on a relatively small number of pages, all that is necessary for the comprehension and application of kinetic enzymes. It is quite certain that such a book can only be written by a successful scientist and a pedagogue with great experience.

Students, professors, and researchers would greatly benefit if this excellent book "*Comprehensive Enzyme Kinetics*" by Professor Leskovac could be found in the libraries of their faculties, institutes and industry, as well as in the laboratories – in all places where enzymes are taught and dealt with.

Miroslav M. Vrvic, D. Sc. Chem.  
Professor of Biotechnology  
Faculty of Chemistry,  
University of Belgrade, P. O. Box 158,  
11001 Belgrade, Studentski trg 16, Serbia and Montenegro,  
E-mail: mmvchem@drenik.net

# CONTENTS OF VOLUME 68

## NUMBER 1

### Organic Chemistry and Biochemistry

<i>R. Marković, A. Shirazi, Z. Džambaski, M. Baranac and D. Minić</i> : Hydrogen bonding in push-pull 5-substituted-2-alkylidene-4-oxothiazolidines: <sup>1</sup> H-NMR spectroscopic study .....	1
<i>N. C. Nikolić and M. Z. Stanković</i> : Kinetics of solanidine hydrolytic extraction from potato ( <i>Solanum tuberosum</i> L) haulm solid-liquid systems .....	9
<i>D. T. Veličković, N. V. Randjelović, M. S. Ristić, A. S. Veličković and A. Šmelcerović</i> : Chemical constituents and antimicrobial activity of the ethanol extracts obtained from the flower, leaf and stem of <i>Salvia officinalis</i> L.....	17
<i>N. Tomašević, M. Nikolić, K. Klappe, D. Hoekstra and V. Niketić</i> : Insulin-induced lipid binding to hemoglobin .....	25

### Physical Chemistry

<i>M. Lj. Kijevčanin, A. B. Djordjević, I. R. Grgurić, B. D. Djordjević and S. P. Šerbanović</i> : Simultaneous correlation of the excess enthalpy and W-shaped excess heat capacity of 1,4-dioxane- <i>n</i> -alkane systems by PRSV-HVOS CEOS .....	35
<i>I. R. Grgurić, M. Lj. Kijevčanin, B. D. Djordjević, A. Ž. Tasić and S. P. Šerbanović</i> : Excess molar volume of acetonitrile + alcohol systems at 298.15 K. Part II: Correlation by cubic equation of state.....	47
<i>M. M. Ačanski, S. Jovanović-Šanta and L. R. Jevrić</i> : Normal and reversed phase thin-layer chromatography of new 16,17-secoestrone derivatives.....	57

### Analytical Chemistry

<i>R. P. Mihajlović, N. R. Ignjatović, M. R. Todorović, I. Holclajtner-Antunović and V. M. Kaljević</i> : Spectrophotometric determination of phosphorus in coal and coal ash using bismuth-phosphomolybdate complex .....	65
--	----

## NUMBER 2

### Organic Chemistry

<i>N. V. Valentić, Ž. Vitnik, S. I. Kozhushkov, A. De Majere, G. S. Ušćumlić and I. O. Juranić</i> : Effect of substituents on the <sup>13</sup> C-NMR chemical shifts of 3-methylene-4-substituted-1,4-pentadienes. Part I. ....	67
<i>V. Leskovac, S. Trivić and D. Peričin</i> : Isomerization of an enzyme-coenzyme complex in yeast alcohol dehydrogenase-catalysed reactions.....	77

### Inorganic Chemistry

<i>L. Larabi, Y. Harek, A. Reguig and M. M. Mostafa</i> : Synthesis, structural study and electrochemical properties of copper(II) complexes derived from benzene- and <i>p</i> -toluenesulphonylhydrazones. ....	85
---	----

**Physical Chemistry**

- P. I. Premović*: Thermochemical equilibrium calculations of high-temperature O<sub>2</sub> generation on the early Earth: Giant asteroid impact on land ..... 97
- M. Rašković, I. Holclajtner-Antunović, M. Tripković and D. Marković*: Excitation and analytical characteristics of an ethanol loaded U-shaped arc ..... 109

**Electrochemistry**

- B. Blizanac, S. Mentus, N. Cyjetićanin and N. Pavlović*: Temperature effect on graphite KS44 lithiation in ethylene carbonate + propylene carbonate solution: galvanostatic and impedance study ..... 119

**Analytical Chemistry**

- A. I. Igov, R. M. Simonović and R. P. Igov*: Kinetic determination of ultramicro amounts of As(III) in solution..... 131

**Chemical Engineering**

- M. Ilić, B. Grubor and V. Manović*: Sulfur retention by ash during coal combustion. Part I. A model of char particle combustion..... 137

## NUMBER 3

**Macromolecules**

- B. Dunjić, J. Djonlajić, S. Vukašinović, M. Sepulchre, M. O. Sepulchre and N. Spassky*: Rheokinetic study of crosslinking of  $\alpha,\omega$ -dihydroxy oligo(alkylene maleate)s with a trisisocyanate ..... 147

**Physical Chemistry**

- M. M. Ačanski*: Retention behaviour of some estradiol derivatives on alumina in normal phase chromatography ..... 163
- V. Manović, B. Grubor, M. Ilić and B. Jovančević*: Sulfur retention by ash during coal combustion. Part II. A model of the process ..... 171
- H. Hubicka and D. Kolodnyńska*: Separation of Y(dcta)<sup>-</sup> complexes from Nd(dcta)<sup>-</sup> and Sm(dcta)<sup>-</sup> complexes on polyacrylate anion-exchangers (Short communication)..... 183

**Electrochemistry**

- B. N. Grgur, N. M. Marković and P. N. Ross Jr.*: Electrochemical oxidation of carbon monoxide: from platinum single crystals to low temperature fuel cells catalysts. Part II. Electrooxidation of H<sub>2</sub>, CO and H<sub>2</sub>/CO mixtures on well characterized PtMo alloy..... 191
- S. Stanković, B. Grgur, N. Krstajić and M. Vojnović*: Kinetics of the zinc anodic dissolution reaction in near neutral EDTA solutions ..... 207

**Analytical Chemistry**

- Z. M. Grahovac, S. S. Mitić and E. T. Pecev*: Kinetic determination of ultramicro amounts of Cu(II) ion in solution ..... 219

**Environmental Chemistry**

- T. Šolević, B. Jovančević, M. Vrvić and H. Wehner*: Oil pollutants in alluvial sediments – influence of the intensity of contact with ground waters on the effect of microorganisms ..... 227

**Organic Chemistry**

<i>N. Djapić, Z. Djarmati, S. Filip and R. M. Jankov: A stilbene from the heartwood of <i>Maclura pomifera</i> (Note) .....</i>	235
---	-----

## NUMBER 4–5

<i>D. Vitorović: Professor Miroslav J. Gašić: On the occasion of his 70<sup>th</sup> birthday.....</i>	239
--	-----

**Organic Chemistry**

<i>I. Novaković, Z. Vujčić, T. Božić, N. Božić, N. Milosavić and D. Sladić: Chemical modification of <math>\beta</math>-lactoglobulin by quinones.....</i>	243
<i>S. De Rosa, C. Iodice, J. Nechev, K. Stefanov and S. Popov: Composition of the lipophilic extract from the sponge <i>Suberites domuncula</i> .....</i>	249
<i>W. E. G. Müller and I. M. Müller: The hypothetical ancestral animal. The Urmetazoa: telomerase activity in sponges (Porifera).....</i>	257
<i>Z. G. Kamenarska, S. D. Dimitrova-Konaklieva, K. Lj. Stefanov and S. S. Popov: A comparative study on the sterol composition of some brown algae from the Black Sea .....</i>	269
<i>S. Trifunović, V. Vajs, V. Tešević, D. Djoković and S. Milosavljević: Lignans from the plant species <i>Achillea lingulata</i> .....</i>	277
<i>S. Milosavljević, I. Juranić, I. Aljančić, V. Vajs and N. Todorović: Conformational analysis of three germacranolides by the PM3 semi-empirical method.....</i>	281
<i>D. Opsenica, D. E. Kyle, W. K. Milhous and B. A. Šolaja: Antimalarial, antimycobacterial and antiproliferative activity of phenyl substituted mixed tetraoxanes .....</i>	291
<i>M. S. Bjelaković, V. D. Pavlović, M. M. Dabović and Lj. B. Lorenc: Acid-catalyzed and photolytic reactivity of some unsaturated B-nor-5,10-secosteroidal ketones .....</i>	303
<i>G. Petrović and Ž. Čeković: Synthesis of tetrahydrokhusitone. Annulation of the cyclohexane ring by free radical and carbanionic sequence of reactions.....</i>	313
<i>M. N. Stojanović, D. B. Nikić and D. Stefanović: Implicit-OR tiling of deoxyribozymes: Construction of molecular scale OR, NAND, and four-input logic gates.....</i>	321
<i>M. M. Crnogorac and N. M. Kostić: Effects of pH on kinetics of the structural rearrangement that gates the electron-transfer reaction between zinc cytochrome <i>c</i> and plastocyanin. Analysis of protonation states in a diprotein complex .....</i>	327
<i>A. Papakyriakou, I. Bratsos and N. Katsaros: Structural studies on metallobleomycins: The interaction of Pt(II) and Pd(II) with bleomycin.....</i>	339
<i>I. Tabaković and S. Riemer: Roughness development in electrodeposited soft magnetic CoNiFe films in the presence of organic additives .....</i>	349
<i>S. Jerosimić and M. Perić: Use of the group theory for classification of electronic states of acetylene. ....</i>	363
<i>R. Marković, Z. Džambaski, M. Stojanović, P. Steel and M. Baranac: Regiospecificity in the heterocyclization of <math>\beta</math>-oxonitriles to 5-substituted 4-oxothiazolidine derivatives .....</i>	383
<i>I. Gutman: Algebraic structure count of liner phenylenes and their congeners.....</i>	391
<i>I. Gutman, D. Vidović, B. Furtula and I. G. Zenkevich: Wiener-type indices and internal molecular energy .....</i>	401
<i>V. Rakić, V. Dondur and R. Hercigonja: FTIR study of carbon monoxide adsorption on ion-exchanged X, Y and mordenite type zeolites .....</i>	409
<i>M. M. Vrvić, V. Dragutinović, V. Matić, S. Spasić, O. Cvetković and D. Vitorović: A kinetic study of the depyritization of oil shale HCl-kerogen concentrate by <i>Thiobacillus ferrooxidans</i> at different temperatures.....</i>	417



- V. M. Leovac, V. Divjaković, V. I. Češljević and R. Fazlić:* Transition metal complexes with thiosemicarbazide-based ligand. Part 45. Synthesis, crystal and molecular structure of [2,6-di-acetylpyridine bis(S-methylisothiosemicarbazonato)]diazide-iron(III) ..... 425

## NUMBER 6

**Organic Chemistry**

- A. S. Veličković, M. S. Ristić, D. T. Veličković, S. N. Ilić and N. D. Mitić:* The possibilities of the application of some species of sage (*Salvia* L) as auxiliaries in the treatment of some diseases..... 435
- M. Carposu, L. Odochian, St. Dima, M. Dumitras and M. Petrovanu:* Thermokinetic study of the in-activation reaction of 1-methylphthalazinium ylids..... 447

**Inorganic Chemistry**

- R. N. Prasad and N. Gupta:* Template synthesis of Mn(II) complexes of tetraazamacrocycles derived from diaminoalkanes and 3,4-hexanedione or benzil ..... 455
- M. G. Abd El Wahed:* Thermodynamic and structural studies of complexes of manganese(II), cobalt(II), nickel(II) and copper(II) with aminofuopyridine carboxamide (Note)..... 463
- D. Vučinić, I. Miljanović, A. Rosić and P. Lazić:* Effect of Na<sub>2</sub>O/SiO<sub>2</sub> mole ratio on the crystal type of zeolite synthesized from coal fly ash ..... 471

**Physical Chemistry**

- J. D. Jovanović and D. K. Grozdanić:* Saturated-liquid heat capacity: new polynomial models and review of the literature experimental data (Note)..... 479

**Electrochemistry**

- V. Vojinović, S. Mentus and V. Komnenić:* Thermodynamic and kinetic behavior of hydrogen electrode in a solution of 0.5 M KClO<sub>4</sub> in dimethyl sulphoxide ..... 497

**Materials**

- B. Matović, S. Bošković and M. Logar:* Preparation of basalt-based glass ceramics ..... 505
- K. I. Popov, S. B. Krstić and M. G. Pavlović:* The critical apparent density for the free flow of copper powder (Preliminary communication)..... 511

## NUMBER 7

**Organic Chemistry**

- S. Ž. Drmanić, B. Ž. Jovanović, A. D. Marinković and M. Mišić-Vuković:* The kinetics of the reactions of 2-substituted nicotinic acids with diazodiphenylmethane in various alcohols..... 515
- N. V. Valentić and G. S. Ušćumlić:* Effects of substituents on the <sup>1</sup>H-NMR chemical shifts of 3-methylene-2-substituted-1,4-pentadienes ..... 525
- V. W. Bhagwat, J. Tiwari, A. Choube and B. Pare:* Kinetics and mechanism of cetyltrimethylammonium bromide catalyzed oxidation of diethylene glycol by chloramine-T in acidic medium ... 535
- B. Todorović-Marković, Z. Marković, N. Marinković and T. Nenadović:* Experimental study of physical parameters significant in fullerene synthesis (Short communication) ..... 543

**Physical Chemistry**

- I. Gutman, B. Arsić and B. Furtula:* Equiseparable chemical trees ..... 549
- D. Ž. Mijin, D. G. Antonović, G. Bončić-Caričić, B. Ž. Jovanović and O. S. Rajković:* Gas chromatographic retention indices for N-substituted amino *s*-triazines on capillary columns. Part IV. Influence of column polarity on retention index ..... 557

<i>T. J. Janjić, G. Vučković and M. B. Čelap</i> : Investigation of the compatibility between one-dimensional system parameters and the multidimensional Solvation parameter model in RP liquid column chromatography .....	565
<i>S. D. Pawar and P. M. Dhadke</i> : Extraction and separation studies of Ga(III), In(III), and Tl(III) using the neutral organophosphorous extractant, Cyanex-923.....	581
<i>A. Cecal, A. Paraschivescu, K. Popa, D. Colisnic, G. Timco and L. Singenorean</i> : Radiolytic splitting of water molecules in the presence of some supramolecular compounds (Short communication) .....	593

## NUMBER 8–9

**Organic Chemistry and Biochemistry**

<i>A. Georgakopoulos</i> : Aspects of solid state $^{13}\text{C}$ CPMAS NMR spectroscopy in coals from the Balkan peninsula .....	599
<i>R. G. Patel, J. V. Patel, M. P. Patel and R. G. Patel</i> : Synthesis and characterization of ether linkage containing bis-fluoran compounds.....	607
<i>D. Marković</i> : Energy storage in the photosynthetic electron-transport chain. An analogy with Michaelis-Menten kinetics .....	615

**Polymers**

<i>S. Koseva, S. Brezovska, V. Boševska and D. Burevski</i> : Bentonite, stabilizer for suspension polymerization .....	629
---	-----

**Inorganic Chemistry**

<i>S. S. Konstantinović, B. C. Radovanović, Ž. Cakić and V. Vasić</i> : Synthesis and characterization of Co(II), Ni(II), Cu(II) and Zn(II) complexes with 3-salicylidenehydrazono-2-indolinone.....	641
--	-----

**Electrochemistry**

<i>M. G. Pavlović, N. D. Nikolić and K. I. Popov</i> : The current efficiency during the cathodic period of reversing current in copper powder deposition and the overall current efficiency.....	649
---	-----

**Materials**

<i>B. R. Simonović, S. V. Mentus and R. Dimitrijević</i> : Kinetic and structural aspects of tantalum hydride formation.....	657
<i>D. Manasijević, D. Živković, I. Katayama and Ž. Živković</i> : Calculation of activities in some gallium-based systems with a miscibility gap .....	665
<i>E. Garskaite, D. Jasaitis and A. Kareiva</i> : Sol-gel preparation and electrical behaviour of Ln: YAG (Ln = Ce, Nd, Ho, Er) .....	677

**Analytical Chemistry**

<i>D. K. Singh, B. Srivastava and A. Sahu</i> : Spectrophotometric determination of ajmaline and brucine by Folin Ciocalteu's reagent.....	685
<i>M. Jelikić-Stankov, P. Djurdjević and D. Stankov</i> : Determination of uric acid in human serum by an enzymatic method using <i>N</i> -methyl- <i>N</i> -(4-aminophenyl)-3-methoxyaniline reagent.....	691

## NUMBER 10

**Organic Chemistry**

- G. S. Uščumlić, A. A. Kshad and D. Ž. Mijin*: Synthesis and investigation of solvent effects on the ultraviolet absorption spectra of 1,3-bis-substituted-5,5-dimethylhydantoins..... 699
- K. Penov-Gaši, S. Stojanović, M. Sakač, E. Djurendić, S. Jovanović-Šanta, S. Stanković, N. Andrić and M. Popsavin*: Synthesis, crystal structure and antiaromatase activity of 17-halo-16,17-seco-5-androstene derivatives..... 707
- A. D. Nikolić, M. R. Mladenović, L. Gobor, D. G. Antonović and S. D. Petrović*: FTIR study of N-H..... $\pi$  hydrogen bonding: *N*-alkylpropanamides – aromatic donor systems ..... 715
- Z. D. Petrović, D. Andjelković and Lj. Stevanović*: Vitamin B<sub>12</sub>-catalyzed synthesis of some peracetylated alkyl  $\beta$ -D-xylopyranosides (Short communication) ..... 719
- V. V. Dabholkar and R. P. Gavande*: A microwave-catalyzed rapid, efficient and ecofriendly synthesis of substituted pyrazol-5-ones (Short communication) ..... 723

**Inorganic Chemistry**

- H. S. Seleem, B. A. El-Shetary, S. M. E. Khalil and M. Shebl*: Potentiometric and spectrophotometric studies of the complexation of Schiff-base hydrazones containing the pyrimidine moiety ..... 729
- W. Ferenc, A. Walków-Dziewulska and J. Chruściel*: Spectral and thermal behaviours of rare earth element complexes with 3,5-dimethoxybenzoic acid..... 751

**Analytical Chemistry**

- S. M. Rančić, R. P. Igov and T. G. Pecev*: Kinetic determination of As(III) in solution..... 765

**Materials**

- K. I. Popov, S. B. Krstić, M. Č. Obradović, M. G. Pavlović, Lj. J. Pavlović and E. R. Ivanović*: The effect of the particle shape and structure on the flowability of electrolytic copper powder. I. Modeling of a representative powder particle ..... 771
- K. I. Popov, M. G. Pavlović, Lj. J. Pavlović, E. R. Ivanović, S. B. Krstić and M. Č. Obradović*: The effect of the particle shape and structure on the flowability of electrolytic copper powder. II. The experimental verification of the model of the representative powder particle..... 779

## NUMBER 11

**Organic Chemistry**

- N. M. Krstić, M. S. Bjelaković, Lj. B. Lorenc and V. D. Pavlović*: Oxidative fragmentation of 5-hydroxy-1-oxo-5 $\alpha$ -cholestan-3 $\beta$ -yl acetate ..... 785
- V. Popsavin, S. Grabež, I. Krstić, M. Popsavin and D. Djoković*: A formal synthesis of (+)-muricatacin from D-xylose ..... 795
- D. Zlatković, D. Jakovljević, Dj. Zeković and M. M. Vrvic*: A glucan from active dry baker's yeast (*Saccharomyces cerevisiae*): chemical and enzymatic investigation of the structure (Preliminary communication) ..... 805

**Biochemistry**

- R. Masnikosa, J. Anna Nikolić and O. Nedić*: Membrane-associated insulin-like growth factor (IGF) binding structures in placental cells ..... 811
- R. M. Prodanović, M. B. Simić and Z. M. Vujčić*: Immobilization of periodate oxidized invertase by adsorption on sepiolite ..... 819

**Physical Chemistry**

- D. Ž. Mijin, D. G. Antonović and B. Ž. Jovanović*: Gas chromatographic retention indices for N-substituted amino *s*-triazines on capillary columns. Part V. Temperature dependence of the retention index ..... 825
- A. Vujaković, A. Daković, J. Lemić, A. Radosavljević-Mihajlović and M. Tomašević-Čanović*: Adsorption of inorganic anionic contaminants on surfactant modified minerals ..... 833
- J. P. Popić and D. M. Dražić*: Electrochemistry of active chromium. Part III. Effects of temperature ... 843

**Electrochemistry**

- X. Yang, Sh. Chen, Sh. Zhao, D. Li and H. Ma*: Synthesis of copper nanorods using electrochemical methods..... 849
- A. V. Tripković, K. Dj. Popović and J. D. Lović*: Comparison of formic acid oxidation at supported Pt catalyst and at low-index Pt single crystal electrodes in sulfuric acid solution..... 859
- S. Lj. Gojković*: Electrochemical oxidation of methanol on Pt<sub>3</sub>Co bulk alloy ..... 871

**Analytical Chemistry**

- D. Zendelovska and T. Stafilov*: High-performance liquid chromatographic determination of famotidine in human plasma using solid-phase column extraction ..... 883

**Materials**

- V. Maksimović, S. Zec, V. Radmilović and M. T. Jovanović*: The effect of microalloying with silicon and germanium on microstructure and hardness of a commercial aluminium alloy..... 893
- K. I. Popov, P. M. Živković and S. B. Krstić*: The apparent density as a function of the specific surface of copper powder and the shape of the particle size distribution curve ..... 903
- Errata ..... 909

## NUMBER 12

**Biochemistry**

- V. D. Dragičević, S. Sredojević, M. B. Spasić and M. M. Vrvic*: Ageing-induced changes of reduced and oxidized glutathione in fragments of maize seedlings ..... 911

**Inorganic Chemistry**

- V. M. Leovac, Lj. S. Vojinović, K. Mészáros Szécsényi and V. I. Češljević*: Transition metal complexes with thiosemicarbazide-based ligands. Part 46. Synthesis and physico-chemical characterization of mixed ligand cobalt(III)-complexes with salicylaldehyde semi-, thiosemi- and isothiosemicarbazone and pyridine ..... 919
- V. S. Jevtović, Lj. S. Jovanović, V. M. Leovac and L. J. Bjelica*: Transition metal complexes with thiosemicarbazide-based ligands. Part 47. Synthesis, physicochemical and voltammetric characterization of iron(III) complexes with pyridoxal semi-, thiosemi- and S-methylisothiosemicarbazones ..... 929

**Physical Chemistry**

- I. Gutman, B. Furtula and J. Belić*: Note of the Hyper-Wiener index (Note) ..... 943
- I. Gutman*: Hyper-Wiener index and Laplacian spectrum ..... 949
- I. Hinić, G. Stanišić and Z. Popović*: Influence of the synthesis conditions on the photoluminescence of silica gels..... 953
- B. F. Abramović, V. B. Anderluh, A. S. Topalov and F. F. Gaál*: Direct photolysis and photocatalytic degradation of 2-amino-5-chloropyridine ..... 961
- M. M. Ačanski*: Normal-phase high performance liquid chromatography of estradiol derivatives on amino- and diol-columns ..... 971

**Electrochemistry**

- V. V. Panić, A. B. Dekanski, V. B. Mišković-Stanković, S. K. Milonjić and B. Ž. Nikolić:* The role of the concentration profile of titanium oxide in RuO<sub>2</sub>–TiO<sub>2</sub> coatings obtained by the sol-gel procedure on its electrochemical behavior ..... 979
- K. Babić-Samardžija, S. P. Sovilj and V. M. Jovanović:* Comparative electrochemical study of some cobalt(III) and cobalt(II) complexes with azamacrocycles and β-diketonato ligands ..... 989

**Materials**

- A. Golubović, S. Nikolić, R. Gajić, S. Djurić and A. Valčić:* The growth of Nd:CaWO<sub>4</sub> single crystals... 1001

**Book Review**

- M. M. Vrvic:* Comprehensive enzyme kinetics by V. Leskovac ..... 1011
- Contents of Volume 68 ..... 1013
- Subject index ..... 1021
- Author index ..... 1025

## Subject index\*

- Acetonitrile + alcohol systems, 47  
Acetylene, classification of electronic states of, 363  
*Achillea tingulata*, lignans of, 277  
Ajmaline and brucine determination, 685  
Algae, chemoevolution of, 269  
Aluminum alloy, microalloying with Si and Ge, 893  
2-Amino-5-chloropyridine, photolysis of, 961  
Antiaromatase activity of androstene derivatives, 707  
Arsenic (III) detn. in soln., 131  
As(III) kinetic detn. in solution, 765  
Asteroid impact on Earth, 97
- Balkan endemic nephropathy, 599  
Bentonite stabilizer, 629  
Bis-fluoran compounds, 607  
Bismuth-phosphomolybdate complex, 65  
Bleomycin, interaction of Pt(II) and Pd(II) with, 339  
B-nor-secosteroidal ketones, 303
- Carbon monoxide adsorption on X, Y and mordenite zeolites, 409  
Carbon monoxide, oxidation of, 191  
Char combustion, 137  
Chemical trees, equiseparable, 549  
Chromium, anodic dissolution of, 871  
Co(II) and Co(III) complexes with azamacrocycles, 989  
Co(II), Ni(II), Cu(II) and Zn(II) complexes with isatin, 641  
Cobalt(III) complexes with salicylaldehyde, 919  
CoNiFe films in presence of organic additives, 349  
Contaminants, anionic, 833
- Copper powder deposition, 649  
Copper nanorods, 843  
Copper powder, apparent density of, 903  
Copper powder, electrolytic, 771, 779  
Copper powder, free flow of, 511  
Copper(II), detn. of ultramicro amounts, 219  
Cyanex-923, use in separation of Ga(III), In(III) and Tl(III), 581
- DC arc, ethanol loaded, plasma composition, 109  
Deoxyribozymes, tiling of, 321  
Diethylene glycol oxidation by chloramine-T, 535  
Dihydroxy oligo(alkylene maleate) crosslinking in, 147  
Dimethyl hydantoins, UV absorption spectra, 699  
3,5-Dimethoxy benzoates, rare earth complexes, 751  
1,4-Dioxane + *n*-alkane systems, 35  
D-xylopyranosides, vitamin B<sub>12</sub> catalyzed synthesis, 719
- Estradiol derivatives, chromatography of, 971  
Estradiol derivatives, retention on alumina, 163  
Ethanol in *Salvia officinalis*, 17
- Famotidine in human plasma, detn., 883  
Formic acid oxidation at platinum, 849  
Fullerene synthesis, significant physical parameters, 543
- Gallium-based systems with a miscibility gap, 665  
Germacranolides, conformational analysis of, 281

\* Indices were kindly prepared by Professor Slobodan Ribnikar

- Glass ceramics, basalt-based, properties of, 505  
 Glutathione in maize seedlings, 911  
 Graphite lithiation, 119
- Hemoglobin, lipid bonding to, 25  
 Hydrogen electrode in a soln. of  $\text{KClO}_4$  in dimethyl sulfoxide, 497  
 Hyper-Wiener index and Laplacian Spectrum, 947  
 Hyper-Wiener index of a chemical tree, 943
- Iron(III) complex with thiosemicarbazide-based ligands, 425  
 Iron(III) complexes with semicarbazones, 927
- Lactoglobulin, modification by quinones, 243
- Maclura pomifera*, a stilbene from, 235  
 Methanol, electrochemical oxidation of, 859  
 3-Methylene-2-substituted-1,4-pentadienes, chemical shifts with, 525  
 Methylphthalazinium ylids, inactivation reactions with, 447  
 Mn(II) complexes of tetraazamacrocycles, 455  
 Mn(II), Co(II), Ni(II) and Cu(II) complexes with aminofuopyridine carboxamide 463  
 Muricatacin synthesis from D-xylose, 795
- Nd: $\text{CaWO}_4$  single crystals, 1001  
 N-H... $\pi$  hydrogen bonding, 715  
 Nicotinic acids, 2-substituted, reaction with diazodiphenylmethane, 515
- Oil pollutants in alluvial sediments, 227  
 Oxonitriles, heterocyclization of, 383  
 Oxygen ( $\text{O}_2$ ) in early Earth, 97
- Pentadienes,  $^{13}\text{C}$ -NMR chem. shifts of, 67  
 Phenylenes, linear, algebraic structure count, 391  
 Phosphorus, detn. in coal and coal ash, 65  
 Photosynthetic electron-transport chain, 615  
 Placental cell membranes, insulin-like growth factor, 811
- Polyurethane, rheokinetic analysis, 147  
 Push-pull alkenes, hydrogen bonding in, 1  
 Pyrazol-5-ones, ecofriendly synthesis of, 723
- Retention indices of capillary columns, 557  
 RP liquid column chromatography, 565  
 $\text{RuO}_2$ - $\text{TiO}_2$  coating, 979
- Saccharomyces cerevisiae*, glucan from, 805  
*Salvia* L. in the treatment of some diseases, 435  
*Salvia officinalis*, chemical composition of, 17  
 Saturated-liquid heat capacity, polynomial models, 479  
 Schiff-base hydrazones complexation, 729  
 16,17-Secosterone derivatives, 57  
 Sepiolite, immobilization of invertase, 819  
 Silica gels, photoluminescence of, 953  
 Solanidine extraction, 9  
*Solanum tuberosum*, solanidine from, 9  
*s*-Triazines, retention indices, 825  
*Suberites domuncula*, composition of lipophilic extract, 249  
 Sulfur, retention by ash, 137, 171  
 Sulphonylhydrazone-Cu(II) complex, 85  
 Suspension polymerization, 629
- Tantalum hydride formation, 657  
 Telomerase activity in sponges, 257  
 Tetrahydrokhusitone, synthesis of, 313  
 Tetraoxanes, phenyl substituted, antimycobacterial activity of, 291  
 Thiobacillus ferrooxidans depyritization of oil shale kerogen, 417  
 Triisocyanate in rheokinetic study, 147
- Uric acid, detn. in human serum, 691
- Water radiolysis, catalyzed, 593  
 Wiener-type indices and internal molecular energy, 401
- Yeast alcohol dehydrogenase, 77  
 Yttrium aluminium garnet preparation, 677

Yttrium and neodymium complexes, 183

Zeolite synthesized from coal fly ash, 471

Zinc anodic dissolution, 207

Zinc cytochrome c and plastocyanin, gated  
electron transfer, 327.



## Author index

- Abd el Waheed M. G., 463  
Abramović B. F., 961  
Ačanski M. M., 57, 163, 971  
Aljančić I., 281  
Anderluh V. B., 961  
Andjelković D., 719  
Andrić N., 707  
Antonović D. G., 557, 715, 825  
Arsić B., 549  
  
Babić-Samardžija K., 989  
Baranac M., 1, 383  
Belić J., 941  
Bhagwat V. W., 535  
Bjelaković M. S., 303, 785  
Bjelica L. J., 929  
Blizanac B., 119  
Bončić-Caričić G., 557  
Boševska V., 629  
Bošković S., 505  
Božić N., 243  
Božić T., 243  
Bratsos I., 329  
Brezovska S., 629  
Burevski D., 629  
  
Cakić Ž., 641  
Caprosu M., 447  
Cecal A., 593  
Choube A., 535  
Chrusciel J., 751  
Colisnic D., 593  
Crnogorac M. M., 327  
Cvetković O., 417  
Cvijetićanin N., 119  
  
Češljević V. I., 425, 919  
Čeković Ž., 313  
  
Ćelap M. B., 565  
Dabholkar V. V., 723  
  
Dabović M. M., 303  
Daković A., 833  
De Meijere, A., 67  
De Rosa S., 249  
Degang Li, 843  
Dekanski A. B., 979  
Dhadke P. M., 581  
Dima St., 447  
Dimitrijević R., 657  
Dimitrova-Konaklieva S., 269  
Divjaković V., 425  
Djapić N., 235  
Djarmati Z., 235  
Djoković D., 277  
Djoković D., 795  
Djonlagić J., 147  
Djordjević A. B., 35  
Djordjević B. D., 35, 47  
Djurdjević P., 691  
Djurendić E., 707  
Djurić S., 1001  
Dondur V., 409  
Dražić D. M., 871  
Dragičević V. D., 911  
Dragutinović V., 417  
Drmanić S. Ž., 515  
Dumitras M., 447  
Dunjić B., 147  
  
Džambaski Z., 1, 383  
  
El-Shetary B. A., 729  
**F**  
Fazlić R., 425  
Ferenc W., 751  
Filip S., 235  
Furtula B., 401, 549, 943  
  
Gaál F. F., 961  
Gajić R., 1001  
Garskaite E., 677

- Gavande R. P., 723  
 Georgakopoulos A., 599  
 Gobor L., 715  
 Gojković S. Lj., 859  
 Golubović A., 1001  
 Grabež S., 795  
 Grahovac Z. M., 219  
 Grgur B., 307  
 Grgur B. N., 191  
 Grgurić I. R., 35, 47  
 Grozdanić D. K., 479  
 Grubor B., 137, 171  
 Gupta N., 455  
 Gutman I. 391, 401, 549, 943, 949  
  
 Harek Y., 85  
 Hercigonja R., 409  
 Hinić I., 953  
 Hoekstra D., 25  
 Holclajtner-Antunović I., 65, 109  
 Houyi Ma, 843  
 Hubicka H., 183  
  
 Ignjatović N. R., 65  
 Igov A. R., 131  
 Igov R. P., 131, 765  
 Ilić M., 171, 137  
 Ilić S. N., 435  
 Iodice C., 249  
 Ivanović E. R., 771, 779  
  
 Jakovljević D., 805  
 Janjić T. J., 565  
 Jankov R. M., 235  
 Jasaitis D., 677  
 Jelikić-Stankov M., 691  
 Jerosimić S., 363  
 Jevrić L., 57  
 Jevtović V. S., 927  
 Jovančičević B., 171, 227  
 Jovanović B. Ž., 515, 557, 825  
 Jovanović J. D., 479  
 Jovanović Lj. S. 927  
 Jovanović M. T., 893  
 Jovanović V. M., 987  
 Jovanović-Šanta S., 57, 707  
 Juranić I., 281  
 Juranić I. O., 67  
  
 Kaljević V. M., 65  
 Kamenarska Z. G., 269  
 Kareiva A., 677  
 Katayama I., 665  
 Katsaros, N., 339  
 Khalil S. M. E., 729  
 Kijevčanin M. Lj., 35, 47  
 Klappe K., 25  
 Kolodynska D., 183  
 Komnenić V., 497  
 Konstantinović S. S., 641  
 Koseva S., 629  
 Kostić N. M., 327  
 Kozhushkov S. I., 67  
 Krstajić N., 207  
 Krstić I., 795  
 Krstić N. M., 785  
 Krstić S. B. 511, 771, 779, 903  
 Kshad A. A., 699  
 Kyle D. E., 291  
  
 Larabi L., 85  
 Lazić P., 471  
 Lemić J., 833  
 Leovac V. M., 425, 919, 929  
 Leskovac V. 77, 1011  
 Logar M., 505  
 Lorenc Lj. B., 303, 785  
 Lović J. D., 849  
  
 Maksimović V., 893  
 Manasijević D., 665  
 Manović V., 171, 137  
 Marinković A. D., 515  
 Marinković M., 543  
 Marković D., 109, 615  
 Marković N. M., 191  
 Marković R., 1, 383  
 Marković Z., 543  
 Masnikosa R., 811  
 Matić V., 417  
 Matović B., 505  
 Mentus S., 119, 497, 657  
 Mészáros Szécsényi K., 919  
 Mišić-Vuković M. M., 515  
 Mišković-Stanković V. B., 979  
 Mihajlović R. P., 65  
 Mijinić D. Ž., 557, 699, 825  
 Milhous W. K., 291

- Miljanović I., 471  
 Milonjić S. K., 977  
 Milosavić N., 243  
 Milosavljević S., 277, 281  
 Minić D. I  
 Mitić N. D., 435  
 Mitić S.S., 219  
 Mladenović M. R., 715  
 Mostafa M. M., 85  
 Müller I. M., 257  
 Müller W. E. G., 257
- Nechev J., 249  
 Nedić O., 811  
 Nenadović T., 543  
 Niketić V., 25  
 Nikić D. B., 321  
 Nikolić A. D., 715  
 Nikolić A. J. 811  
 Nikolić B. Ž., 977  
 Nikolić M., 25  
 Nikolić N. Č, 9  
 Nikolić N. D., 649  
 Nikolić S., 1001  
 Novaković I. , 243
- Obradović M. Č., 771, 779  
 Odochian L. , 447  
 Opsenica D., 291
- Panić V. V., 977  
 Papakyriakou A., 329  
 Paraschivescu A., 593  
 Pare B., 535  
 Patel J.V., 607  
 Patel M. P., 607  
 Patel R. G., 607  
 Pavlović Lj. J., 771, 779  
 Pavlović M. G., 511, 649, 771, 779  
 Pavlović N., 119  
 Pavlović V. D., 303, 785  
 Pawar S. D., 581  
 Pecev E. T., 219  
 Pecev T. G., 765  
 Penov-Gaši K., 707  
 Perić M., 363  
 Peričin D., 77  
 Petrovanu M., 447
- Petrović G., 313  
 Petrović S. D., 715  
 Petrović Z. D., 719  
 Popa K., 593  
 Popić J. P., 871  
 Popov K. I., 511, 649, 771, 779, 903  
 Popov S. S., 269  
 Popov S., 249  
 Popović K. Dj ., 849  
 Popović Z., 951  
 Popsavin M. 707, 795  
 Popsavin V., 795  
 Prasad R. N., 455  
 Premović P. I., 97  
 Prodanović R. M., 819
- Rašković M., 109  
 Radmilović V., 893  
 Radosavljević-Mihajlović A., 833  
 Radovanović B. S., 641  
 Rajković O. S., 557  
 Rakić V., 409  
 Rančić S. M., 765  
 Randjelović N. V., 17  
 Reguig A., 85  
 Riemer S. , 349  
 Ristić M. S., 17, 435  
 Rosić A., 471  
 Ross Ph. N. Jr., 191
- Sahu A., 685  
 Sakač M., 707  
 Seleem H. S., 729  
 Sepulchre M., 147  
 Sepulchre M.-O., 147  
 Shebl M., 729  
 Shenhao Chen, 843  
 Shirazi A, 1  
 Shiyong Zhao, 843  
 Simić M. B., 819  
 Simonović B. R., 657  
 Simonović R. M., 131  
 Singerean L., 593  
 Singh D. K., 685  
 Sladić D., 243  
 Sovilj S. P., 989  
 Spasić M. B., 911  
 Spasić S., 417

- Spassky N. , 147  
 Sredojević S., 911  
 Srivastava B., 685  
 Stařilov T., 883  
 Stanišić G., 951  
 Stankov D., 691  
 Stanković M. Z., 9  
 Stanković S., 207, 707  
 Steel P., 383  
 Stefanov K., 249  
 Stefanov Lj. K., 269  
 Stefanović D., 321  
 Stevanović Lj., 719  
 Stojanović M., 383  
 Stojanović M. N., 321  
 Stojanović S., 707  
  
 Šerbanović S. P. 35, 47  
 Šmelcerović A. A.. 17  
 Šolaja B. A., 291  
 Šolević T., 227  
  
 Tabaković I., 349  
 Tasić A. Ž, 47  
 Tešević V. 277  
 Timco G., 593  
 Tiwari J., 535  
 Todorović M. R., 65  
 Todorović N., 281  
 Todorović-Marković B., 543  
 Tomašević N., 25  
 Tomašević-Čanović M., 833  
 Topalov A. S., 961  
 Trifunović S., 277  
 Tripković A. V., 849  
 Tripković M., 109  
 Trivić S., 77  
  
 Ušćumlić G. S., 67, 525, 699  
  
 Vajs V., 277, 281  
 Valčić A., 1001  
 Valentić N. V., 67, 525  
 Vasić V., 641  
 Veličković A. S., 17, 435  
 Veličković D. T., 17, 435  
 Vidović D., 401  
 Vitnik Ž., 67  
 Vitorović D., 242, 417  
 Vojinović Lj. S., 919  
 Vojinović V., 497  
 Vojnović M., 207  
 Vrvic M. M. , 227, 417, 805, 911, 1011  
 Vučinić D. A., 471  
 Vučković G., 565  
 Vujčić Z., 243  
 Vujčić Z. M., 819  
 Vujaković A., 833  
 Vukašinović S., 147  
  
 Walkow-Dziewulska, 751  
 Wehner H., 227  
  
 Xuegeng Yang, 843  
  
 Zec S., 893  
 Zeković Dj., 805  
 Zendelovska D., 883  
 Zenkevich I. G., 401  
 Zlatković D., 805  
  
 Živković Ž., 665  
 Živković D., 665  
 Živković P. M., 903